

UNIVERSITÉ DU QUÉBEC À MONTRÉAL

DÉVELOPPEMENT DE NANOMATÉRIAUX FONCTIONNELS À PARTIR DE
POLYMÈRES ET DENDRIMÈRES AMPHIPHILES POUR DE APPLICATIONS
POTENTIELLES EN NANOMEDICINE

MÉMOIRE
PRÉSENTÉ
COMME EXIGENCE PARTIELLE
DE LA MAÎTRISE EN CHIMIE

PAR
BRANDON ANDRADE-GAGNON

OCTOBRE 2021

UNIVERSITÉ DU QUÉBEC À MONTRÉAL

DEVELOPMENT OF FUNCTIONAL NANOMATERIALS FROM AMPHIPHILIC
POLYMERS AND DENDRIMERS FOR POTENTIAL APPLICATIONS IN
NANOMEDICINE

THESIS
PRESENTED
AS A REQUIREMENT
FOR THE MASTER'S IN CHEMISTRY

BY
BRANDON ANDRADE-GAGNON

OCTOBER 2021

UNIVERSITÉ DU QUÉBEC À MONTRÉAL
Service des bibliothèques

Avertissement

La diffusion de ce mémoire se fait dans le respect des droits de son auteur, qui a signé le formulaire *Autorisation de reproduire et de diffuser un travail de recherche de cycles supérieurs* (SDU-522 – Rév.04-2020). Cette autorisation stipule que «conformément à l'article 11 du Règlement no 8 des études de cycles supérieurs, [l'auteur] concède à l'Université du Québec à Montréal une licence non exclusive d'utilisation et de publication de la totalité ou d'une partie importante de [son] travail de recherche pour des fins pédagogiques et non commerciales. Plus précisément, [l'auteur] autorise l'Université du Québec à Montréal à reproduire, diffuser, prêter, distribuer ou vendre des copies de [son] travail de recherche à des fins non commerciales sur quelque support que ce soit, y compris l'Internet. Cette licence et cette autorisation n'entraînent pas une renonciation de [la] part [de l'auteur] à [ses] droits moraux ni à [ses] droits de propriété intellectuelle. Sauf entente contraire, [l'auteur] conserve la liberté de diffuser et de commercialiser ou non ce travail dont [il] possède un exemplaire.»

ACKNOWLEDGMENT

First and foremost, I would like to express my sincere gratitude to my supervisor Professor Ali Nazemi, for giving me the opportunity to work in his research group, where I was able to discover and learn the basis of polymers, dendrimers, and self-assembly aspects. I would like to take this time to thank him for his guidance, great support, kind advice, constructive suggestions, and for his confidence in me. His understanding and patience have allowed me to carry out all of my projects successfully and be able to overcome various obstacles that were encountered.

I would also like to thank Professor Steve Bourgault for his great support and significant impact throughout my research.

I would also like to express my sincere gratitude to my colleagues Marilyne Bélanger-Bouliga and Thi Hong Diep Nguyen for their collaboration and support with my research.

I would also like to mention my gratitude to all the members of the department of chemistry, and biochemistry at UQAM, particularly the administration, professors, and technicians who have helped me during the course of my master's program.

Last, but certainly not least, I would like to give a special thanks to my mom for her unlimited encouragement, love, and support during my studies! If not for her, I would not have reached my full potential! This thesis is a representation of all her hard work paying off!

TABLE OF CONTENTS

LIST OF FIGURES	viii
LIST OF TABLES	x
LIST OF SCHEMES	xi
LIST OF ABBREVIATIONS	xii
RÉSUMÉ	xv
ABSTRACT	xvii
CHAPTER I SYNTHESIS & CHARACTERIZATION OF POLYMERIC & DENDRITIC MATERIALS	1
1.1 Macromolecules	1
1.2 Polymers	2
1.2.1 Polymer Topology and Composition	2
1.2.2 Classification of Polymerization Reactions	5
1.2.3 Step-Growth Polymerization	7
1.2.4 Chain-Growth Polymerization	9
1.2.5 Concept of “Click” Chemistry	13
1.2.6 Copper-Catalyzed Azide-Alkyne Cycloaddition “Click” Chemistry	15
1.2.7 “Click” Chemistry for the Construction of Polymers	18
1.3 Dendrimers	20
1.3.1 Symmetrical (Conventional) Dendrimers	21
1.3.2 Dendrimer Synthetic Methods	24
1.3.3 Asymmetrical (Janus) Dendrimers	26
1.3.4 Janus Dendrimer Synthetic Methods	28
1.3.5 Dendrimers Constructed by Copper-Catalyzed Azide-Alkyne “Click” Reaction	30
1.4 Self-Assembly	31
1.4.1 Self-Assembly of Amphiphilic Polymers	33

1.4.2 Self-Assembly of Amphiphilic Janus Dendrimers.....	36
1.5 Application of Self-Assembled Soft Nanomaterials in Nanomedicine	38

CHAPTER II DEGRADABLE SPIROCYCLIC POLYACETAL-BASED CORE AMPHIPHILIC ASSEMBLIES FOR ENCAPSULATION & RELEASE OF HYDROPHOBIC CARGO.....	42
2.1 Abstract	42
2.2 Introduction	43
2.3 Results & Discussion	46
2.3.1 Synthesis & Characterization of Spirocyclic Polyacetals	46
2.3.2 Self-Assembly of Spirocyclic Polyacetals (7) & (8)	51
2.3.3 Encapsulation & pH-Triggered Release of Nile Red from Particles	54
2.3.4 Cytocompatibility & Interactions of Nile Red-Loaded Particles with Cells	56
2.4 Materials & Methods.....	59
2.4.1 Synthesis of Compound (2).....	60
2.4.2 Synthesis of Compound (3).....	61
2.4.3 Synthesis of Compound (4)	61
2.4.4 Synthesis of Compound (5).....	62
2.4.5 Synthesis of Compound (6)	62
2.4.6 Synthesis of Polymer (7).....	63
2.4.7 Synthesis of Polymer (8).....	64
2.4.8 Procedure for Self-Assembly of (7) & (8)	65
2.4.9 Procedure for the Encapsulation of Nile Red by Particles Formed by Polymer (7)	65
2.4.10 Procedure for the Degradation Study of Polymers (7) & (8) by ¹ H-NMR	65
2.4.11 Procedure for Nile Red Release Study	66
2.4.12 Procedure for Cell Viability Assays	66
2.4.13 Procedure for Evaluation of Cellular Uptake	67
2.5 Conclusion	67

CHAPTER III SYNTHESIS & SELF-ASSEMBLY OF AMPHIPHILIC JANUS DENDRIMERS WITH AGGREGATION-INDUCED EMISSION PROPERTY TO POTENTIAL THERANOSTICS	69
3.1 Abstract	69
3.2 Introduction	70
3.3 Results & Discussion	74
3.3.1 Synthesis of Hydrophobic Aryl Ether-Based Dendrons	74
3.3.2 Synthesis of Azido-Propoxy Tetraphenylethylene	76
3.3.3 Synthesis of Hydrophilic Alkyne-Functionalized Oligoethylene Glycol Gallate	78
3.3.4 Synthesis of Amphiphilic Janus Dendrimers	79
3.3.5 Characterization of Amphiphilic Janus Dendrimers	83
3.3.6 AIE Absorption & Emission Properties	85
3.3.7 Self-Assembly of Amphiphilic Janus Dendrimers	88
3.4 Materials & Methods.....	93
3.4.1 Experimental Section	94
3.4.2 Synthesis of Reduced Benzoate (9).....	94
3.4.3 Synthesis of First-Generation Alkyne (10)	95
3.4.4 Synthesis of Brominated First-Generation Alkyne (11)	95
3.4.5 Synthesis of Second-Generation Alkyne (12).....	96
3.4.6 Synthesis of Brominated Second-Generation Alkyne (13).....	97
3.4.7 Synthesis of Third-Generation Alkyne (14).....	97
3.4.8 Synthesis of Methoxy-Functionalized TPE (15).....	98
3.4.9 Synthesis of Hydroxy-Functionalized TPE (16).....	99
3.4.10 Synthesis of Bromo-Propoxy TPE (17)	100
3.4.11 Synthesis of Azido-Propoxy TPE (18).....	100
3.4.12 Synthesis of Tosylated TEG (19).....	101
3.4.13 Synthesis of Oligoethylene Glycol Gallate (20)	101
3.4.14 Synthesis of Oligoethylene Glycol Gallic Acid (21)	102
3.4.15 Synthesis of Alkyne-Functionalized Oligoethylene Glycol Gallate (22)	102
3.4.16 Synthesis of First-Generation TPE-Conjugated Dendron (23)	103

3.4.17 Synthesis of Second-Generation TPE-Conjugated Dendron (24)	103
3.4.18 Synthesis of Third-Generation TPE-Conjugated Dendron (25)	104
3.4.19 Synthesis of First-Generation Azido-Functionalized TPE-Conjugated Dendron (26)	105
3.4.20 Synthesis of Second-Generation Azido-Functionalized TPE-Conjugated Dendron (27)	106
3.4.21 Synthesis of Third-Generation Azido-Functionalized TPE-Conjugated Dendron (28)	107
3.4.22 Synthesis of First-Generation Amphiphilic Janus Dendrimer (29)	108
3.4.23 Synthesis of Second-Generation Amphiphilic Janus Dendrimer (30)	109
3.4.24 Synthesis of Third-Generation Amphiphilic Janus Dendrimer (31)	110
3.4.25 Procedure for the Self-Assembly of Janus Dendrimers (29) , (30) & (31)	111
3.4.26 Procedure for the TEM Images of Janus Dendrimers (29) , (30) & (31)	111
3.5 Conclusion	111
CONCLUSION & FUTURE PERSPECTIVES	113
APPENDIX A	115
APPENDIX B	123
REFERENCES	146

LIST OF FIGURES

Figure	page
1.1 Schematic representation of linear, cyclic, branched & network polymers	3
1.2 Schematic representation of more complicated branched & combined polymers .	4
1.3 Schematic representation of various copolymers	5
1.4 Schematic representation of step-growth & chain-growth polymerization	6
1.5 Comparison of polycondensation and polyaddition	7
1.6 General mechanism of NMP polymerization	10
1.7 General mechanism of ATRP polymerization	11
1.8 General mechanism of RAFT polymerization	12
1.9 Schematic representation of “Click” reactions	14
1.10 Mechanism pathway for CuAAC	17
1.11 Representative structure of graft copolymer as both a construction & modification reaction	19
1.12 Representative structures of ATRP polymers prepared by CuAAC connection of polymeric building blocks	20
1.13 Representation of dendritic architecture	22
1.14 General structure of dendrimers & dendrons	23
1.15 Synthesis of dendrimers according to the divergent method	25
1.16 Synthesis of dendrimers according to the convergent method	26
1.17 Coin representing Janus, the two-faced God	27
1.18 Schematic representation of a Janus dendrimer	28
1.19 Synthetic approaches of Janus dendrimers	29
1.20 General structure of a surfactant molecule	32
1.21 Self-assembled structures formed by amphiphilic BCPs	34
1.22 Schematic representation of dendrimersomes	37
1.23 Schematic illustration of established nanotherapeutic platforms	39

2.1 ¹ H-NMR, SEC & DSC analysis of polymers (7) & (8)	49
2.2 A pH-triggered degradation reaction of (7) in acidic media	51
2.3 TEM & AFM images of P1 & P2	53
2.4 DLS data for the Nile red-encapsulated P1 in phosphate buffer at pH 7.4 & pH 5.5 after 84h	55
2.5 CHO-K1 cells treated for 24h with increasing concentration of P1 for study of cell viability & cellular uptake	58
3.1 ¹ H-NMR of the third generation amphiphilic Janus dendrimer (31)	82
3.2 SEC refractive index of TPE-conjugated dendrons & Janus dendrimers	83
3.3 UV-Vis absorption spectra for Janus dendrimers (29), (30), & (31)	86
3.4 Fluorescence emission profile for Janus dendrimers (29), (30), & (31)	88
3.5 Amphiphilic Janus dendrimers under kinetic control	91
3.6 Amphiphilic Janus dendrimers under thermodynamic control	92

LIST OF TABLES

Table	page
3.1 Summary of SEC analysis for each dendron/dendrimer	84
3.2 Summary of DSC analysis for each dendron/dendrimer	85
3.3 Summary of DLS data for the self-assembly of amphiphilic Janus dendrimers under two conditions, before and after removal of DMSO	89

LIST OF SCHEMES

Scheme	page
1 Illustration of Nile red-loaded core amphiphilic assembly formation & pH-triggered disassembly & cargo release	46
2 The synthesis of monomers & the spirocyclic polyacetals	47
3 Synthetic approach to three generations of hydrophobic aryl ether dendrons	76
4 Synthetic approach to azido-functionalized tetraphenylethylene derivative (18)....	77
5 Synthetic approach to hydrophilic alkyne-functionalized oligo(ethylene glycol)-decorated gallate (22).....	79
6 Synthesis of TPE-functionalized dendrons & amphiphilic Janus dendrimers	80

LIST OF ABBREVIATIONS

AFM	Atomic Force Microscopy
AIE	Aggregation-Induced Emission
AJD	Amphiphilic Janus Dendrimer
ATRP	Atom Transfer Radical Polymerization
BCP	Block Copolymer
CDCl ₃	Deuterated Chloroform
CHCl ₃	Chloroform
CH ₂ Cl ₂	Dichloromethane
CuAAC	Copper-Catalyzed Azide-Alkyne Cycloaddition
DLS	Dynamic Light Scattering
DMF	N,N-Dimethyl Formamide
DMSO	Dimethyl Sulfoxide

DMSO-d ₆	Deuterated Dimethyl Sulfoxide
DNA	Deoxyribonucleic Acid
DSC	Differential Scanning Calorimetry
EtOAc	Ethyl Acetate
HR-MS	High Resolution Mass Spectrometry
IR	Infra-red
LCM	Large Compound Micelles
M _n	Number Average Molecular Weight
M _w	Average Molecular Weight
NMP	Nitroxide Mediated Polymerization
NMR	Nuclear Magnetic Resonance
PEG	Poly(ethylene glycol)
RAFT	Reversible Addition Fragmentation Chain Transfer
RNA	Ribonucleic Acid

SEC	Size Exclusion Chromatography
TEG	Triethylene glycol
TEM	Transmission Electronic Microscopy
T_g	Glass Transition Temperature
THF	Tetrahydrofuran
TPE	Tetraphenylethylene

RÉSUMÉ

Les macromolécules constituent des molécules de hauts poids moléculaires, fournissant une structure avec répétition de plusieurs unités dérivées de monomères de bas poids moléculaire. Ils peuvent être subdivisés en deux catégories générales : les polymères et les dendrimères. Les macromolécules amphiphiles ont attiré une large attention en tant que blocs de construction pour la fabrication de nano- et micro-matériaux avec des morphologies variées avec des applications dans différents domaines de la science et de la technologie. Dans ce mémoire, nous synthétisons de nouvelles classes de polymères linéaires amphiphiles dégradables, ainsi que des dendrimères Janus amphiphiles (AJDs) bien définis avec une propriété d'émission induite par l'agrégation. Nous étudions le comportement d'auto-assemblage de ces deux classes de macromolécules pour développer des nanomatériaux avec des applications potentielles en nanomédecine. Dans la première partie, nous développons des polymères linéaires amphiphiles dégradables, composés d'acétals spirocycliques, définis comme des matériaux dégradables de manière pH-dépendante qui confèrent une rigidité conformationnelle au squelette polymère qui limitent sa flexibilité et améliorent sa stabilité thermique. Attachés à des poly (éthylène glycol), ces polymères linéaires amphiphiles sont synthétisés par polymérisation « clic » azoture-alcyne catalysée au cuivre. Ces polymères s'auto-assemblent pour former des assemblages micellaires capable d'encapsuler le rouge du Nil en tant que médicament modèle hydrophobe. Des expériences *in vitro* montrent que le pH acide accélère la libération efficace des cargaisons et conduit à la dégradation complète des assemblages. De plus, les analyses cellulaires révèlent que ces matériaux sont entièrement cytocompatibles, interagissent avec la membrane plasmique et peuvent être internalisés par les cellules. Dans la deuxième partie, nous développons des AJDs, composés de dendrons à base d'éther benzylque, conjugués à du tetraphényléthylène (TPE) pour étudier leur

comportement d'émission induite par l'agrégation (AIE). Ces AJDs ont également été synthétisés par réaction de « clic » azoture-alcyne catalysée au cuivre. Ces dendrimères s'auto-assemblent pour former des assemblages vésiculaires fluorescents, qui ont des applications thérapeutiques potentielles.

Mots-clés : macromolécule, polymère, dendrimère, auto-assemblage, thérapeutique.

ABSTRACT

Macromolecules constitute of high molecular weight molecules, providing a structure with repetition of several units derived from low molecular weight monomers. They can be subdivided into two general categories: polymers and dendrimers. Amphiphilic macromolecules have attracted widespread attention as building blocks for the fabrication of nano- and micromaterials with varying morphologies with applications in different areas of science and technology. In this memoire, we synthesize new classes of degradable amphiphilic linear polymers as well as amphiphilic Janus dendrimers (AJDs) with aggregation-induced emission property. We study the self-assembly behaviour of these two classes of macromolecules to develop nanomaterials with potential applications in nanomedicine. In the first part, we develop degradable amphiphilic linear polymers, composed of spirocyclic acetals, defined as pH-degradable materials that provide conformational rigidity to the polymer backbone that restrict its flexibility and enhance its thermal stability. Attached with poly (ethylene glycol) units, these amphiphilic linear polymers are synthesized by copper-catalyzed azide-alkyne “click” polymerization, which self-assemble to form micellar assemblies, capable of encapsulating Nile red as a hydrophobic model drug. In vitro experiments show that acidic pH accelerates efficient cargo release and leads to the complete degradation of the assemblies. Moreover, cellular assays reveal that these materials are fully cytocompatible, interact with the plasma membrane, and can be internalized by cells. In the second part, we develop AJDs, composed of aryl ether-based dendrons, conjugated with tetraphenylethylene (TPE) to investigate their aggregation-induced emission (AIE) behaviour. These AJDs were also synthesized by copper-catalyzed azide-alkyne “click” reaction. These dendrimers self-assemble to form fluorescent vesicular assemblies, which have potential theranostic applications.

Keywords: macromolecules, polymers, dendrimers, self-assembly, theranostic.

CHAPTER I

SYNTHESIS AND CHARACTERIZATION OF POLYMERIC AND DENDRITIC MATERIALS

1.1 Macromolecules:

What are macromolecules? They constitute high molecular weight molecules, providing a structure with several repeat units derived from low molecular weight monomers.[27] The repeat unit concept refers to the structure of the macromolecular chain. The monomeric unit is based on the polymerization process; it refers to the largest constitutional unit contributed by a single monomer during a polymerization process. Consequently, the constitutional repeat unit may, according to the structure or method of synthesis, be the same size, smaller or larger than the monomer unit.[27, 46] Macromolecules can be of natural origin, such as nucleic acids, proteins, lipids, and carbohydrates, which are the four major classes of organic macromolecules that are essential to life, or they can be synthetically produced, such as poly(ethylene), nylon, and silicones, which are held together by covalent, ionic, and coordinate bonds. Macromolecular chains possess flexibility, which lead to spatial geometries; among these are (i) chain-folding, in which a long macromolecule folds back on itself to form a mini-crystal, (ii) interchain supercoiling in which two or more macromolecules wrap around one another to generate a braided-rope structure, and (iii) extended aggregation in which macromolecular chains are cross-linked to form two-dimensional networks which act as unique molecular entities.[27, 46] Overall, macromolecules can be subdivided into two categories: polymers and dendrimers.

1.2 Polymers:

Polymers are composed of long sequences of one or more species of atoms or groups of atoms linked together by covalent bonds. They have existed in natural form since life began, such as in deoxyribonucleic acid (DNA), ribonucleic acid (RNA), proteins, and polysaccharides.[135] Polymers can carry reactive functional groups that can participate in chemical processes without degradation of the original polymer chains. Although polymers are abundant in nature, synthetic functional polymers are obtained by covalent polymerization of simple monomers.[33] Depending on the process used, the reactive groups of functional polymers may be incorporated into the main chain, as pendant groups, or even as the chain ends.[19, 33, 135] Examples of functional polymers with reactive groups in the main chain or in the side chain are poly-(isoprene) (natural rubber) and poly(acrylamide), polymers that have carbon-carbon double bonds or primary amide functional groups at regular intervals throughout their main chain or pendant to the main chain, respectively.[19, 33, 135]

1.2.1 Polymer Topology and Composition:

The properties of polymers are directly connected to their size and shape. The shape of polymers is also directly connected to the size of the various primary and secondary bonding forces that are present within and between the chains.[19] The most commonly known topologies are linear, cyclic, branched and network polymers (**Figure 1.1**).

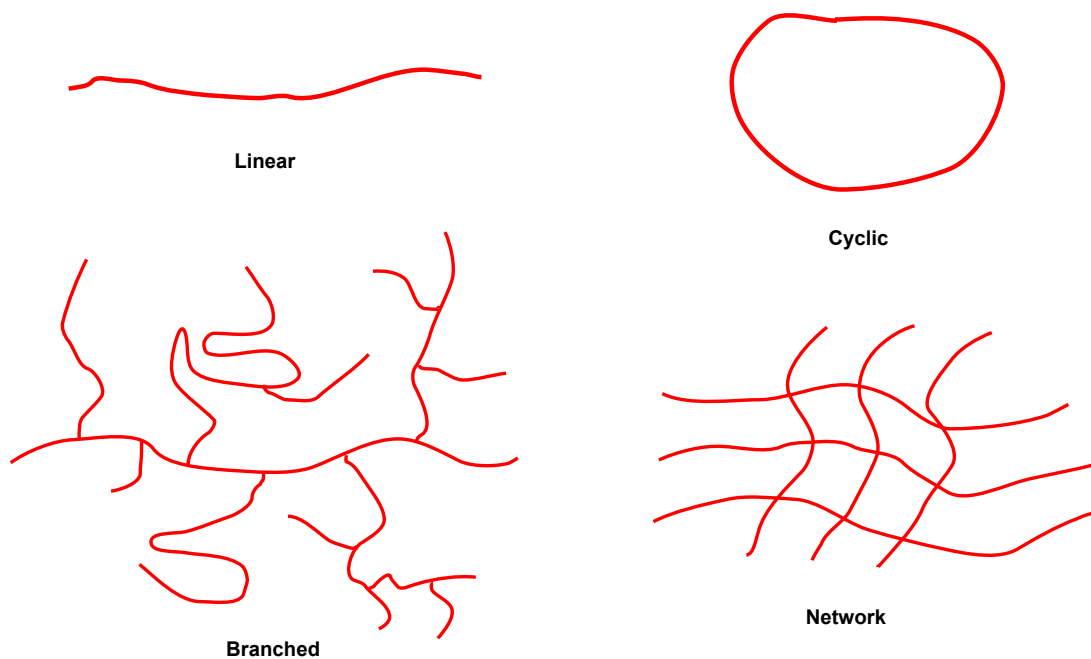


Figure 1.1. Schematic representation of linear, cyclic, branched and network polymers.

Cyclic polymers have no chain ends and show properties that are different than their linear counterparts.[135] Branched polymers have side chains bonded to the main chain and are characterized based on the number and size of the branches. Network polymers have three-dimensional structures where each chain is connected to all the others by various junction points, which are characterized by their cross-linking.[135] In addition, both branched and network polymers can be formed either through polymerization or linking together pre-existing chains.[135] From these basic topologies, subsections of more complexed topologies can occur. One such example are branched polymers, where the complexity can lead to star polymers, “H” shaped polymers, and “pom-pom” shaped polymers. There can also be combined polymer topology, such as cyclic branched polymers, ring polymers, rotaxanes, catenanes and knot polymers (Figure 1.2).[124]

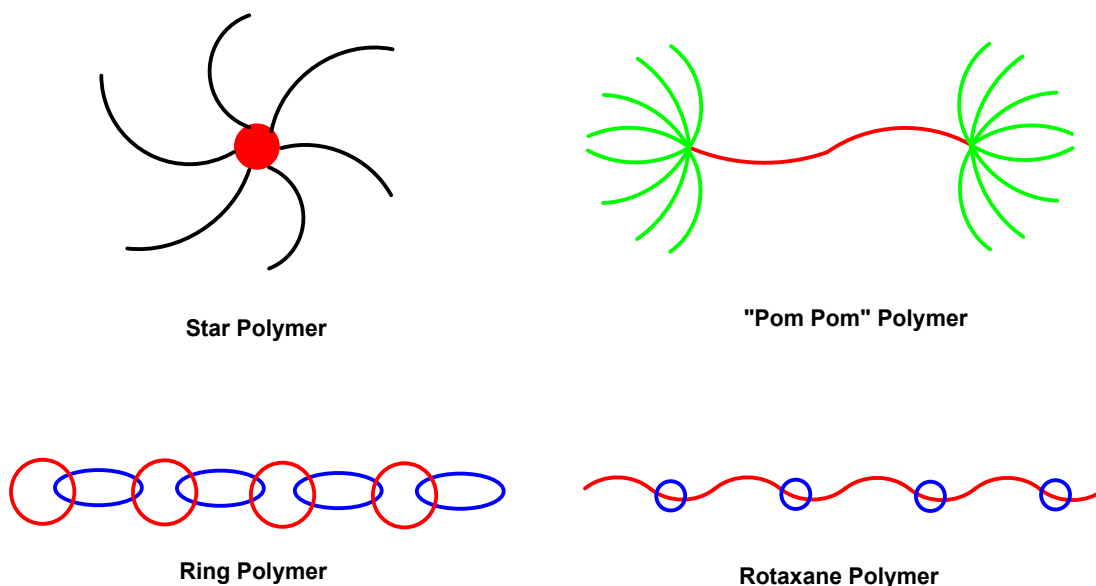


Figure 1.2. Schematic representation of more complexed branched and combined polymers.

The naming of polymers, based on the visualization of its chemical structure, is often an area of difficulty. Most polymers have more than one correct name, leading to a variety of complicated trade names which are also used to describe certain polymers.[124] The best approach adopted is to use names which most clearly and simply indicate the chemical structures of the polymers.[124]

The term homopolymer is often used to describe polymers that are derived from one type of monomer.[135] However, polymers can be synthesized from two or more monomers. These are specifically known as copolymers, leading to more complex topologies.[135] Copolymerization provides controlled parameters over its chemical composition and diversity for the assembly of two monomers (**Figure 1.3**).[136] Applying two to three simplistic monomers, in which an abrupt change in composition at the connection point from one monomer to the next, is defined as block copolymers.[8] Alternating copolymers have only two different types of repeat units, which are arranged alternatively along the polymer chain. Statistical (or random)

copolymers have a random distribution of the monomers along the polymer backbone.[135] Gradient copolymers are macromolecules that contain at least one section of continuously changing monomer compositions. This unusual composition is reflected in their structure and properties, which are different from those of their nearest relatives, which are statistical and block copolymers. [8, 136] Therefore, there are considerable opportunities for creating fundamentally new macromolecular structures and hence materials with new end properties.[136]

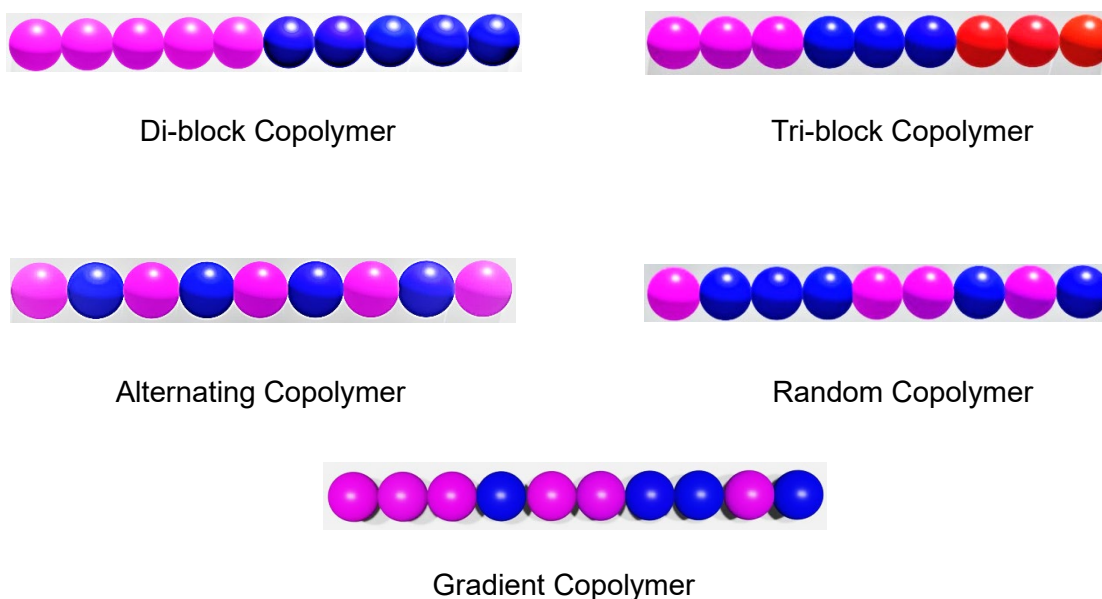


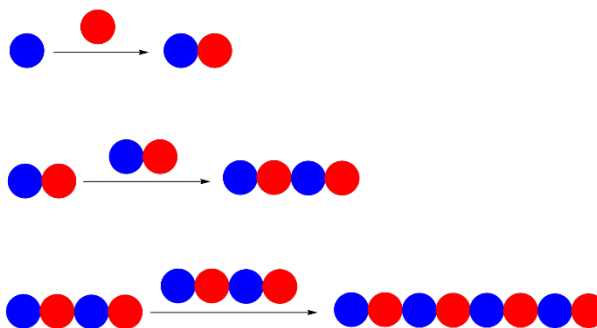
Figure 1.3. Schematic representation of various copolymers.

1.2.2 Classification of Polymerization Reactions:

Polymerization reactions can be classified into two general categories: (i) step-growth polymerization and (ii) chain-growth polymerization. Step-growth polymerization was the first polymerization to be understood from a fundamental perspective.[26, 50] It involves the reaction between pairs of mutually reactive functional groups of the

monomers, where the monomer's concentration is consumed very rapidly early in the reaction, allowing the molecular weight of the polymers formed to increase with reaction time. The final reaction mixture is composed of little monomer content, but large content of oligomers/polymers with various numbers of repeat units.[26, 50] The chain-growth polymerization involves the concentration of the monomers being consumed very slowly in which high molecular weight polymer is formed early in the polymerization process and the polymer yield gradually increases with time (**Figure 1.4**).[102]

Step-Growth Polymerization:



Chain-Growth Polymerization:

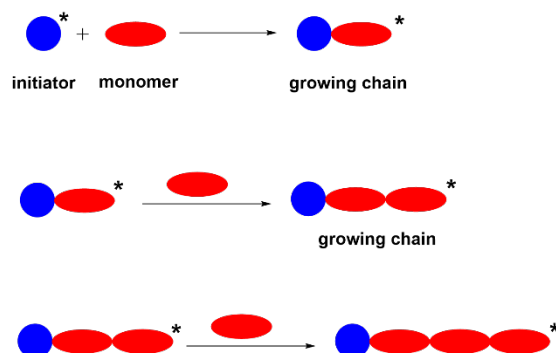
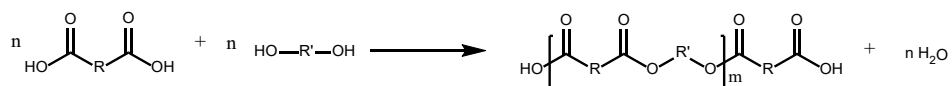


Figure 1.4. Schematic representation of step-growth and chain-growth polymerization.

1.2.3 Step-Growth Polymerization:

Step-growth polymerization can be broken down even further to polycondensation and polyaddition.[26, 50] Polycondensation involves monomers reacting together with the elimination of by-products. Polyaddition, on the other hand, involves monomers reacting together without the elimination of by-products, as everything has been atom economized (Figure 1.5).[26, 50]

Polycondensation:



Polyaddition:

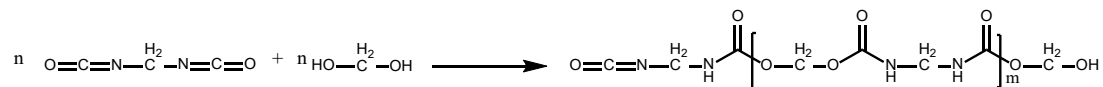


Figure 1.5. Comparison of polycondensation and polyaddition.

Polycondensation, due to its common use, has been extensively investigated, favored by the variety of possible monomers and the respective range of reaction schemes.[26, 50] Typical classes of polycondensates are polyesters, polyamides, polyurethanes, polyureas, poly-sulfides and polyethers, with a number of these polymers being bio-based and/or biodegradable. During a polycondensation process, the main reaction involves the interaction of two functional groups of different or same type of molecules, resulting in the formation of a new intermolecular bond.[26, 50] The reacting molecules can be a combination of monomers, oligomers, or short-chain polymers, resulting in higher molecular weight molecules. In the perspective of its kinetics, polycondensation reactions are equilibrium systems; the reverse reaction is the depolymerization of a polymer molecule, the rate of which is mainly determined by the equilibrium constant.[26, 50] In order to achieve equilibrium, it is necessary to slowly remove

enough of the by-product from the reaction zone, while a reversible polycondensation will proceed under non-equilibrium, when the rate of the by-product removal is high enough and comparable with that of its formation.[26, 50] The difficulty in complete removal of by-products from highly viscous reaction mixture leads to polymers with low molecular weight (<50,000 g/mol).[26, 50] The most commonly used polymers synthesized by polycondensation are the polyesters and polyamides (nylons). Their use as textile and technical fibers, along with their role as engineering plastics, has led to extensive applications in packaging material as a result of their transparency, chemical resistivity, gas and vapor non-permeability.[31]

In contrast to polycondensation, polymerizations of the polyaddition type are the formation of polyurethanes and polyurea.[9] Polyaddition is limited in scope due lack of functionalities on the backbone for further modification. The introduction of functional side groups by step-growth polymerization is, in general, not straightforward since reaction conditions can be drastic (high temperatures, vacuum); it requires additional protecting and deprotecting steps, which may be an important restriction for industrial manufacturing.[9] The chemical modification of functional polymers can suffer from a lack of efficiency because the reactivity of functional groups may be affected by the structure of the polymer and by the efficiency of the modification reactions used.[9] In addition, in order to achieve high molecular weight polymers through step-growth polymerization, certain criteria must be met: (i) high reaction conversion, (ii) absence of side reactions and (ii) efficient removal of by-products formed.[9] As a result, the focus on the research of functionalization of polymers has been moving during the last decade toward the use of highly efficient combination approaches, often referred to as ‘click’ chemistry, which will be described in detail in the sections following chain-growth polymerization.[9]

1.2.4 Chain-Growth Polymerization:

Chain-growth polymerization is broken down into two main categories: (i) ionic and (ii) radical polymerization.[43, 123, 134] Ionic polymerization involves the growth of a polymer, accompanied by a counter-ion (cationic or anionic), where the monomeric substituents must be capable of stabilizing the ionic center generated.[43, 134] The difference between the cationic and anionic polymerization is the absence of any termination group for the anionic reactions, indicating no self-quenching present. This is known as a living polymerization, where the active centers are persistent, in that there is no termination process or chain transfer reactions.[43, 134] The growth of these polymers stays active until one deliberately quenches the reaction after a certain period of time.[43, 134] In contrast to ionic polymerization, radical polymerization involves the formation of reactive intermediates by the action of an initiator on an alkene. This type of polymerization represents approximately 50% of all polymers formed in the industry.[20] The drawback of using radicals is that the intermediates formed are very reactive (lifetime is less than one second).[20] This makes it nearly impossible to control the molecular weight and structure of the polymers. So how do we control the reactivity of the radicals? Simple, we increase the intermediates lifetime; if we can insert 1 minute of dormancy after each 1 millisecond of activity, the duration of the radical's lifetime can be extended by approximately one second to more than a day.[20] There are three main radical methods that can apply proper control to its polymerization: (i) nitroxide mediated polymerization (NMP), (ii) atom transfer radical polymerization (ATRP) and (iii) reversible addition fragmentation chain transfer (RAFT).[42, 44, 60, 81, 95, 104]

NMP is based on the mechanism of reversible termination between the (macro) growing propagating radical and nitroxide, acting as a control to make (macro) alkoxyamine as a predominant species (**Figure 1.6**). This dormant species re-generates

the propagating radical and nitroxide by homolytic cleavage when the temperature rises.[42, 44]

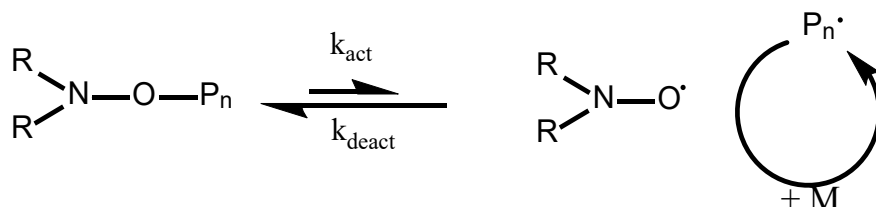


Figure 1.6. General mechanism for NMP polymerization. Note: k_{act} = rate constant of activation, k_{deact} = reversible deactivation rate constant, M = monomer, and $\text{P}_n \cdot$ = propagating radical polymer with “n” repeat units.

More versatile and simpler approaches involve ATRP and RAFT polymerization. ATRP is a radical pseudo-living polymerization, catalyzed by a transition metal, which is also called an activator. The initiation occurs through a transfer of single electrons from the metal to the halogen in the covalent bond, which leads to the homolysis to give the radical, oxidizing the metal complex by a (+1), causing an attachment of the free halide (Figure 1.7).[81, 95, 104]

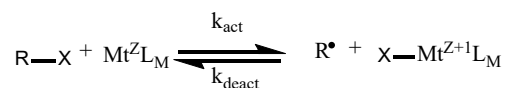
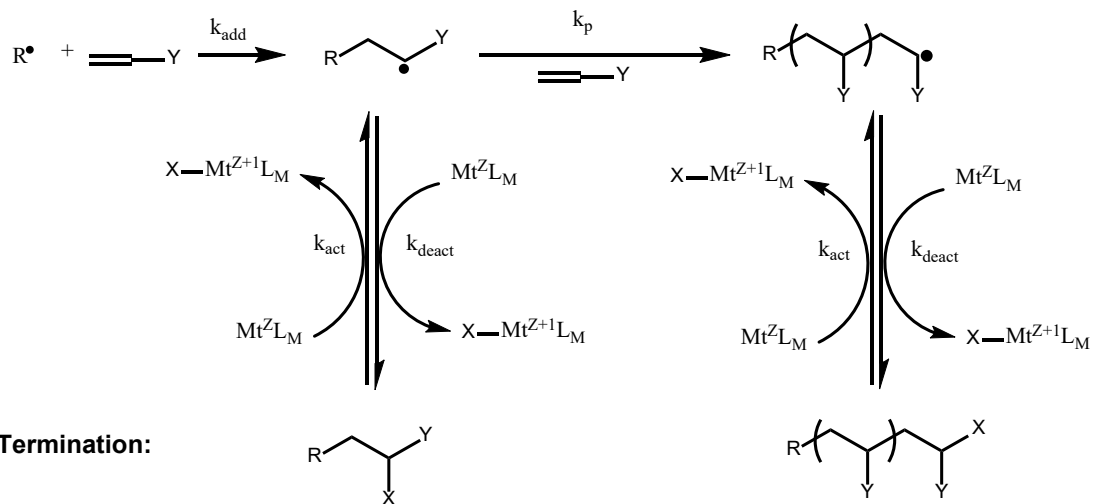
Initiation:**Propagation:****Termination:**

Figure 1.7. General mechanism for ATRP polymerization. Note: R^{\bullet} = radical species, Mt = metal species, L_{M} = ligand, k_{act} = rate constant of activation, k_{deact} = reversible deactivation rate constant, k_{add} = addition rate constant, and k_{p} = propagating chain rate constant.

What has been a more convenient approach to ATRP is RAFT (**Figure 1.8**). In NMP and ATRP, the equilibrium is established by a reversible termination mechanism of the propagating chain, in which the balance strongly favors the dormant species. RAFT proceeds through a degenerative chain transfer process, where the reproduced species are balanced with the dormant species.**[60]**

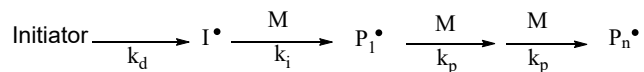
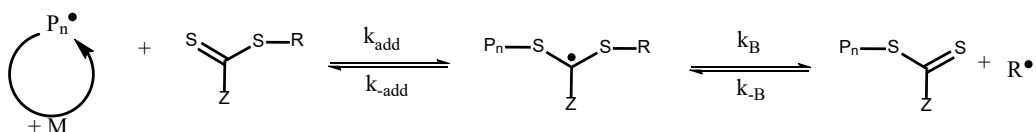
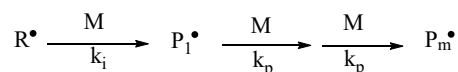
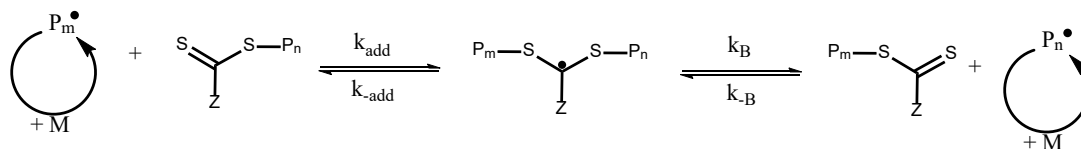
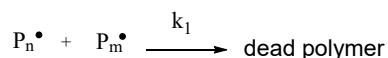
Initiation:**Initialization/Pre-equilibrium:****Reinitiation:****Main equilibrium:****Termination:**

Figure 1.8. General mechanism for RAFT polymerization. Note: I^\bullet = initiator, M = monomer, P_n^\bullet = propagating radical polymer with “n” repeat units, and P_m^\bullet = new propagating radical polymer with “m” repeat units.

The Z and R groups of the RAFT agent play an important role on its performance and activity. The Z groups adjust the reactivity of the C=S bond, which influences the addition rate and the radical fragmentation.[60] The R groups must form the stable free radical. Initially, the RAFT mechanism begins through the formation of an initiator

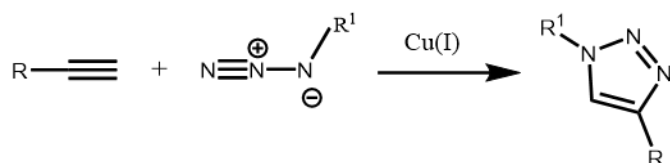
derived radical (I^\bullet) that propagates with monomer (M) to give a polymeric radical (P_n^\bullet).^[60] The polymeric radical then reacts with a thiocarbonylthio chain transfer (or RAFT agent) with the RAFT process effectively swapping the thiocarbonylthio functionality ($ZC(=S)S-$) between growing polymer chains. The control over molar mass and dispersity arises from the rapid equilibration of chains with respect to the polymerization rate ($k_{add} \gg k_p$ and $k_b \gg k_p$).^[60] Upon completion of a RAFT polymerization, the vast majority of chains will possess a thiocarbonylthio end-group, with the overall process of an insertion of monomer units between the S–R bond of the RAFT agent to give a polymer. The conserved RAFT end-group of the polymer is itself a macro-RAFT agent, which facilitates the synthesis of block copolymers through the polymerization of a second monomer.^[60] The RAFT process does not prevent the formation of dead chains but reduces that possibility through the formation of many more, shorter chains.^[60] Due to inherent low concentration of end groups and the possibility of side reactions with other functional groups within the polymer, reactions with high efficiency are a necessity for specific polymer modifications.^[40] With the use of a copper (Cu)(I) catalyst, azide-alkyne coupling reactions result in highly specific and efficient preparation of 1,4-disubstituted 1,2,3-triazole products under moderate reaction conditions.^[40] This particular coupling process can be conducted in aqueous or organic media, and little or no side reactions are observed. The practicality and versatility of the Cu(I)-catalyzed coupling reaction led to its involvement in the classification of efficient and specific organic reactions, commonly termed “click chemistry.”^[40]

1.2.5 Concept of “Click” Chemistry

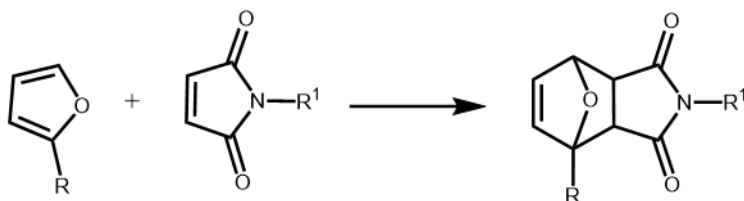
The concept of “click” chemistry for polymers involves a number of polyvalent reactions, which are (i) highly stereo/regioselective, (ii) produce easily separable

products, (iii) generally have excellent yields, (iv) use readily available starting materials and reagents, (v) are tolerant to a wide range of functional groups, and (vi) can be carried out using a wide set of reaction conditions, such as water, air and two-phase systems.[63] The three most commonly used “click” reactions are (i) copper catalyzed azide-alkyne cycloaddition (CuAAC), (ii) Diels-Alder reaction and (iii) thiol-ene “click” reaction (**Figure 1.9**).[63]

Copper-catalyzed azide-alkyne cycloaddition:



Diels-Alder reaction:



Thiol-ene “click” reaction:

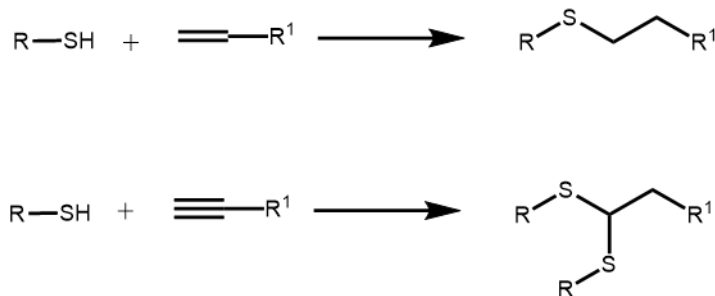


Figure 1.9. Schematic representation of three “Click” reactions.

The Diels–Alder reaction (also known as the [4+2] cycloaddition) involves the reaction between a diene and dienophile, typically bearing an alkenyl moiety.[35] This “click” chemistry is particularly interesting as a result of its thermal reversibility at different

temperature ranges, depending on the actual diene/dienophile combination. The Diels-Alder reaction provides features in its role towards (i) solvents, (ii) Lewis/Bronsted acids or bases as catalysts, (iii) water as a medium, including aqueous emulsions, and (iv) mechanical energy to replace the thermal activation to promote the retro-Diels-Alder reaction of adducts incorporated into polymer chains. The term “click” attributed to reactions involving polymerizations, polymer couplings and other synthetic macromolecular processes does not comply to every situation. Despite being defined as “click”, some Diels-Alder reactions should be viewed instead as modular design reactions or macromolecular conjugations.[35]

The thiol-ene “click” reaction is the hydrothiolation of a carbon-carbon double bond. In the polymer/materials field, this particular reaction has been most widely employed for preparing networks and films.[78] The “thiol-ene” does not indicate a particular mechanistic pathway, making it also applicable to base/nucleophile-mediated thiol additions with activated substrates. However, the thiol-ene reaction has recently attracted researchers as its recognition of its “click” characteristics.[78] Such hydrothiolation reactions can proceed under a variety of conditions such as a radical pathway through catalytic processes mediated by nucleophiles, acids, and bases, in the absence of an added catalyst. This has been conducted under radical conditions, often photochemically induced, where it proceeds through a typical chain process, much like ATRP/RAFT polymerization.[78]

1.2.6 Copper-Catalyzed Azide-Alkyne Cycloaddition “Click” Chemistry

The basic process of the CuAAC generates 1,4-disubstituted 1,2,3-triazoles; nearly all functional groups are compatible with this process, except those that are either self reactive or able to yield stable complexes with the copper metal under catalyst

deactivation.[12, 25] The CuAAC is commonly performed by mixing a source of Cu (II) (mainly copper (II) sulfate) and a reducing agent (such as sodium ascorbate), to generate Cu (I) complex *in situ*. The most commonly used solvent systems are biphasic (mixtures of water/alcohol to water/toluene), which lead to excellent results.[12, 25] However, depending on the proportion of hydrophobicity of the polymers formed, it may cause a distorted coordination environment in the biphasic system, or can be oxygen sensitive, leading to inefficient “click” chemistry.[12, 25] Therefore, a new and highly innovative approach towards a polymeric bound copper (I) catalyst is by attaching a bipyridyl ligand to subsequently ligate a Cu(I) species to the polymer. These Cu(I) species provide high solubility in anhydrous organic solvents.[12, 25]

The mechanism proposed (**Figure 1.10**) for both Cu (I) and Cu(II) species are very similar, which involves the following main features: (a) up to a 1×10^5 rate acceleration and an absolute 1,4-regioselectivity of the copper catalyzed process, (b) kinetic features of the reaction that indicates at least second-order kinetics with respect to the concentration of the copper species, proposing at least two copper centers involved in this reaction, (c) significant auto-acceleration if multiple triazoles are formed, revealing intermolecular ligand effects, (d) significant rate reduction with strongly increasing amount of copper, and (e) the formation of a copper-alkylide, whose primary structure and activity within the transition state cannot be exactly predicted.[12]

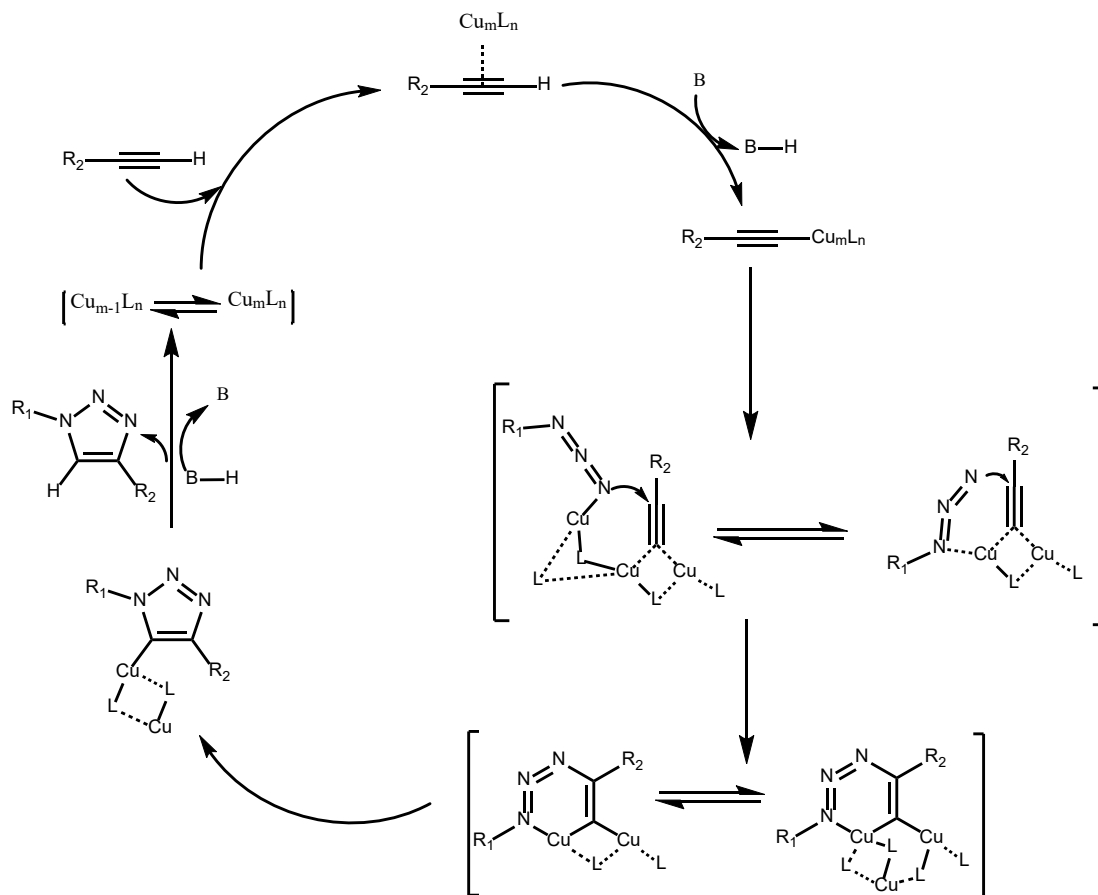


Figure 1.10. Mechanism pathway for CuAAC.

A terminal alkyne is a carbon acid; the triple bond can be a π -donor to an electrophilic center or a π -acceptor from an electron-rich metal center. This is how copper, in either the (+1) or (+2) oxidation state is initially attached.[142] The alkylated nitrogen (N- R_1) of an azido group is Lewis basic and nucleophilic, whereas the terminal nitrogen is electrophilic. Therefore, Lewis acids, proton, or electrophiles tend to interact with the alkylated nitrogen, whereas a nucleophile or a back-bonding metal prefers the terminal nitrogen.[142] Copper (I) and (II)/organic azide complexes that were characterized in the solid state featured organic azides carrying ancillary ligands. In its resonance stabilization, both copper complexes were found to interact with the alkylated

nitrogen.[142] This forms an unusual six membered copper metallocycle, in which the second copper atom acts as a stabilizing donor ligand. Ring contraction to a triazolyl-copper derivative is followed by protonolysis that delivers the triazole product and closes the catalytic cycle.[142] If the two reaction partners (azide and alkyne) are brought into close spatial relationship, the reaction can be fast and efficient.[12]

1.2.7 “Click” Chemistry for the Construction of Polymers

There are two fundamentally different ways to use any reaction in materials synthesis: to construct materials or to modify them.[59] Construction materials pertains to building an architecture and the reactions employed provide the driving force with which the macroscopic building blocks are connected. Furthermore, the more easily the required functional groups can be introduced into potential building blocks, the more structurally and chemically diverse the materials that can be synthesized.[59] This is essential in materials synthesis as high yields and chemo-selectivity are a necessity, where the concept of modularity is crucial. Since azide and alkyne functional groups are readily attached to molecular scaffolds and are stable toward a wide variety of solvents and reaction conditions, CuAAC allows the use of almost any necessary building block without worrying about the connection reaction.[59] Modification of materials pertains to the attachment or removal of functionality to or from an already existing material, ensuring that it is chemo-selective for functionalization at the desired site and high yield.[59] Applications involving CuAAC reactions to materials synthesis involves the modification of polymers, surfaces, dendrimers, nanoparticles, viruses, networks, and other diverse macromolecular structures.[59] In some cases, a reaction can be seen as both a modification and a construction reaction. For example, the attachment of alkyne end-functionalized polymers to azide side-chain derivatized polymers to yield graft copolymers can be considered both the modification of the azide-derivatized polymer and the construction of a graft copolymer (**Figure 1.11**).[59]

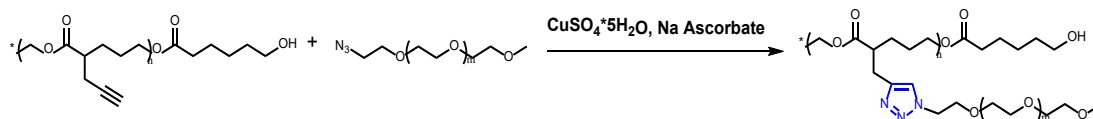


Figure 1.11. Representative structure of graft copolymer as both a construction and modification reaction. Triazole ring shown in blue.

Such cases are mainly considered modification reactions and only limited examples are given.[59] A triazole-containing material is defined from CuAAC “construction” if at least one triazole within the structure can be traced in every direction along the structure to another triazole.[59] Since many known polymerization reactions in macromolecular chemistry require the absence of specific functional groups, there is considerable interest in the fixation of ligands onto polymers after a successful polymerization reaction has been conducted.[11] One particular example are living polymerization reactions, where the highly sophisticated chemical mechanism and equilibria of (quasi-)living polymerization reactions are often highly substrate specific and, therefore, strongly affected by even small amounts of functional groups. The binding of large numbers of ligands onto polymers (i.e., side chain-modified polymers) or dendrimers is a concern as it requires highly efficient coupling reactions.[11] In addition, due to the limited solubility of many polymers, reactants for post-functionalization reactions cannot always be applied in homogeneous solution with the derivatized polymer. In these cases, highly efficient reactions acting in heterogeneous reaction media are desired.[11] Since azide and alkyne functional groups have a narrow spectrum of reactivity, they can be incorporated into polymerization initiators to make end-functionalized macromonomers, such as ATRP-derived polymers, macrocyclic polymers, and pendant functional polymers (Figure 1.12).[59] ATRP has been used extensively in conjunction with the azide/alkyne “click” reaction, and also represent the first, intensely exploited examples of a combination between a (quasi-)living polymerization reaction and the azide/alkyne click chemistry.[11]

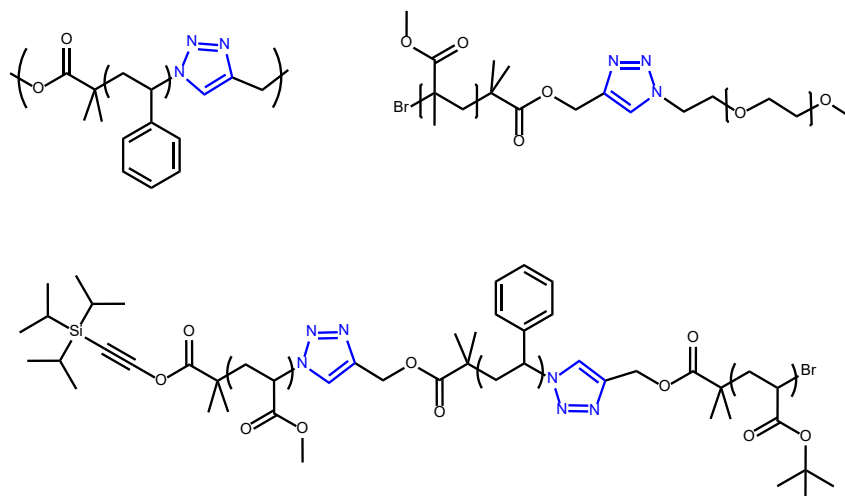


Figure 1.12. Representative structures of ATRP polymers prepared by CuAAC connection of polymeric building blocks. Triazole rings shown in blue.

The click reaction has been used in a variety of other polymerization reactions not related to living or (quasi)living polymerizations.[11] As described previously on the modification of materials, sidechain modifications of polymers have been reported using azido- or acetylene-functionalized polymers or oligomers, as well as biomolecules such as proteins and nucleic acids.[11] As a result of the high yields promoted by “click” chemistry, the application on multiple reaction sites can be easily derived. Thus dendritic systems are an important field of investigation, since the “click” reaction is not only a very high yielding, but also allows reactions in sterically hindered environments.[11]

1.3 Dendrimers:

The progression and advances in structural diversity of macromolecular architecture are important steps towards future high-performance materials.[84] Macromolecules with well-defined structures are in great demand; (i) sequence-controlled insertion of

the monomers within the main chain, (ii) introduction of functional groups in a controlled manner and (iii) that react to external stimuli with great efficiency.[84] While macromolecules consist of high molecular weight molecules, derived from low molecular weight monomers, it does not imply that only polymers fit this category. The highly branched and symmetrical molecules known as dendrimers are the most recently recognized members of the macromolecular family. Dendrimers are globular, monodisperse macromolecules that emerge radically from a central core with regular branching patterns and repeat units that contribute branch points.[34, 70] Dendrimers distinguish themselves from conventional polymers in two critical ways. First, they are constructed from AB_n monomers (n usually 2 or 3), which contain hyperbranched structures, rather than the standard AB monomers which produce linear polymers. Secondly, they are synthesized in a repetitive fashion; the combination of these two features leads to a nonlinear, stepwise synthetic growth, wherein the number of monomer units incorporated after each repetition roughly doubles (AB_2) or triples (AB_3) that in the previous cycle.[137]

1.3.1 Symmetrical (Conventional) Dendrimers:

The word dendrimer comes from the Greek word “dendra”, which signifies “tree” (**Figure 1.13**). Dendrimers are macromolecules made up of a multitude of branches which come from a central point (termed the core). The three distinct regions that represents a dendrimer are: (i) its central core, (ii) its branches and (iii) its terminal (peripheral) groups.[128]

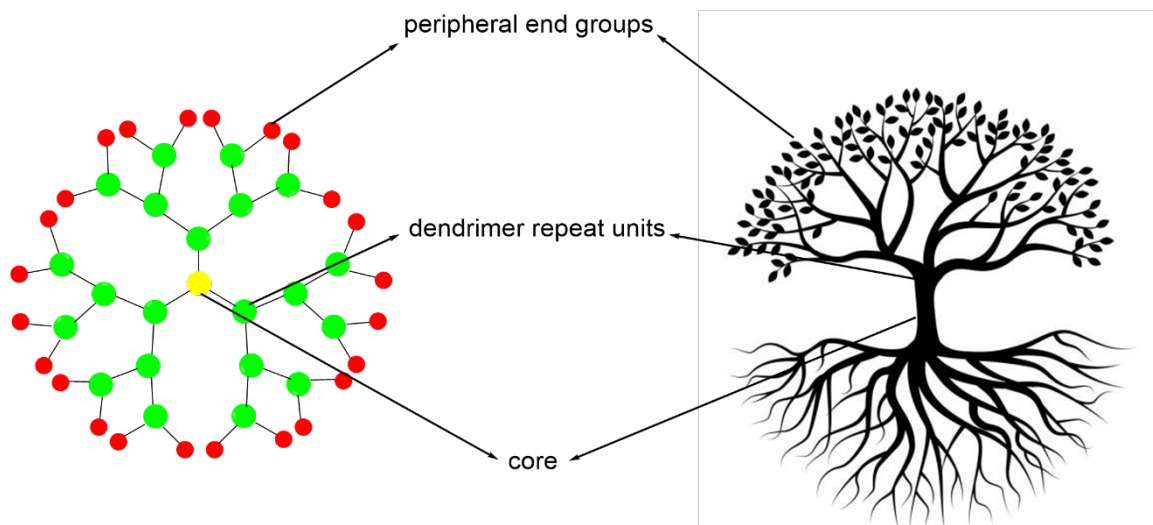


Figure 1.13. Representation of dendritic architecture.

Dendrimers have distinctive properties: (i) can trap small molecules within their central region, (ii) have low intrinsic viscosities in solution, and (iii) presence of large number of terminal groups, influencing its potential applications.[18, 128] The preparation method and properties of dendrimers are radically different from those of conventional polymers. Unlike polymers, the synthesis of dendrimers takes place under well-controlled conditions, which lead to monodisperse compounds with exact molecular weight and branched structure, regulated in the form of a tree.[18] Its synthesis is most often based on multiple sequences of two simple chemical reactions, involving two or three different functional groups. Each subsequent reaction sequence gives a dendrimer of a higher generation and a doubled number of end groups, leading to a two-fold increase in molecular weight (**Figure 1.14**). Dendrimers are comprised of dendrons, which differ as they contain a focal point, known as the point of attachment to a central core.[18]

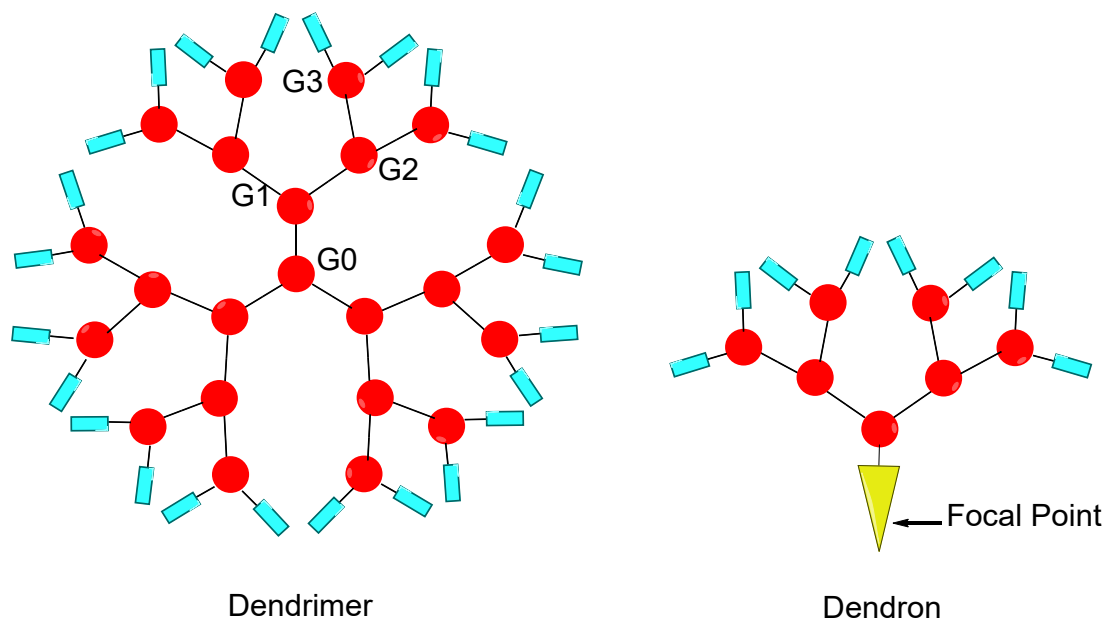


Figure 1.14. General structure of dendrimers and dendrons.

Despite the application of highly selective reactions, there are a few drawbacks: (i) final yield of production is often weak, (ii) high cost of synthesis, (iii) obtaining high-generation dendrimers with structural defects, and (iv) number of end groups increasing faster than the radius of the dendrimer.[117] In addition, there is a limit to the growth of the dendrimers, termed the “starburst limit.” This indicates that as the number of synthetic steps increases, the number ramifications grow exponentially.[117] For each additional generation of branches, the surface area increases by a factor of two, while the volume increases by a factor of three. The surface becomes compact up to a limit, at which point it is no longer possible to place monomers at the ends of the branches. Overall, the “starburst limit” depends on: (i) functionality of the central core, (ii) branching multiplicity and (iii) branch lengths.[117]

1.3.2 Dendrimer Synthetic Methods

For the fabrication of dendrimers, there exist two main synthetic approaches: (i) divergent method and (ii) convergent method.[117] For the divergent method (**Figure 1.15**), a multifunctional core is required, where the dendrimer propagates with the branch growing toward the exterior using the appropriate synthetic techniques. The process efficiency to construct the dendritic scaffolds is strongly influenced by the tedious multistep procedures with repetitive protection–deprotection/activation and chromatographic purification.[24] The drawback of this method is the purity of the target product decreasing as a result of the increased number of reactions carried out on the same molecule, which are continued from one generation to the next.[24] To obtain the desired dendrimer without defects, the reactions must be carried out quantitatively at each coupling and activation step. However, the number of terminal groups increases exponentially at each generation, leading to a compact environment for the functional groups, providing steric hindrance.[24] The possibility of conducting a reaction with 100% conversion decreases with the growth of the dendron/dendrimer; structural defects are often extremely difficult to separate from intact dendrimers because of their similar chemical compositions and physical properties.[80]

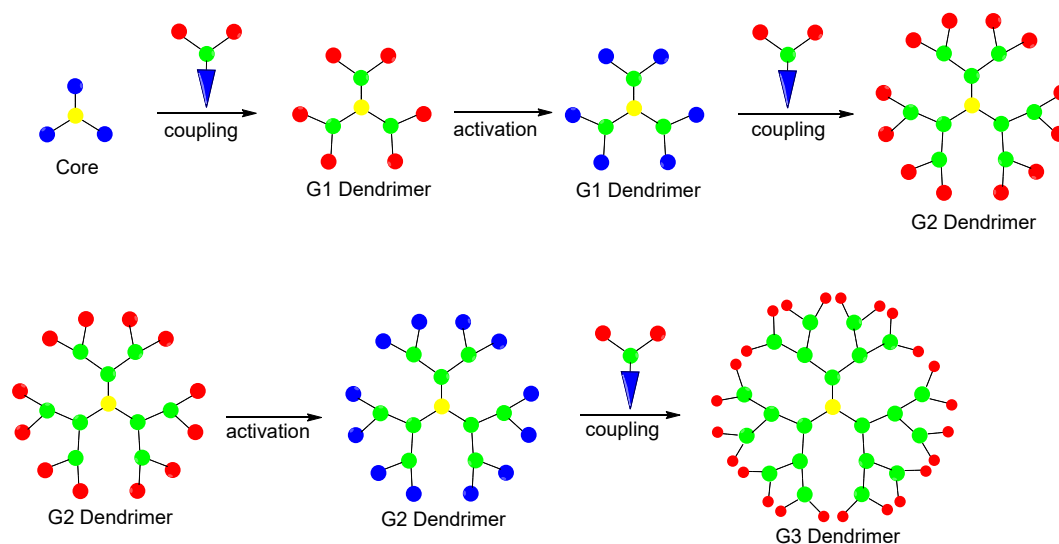


Figure 1.15. Synthesis of dendrimers according to the divergent method.

The convergent method (**Figure 1.16**), on the other hand, is initiated by the (future) periphery of the macromolecule, followed by the appropriate synthetic techniques, where the dendrimer grows inwards progressively until it reaches the central core.[117] Since the number of reactions carried out on the same molecule from one generation to the next is limited, it is possible to obtain dendrimers without structural defects; the use of reagents in equimolar quantities or in slight excess is sufficient to produce good yields. The purification of the product(s) through chromatographic techniques is easier than in the divergent method as a result of the large difference in molecular weights and polarity between the fully substituted dendron(s)/dendrimer(s) and the by-product(s).[117] However, the reactivity to reach the interior core is often considerably reduced because of the increasing steric congestion as the dendrimer generation increases. Larger dendrons can cause shielding of a multifunctional core, thereby leading to incomplete substitution, where only dendrimers of lower generation can be obtained.[79]

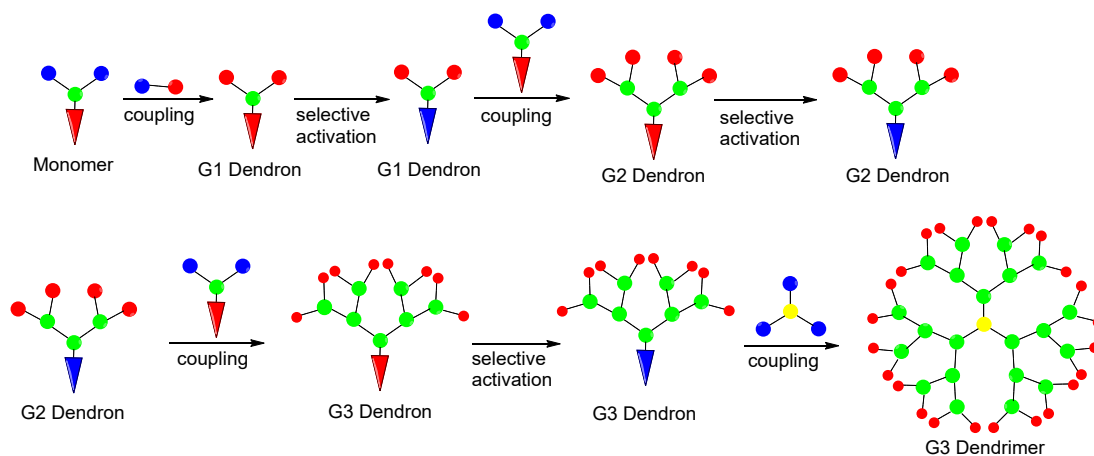


Figure 1.16. Synthesis of dendrimers according to the convergent method.

If desired to go to higher generation dendrimers, it is possible to combine the divergent/convergent approach to apply their advantages, while having little of its drawbacks. Various new synthetic strategies aiming at enhancing the process efficiency have been developed, including those by the double stage and double exponential growth, using branched monomers and orthogonal coupling.[24]

1.3.3 Asymmetrical (Janus) Dendrimers:

Despite their well-defined properties shown in the conventional dendrimer subsection, symmetrical dendrimers possess several limitations in biomedical applications: (i) rapid systemic clearance, (ii) significant toxicological issues, (iii) poor drug loading and (iv) difficulty in achieving controlled drug release.[114] Most dendrimers possess a single type of terminal group because of its simplicity to synthesize. However, having two (or more) types of terminal groups is highly desirable to combine several properties within a single molecule.[114] This can be achieved by grafting two (or more) types of functions either statistically or precisely as terminal groups. Another possibility pertains to grafting two terminal groups on precise areas of the surface. This can be

done by patches of one type of function together with another one, but most generally the dendritic structure is composed of two halves, where each half is composed of different sizes and a number of terminal groups.[17] This leads to the emerging class of Janus dendrimers. The word “Janus” is referenced to the Roman God of beginnings, transitions, and endings, which is represented by two distinct faces (**Figure 1.17**).[17]



Figure 1.17. Coin representing Janus, the two-faced God. This image is in public domain.

Source: <https://commons.wikimedia.org/w/index.php?curid=34884498>

Janus dendrimers are well-defined, asymmetrical dendrimers, with various backbones and peripheral groups. This implies that either the dendrimers have the same interior structure, but different peripheral groups, or the peripheral groups are the same, whereas the interior structure is different. [114]

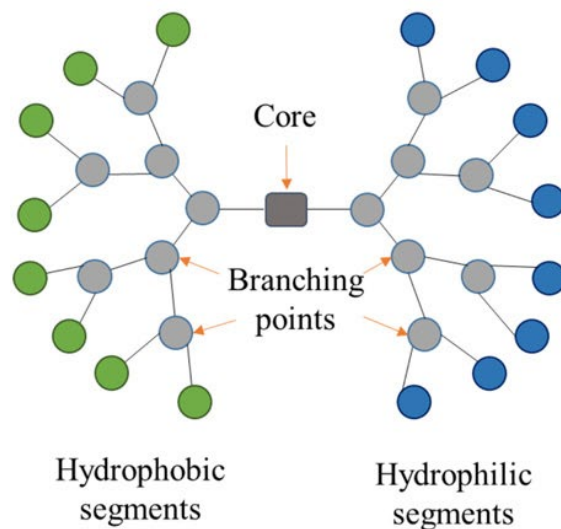


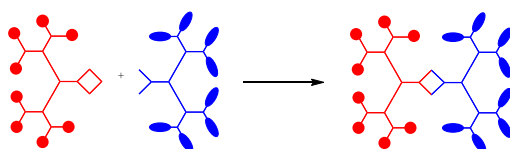
Figure 1.18. Schematic representation of a Janus dendrimer.

1.3.4 Janus Dendrimer Synthetic Methods

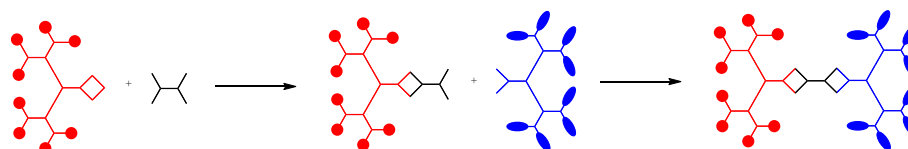
There are three principle synthetic approaches to forming Janus dendrimers: (i) chemo selective coupling, (ii) heterogeneous double exponential growth and (iii) mixed modular approach (**Figure 1.19**).^[120] The chemo selective coupling involves the attachment of two pre-synthesized dendrons having complementary functions at the junction. The heterogeneous double exponential growth consists of the reaction of a first dendron with a multifunctional core, followed by a second dendron grafted to the remaining function(s) of the core.^[120] The mixed modular approach implicates the focal point of a dendron for the growth of new branches through the divergent method. Both the chemo selective coupling and heterogeneous double exponential growth lead to low generation dendrimers, while higher generation dendrimers (G4-G7) are difficult to obtain pure.^[120] The mixed modular approach is considered more versatile

as each step would require purification of small monomers, allowing for higher generation dendrimers with sufficient purification and yield.[120]

a) Chemo selective coupling



b) Heterogeneous double exponential growth



c) Mixed modular approach

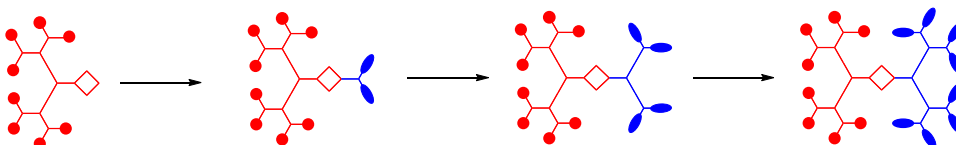


Figure 1.19. Synthetic approaches of Janus dendrimers: (a) chemo-selective coupling, (b) heterogeneous double exponential growth, (c) mixed modular approach.

High yield and completion of each individual reaction at each synthetic step is crucial to maintain the purity and consistency of a dendrimer.[24, 80] “Click” chemistry, by virtue of its high yield, high efficiency, high atom economy, short reaction time, and mild reaction conditions, has emerged as a popular approach for preparing various dendrimers.[24, 80]

1.3.5 Dendrimers Constructed by Copper-Catalyzed Azide-Alkyne “Click” Reaction

An ongoing challenge in developing dendritic macromolecules is the elaboration of new methodologies for their synthesis.[6] Ideally, dendrimer synthesis should be fast, efficient, and rely on simple purification methods, where these attributes are absent in the conventional divergent and convergent methods. A number of accelerated strategies have been developed ranging from a branched AB₄ monomer approach to the rapid synthesis of dendrimers by an orthogonal coupling strategy.[6] To overcome the long-held view that dendrimer synthesis is tedious, expensive, and time-consuming, a highly efficient strategy has been introduced based on the combination of two orthogonal “click” reactions.[6] Successful implementation of “click” chemistry has been achieved in dendrimer synthesis using the divergent, convergent, or combined divergent/convergent methods. In addition, great strides in “click” chemistry have been made to deliver simplified and accelerated dendrimer synthesis yet with diverse structural complexity.[72, 80]

Since neither azide nor alkyne functional groups require protection during other subsequent reactions and can take place in the presence of the unprotected nucleophiles and electrophiles, every step in the synthetic sequence has been used to grow the dendrimer.[68] Dendrimers display a high number of functional groups at their periphery, which strongly determines their solubility and biological properties.[68] They are able to carry a large number of molecular fragments of interest for their physical, catalytic, or biomedical properties. The development of efficient strategies for their peripheral functionalization is therefore of great interest.[68] The CuAAC reaction is modular, specific and regioselective, proven to be a reliable technique for the preparation of new functional materials, as well as the modification of dendrimer periphery.[116]

1.4 Self-assembly

An essential aspect of material chemistry is understanding the behaviour of polymers/dendrimers with other molecules, such as its interaction with solvents, other species, and its behaviour in bulk/solution state. Soft nanomaterials are formed by a process called self-assembly. The self-assembly process involves amphiphiles, which are compounds possessing both hydrophilic (water-loving) and hydrophobic (fat-loving) components (**Figure 1.20**).^[77] Their amphiphilicity (or surface activity) results in the amphiphiles polar head group to interact with water while the nonpolar lipophilic chain will migrate above the interface (either in the air or in a nonpolar liquid).^[77] These amphiphilic molecules are often called *surfactants* (i.e., surface active agents) as a result of their ability to reduce the interfacial tension.^[39] It is the nature of the group forming the polar head that is used to divide the surfactants into different categories, such as cationic, anionic, and neutral surfactants.^[39] The properties of the surfactants also vary according to ionic strength, pH, counterions and temperature.^[39] The main forces acting in the amphiphiles self-assembly are hydrogen bonding, hydrophobic effects, electrostatic interaction, and van der Waals forces, which are considered weak.^[77] Despite the weakness of the forces involved in amphiphiles self-assembly, the relevant number of these soft interactions will produce an overall effect that is strong enough to hold different amphiphile molecules together as well as to ensure their stability in solution.^[77] Moreover, the weakness of the involved interactions makes the structure more flexible, enabling the system to withstand minor perturbation while preserving the reversibility of the self-assembled structure. Stability in solution of the amphiphiles within the aggregates is given both to the hydration of the hydrophilic headgroups and to the insertion of the hydrophobic tail(s) in the solvent.^[77] The first reason of stability in solution is an enthalpic gain in solvation due to hydrogen bond formation while the second reason, called the hydrophobic effect, is a gain in entropy of the bulk water.^[77]

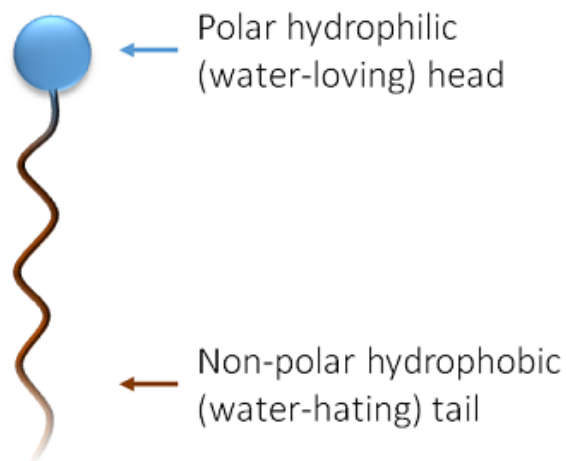


Figure 1.20. General structure of a surfactant molecule.

Hydrogen bonds are essential in biological systems as they are strong enough to bind biomolecules together, but weak enough, when necessary, to be broken inside living cells.[77, 99] Together with the hydrogen bond, the hydrophobic effect is the second main driving force of amphiphile self-assembly into various supramolecular structures; the hydrophobic effect regulates the tendency of nonpolar (hydrophobic) molecules to self-aggregate.[77, 99] When a hydrophobic compound is inserted in water, the disruption of the H-bonding of water favors a rearrangement of the water molecules around the nonpolar molecules. When different nonpolar molecules are dissolved in water, the disruption of the H-bonding of water favors the creation of larger cavities to accommodate an assembly of nonpolar (solute) molecules.[77, 99] In this case, water molecules' structures that are distorted by the presence of the hydrophobe will make new hydrogen bonds, thus inducing an ice-like cage structure around the hydrophobic molecules. This process corresponds to an effective mutual attraction between the nonpolar molecules in water, while entropically more favorable aggregated structures are generated to minimize the disruption of the water structure.[77, 99]

Soft materials based on polymers/dendrimers exhibit higher stability and durability than small molecules as a result of their superior mechanical and physical properties.[39] This has brought significant attention, not only for academic interests, but as potential applications in many fields, such as biomedicine, microelectronics, and catalysts.[39] In the self-assembly of polymers/dendrimers, the two most important factors to control are: (i) minimization of the interface area between adjacent polymers/dendrimers, and (ii) maximizing the entropy of the polymer/dendrimer chains; this is known as the disorder-order transition.[82]

1.4.1 Self-Assembly of Amphiphilic Polymers:

A precisely designed architecture is a key prerequisite for controlling the solution self-assembly process by tuning the interactions between the different polymer segments, both with each other, and with the solvent. The polymers that fit this criterion are amphiphilic block copolymers (BCPs).[125] Well defined BCPs, such as diBCPs, linear, and star triBCPs, are now accessible through a variety of living polymerization techniques, including anionic polymerization and controlled radical polymerization methods, such as RAFT, NMP and ATRP techniques.[13, 125] Amphiphilic BCPs, which consist of covalently linked, and more recently non-covalently linked macromolecular building blocks, represent an important method for the creation of soft-matter-based core-shell nanoparticles with useful properties and functions. Amphiphilic BCPs undergo self-assembly in aqueous solution in order to minimize energetically unfavourable hydrophobe-water interactions.[13, 125] How the amphiphilic BCPs pack, and hence the morphology formed, is related to the amphiphilic shape, which depends on the relative size of the hydrophobic and hydrophilic parts under equilibrium self-assembly conditions as this determines the curvature of the hydrophilic/ hydrophobic interface.[13, 82, 125] Further parameters

that influence the morphology include the polymer concentration, solvent composition, and temperature. The packing preferences can be analyzed in terms of the dimensionless “packing parameter” which is defined as: $P = \frac{v}{a_0 l_c}$, where v is the volume of the hydrophobic hydrocarbon chain, a_0 is the area of the hydrophilic headgroup, and l_c is the length of the hydrophobic tail normal to the interface.[13, 82, 125] Morphologies, such as spheres, cylinders (or worms or rods), and vesicles, are also commonly observed (**Figure 1.21**).

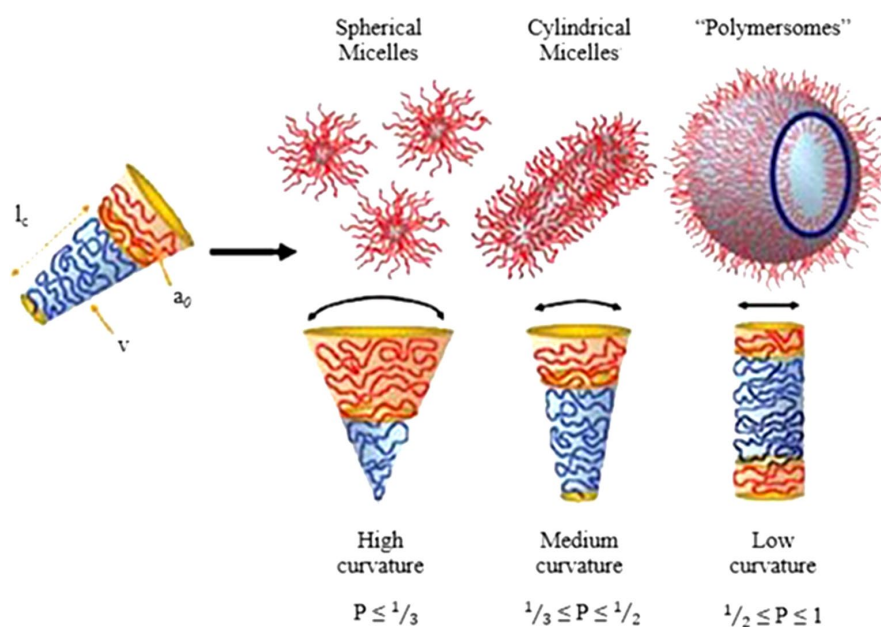


Figure 1.21. Self-assembled structures formed by amphiphilic BCPs. Copyright 2009 Wiley-VCH.

The micelle core is formed by the insoluble, hydrophobic block(s) and the corona (or shell) by the soluble hydrophilic block(s), which leads to colloidal stabilization of the micelle in solution.[13, 125] The role of entropy in self-assembly, however, is smaller (especially in non-aqueous solvents), as a result of the reduced translational freedom

of macromolecules with respect to low molar mass species. There is, nonetheless, an unfavorable entropic contribution from the stretching of the hydrophobic chains within the micellar core.[13, 125] The reduction in interfacial energy between the core-forming block and the presence of repulsive interactions between the hydrophilic coronal chains, constitute additional opposing entropic contributions to the free energy of the system.[13, 125] Amphiphilic BCP cylindrical (or worm-like) micelles are energetically favourable relative to shortened cylinders with incorporated end-defects since these structures allow uniform curvature across the entire aggregate.[13] However, entropic demands and molecular strain induces the formation of defects such as end caps (which are more energetically favourable) and branch points (which are less favourable).[13, 99, 101] Amphiphilic BCP vesicles (a.k.a. ‘polymersomes’) exhibit superior mechanical and physical properties compared to lipid-based vesicles (a.k.a. liposomes). The nature of polymeric vesicles was established in early studies, with micromanipulation verifying a ten-fold increase in critical strain before rupture compared to lipid vesicles.[13] Higher copolymer molecular weights led to an increase in membrane thickness, which in turn led to vesicles with greater bending constriction. Initially, it was hypothesized that polymeric vesicles were non-equilibrium structures based on the glassy nature from initial studies done on polystyrene membrane.[13] It was later discovered that the vesicular morphologies are not dictated by the kinetically frozen glassy nature of the hydrophobic block, since vesicles could be formed with low glass transition temperature (T_g) hydrophobes such as poly(butadiene) and poly(propylene oxide).[13] There is also the possibility of forming lamellar packing, which possess the same characteristics as polymeric vesicles, but are flat rather than enclosed. In comparing these two morphologies, polymeric vesicles are more frequently observed due to their superior thermodynamic stability.[99, 101]

1.4.2 Self-Assembly of Amphiphilic Janus Dendrimers:

The field of dendrimer self-assembly is currently in an explosive growth phase, as it has not been thoroughly examined.[137] The synthetic availability of dendrimers in a wide range of sizes (i.e., generations) combined with their unique structure, makes them versatile building blocks for the construction of several nanoscopic structures, including mono- and multilayers, micellar aggregates, and discrete hydrogen-bonded superstructures. Similar to the self-assembly of polymers, the morphology nanoparticles formed by dendrimers is dependent on the hydrophobic/hydrophilic balance.[137] The variation in the chemical structure of amphiphilic Janus dendrimers leads to a rich palette of morphologies in water, such as cubosomes, disks, tubular vesicles, helical ribbons and bilayered vesicles, termed as dendrimersomes.[28] When synthesized with judiciously tailored hydrophilic and hydrophobic elements, amphiphilic Janus dendrimers can function as powerful structure-directing amphiphiles, with greater versatility than simple lipids, surfactants, or block copolymers.[99] The molecular complexity of amphiphilic Janus dendrimers makes it difficult to apply conventional geometric models for predicting their self-assembly.[28] Most of the reported studies have focused on the prediction of bilayered vesicles' (a.k.a 'dendrimersomes') size, shape and stability; they are mostly based on Percec-type Janus dendrimers (**Figure 1.22**).[28, 101, 139, 140]

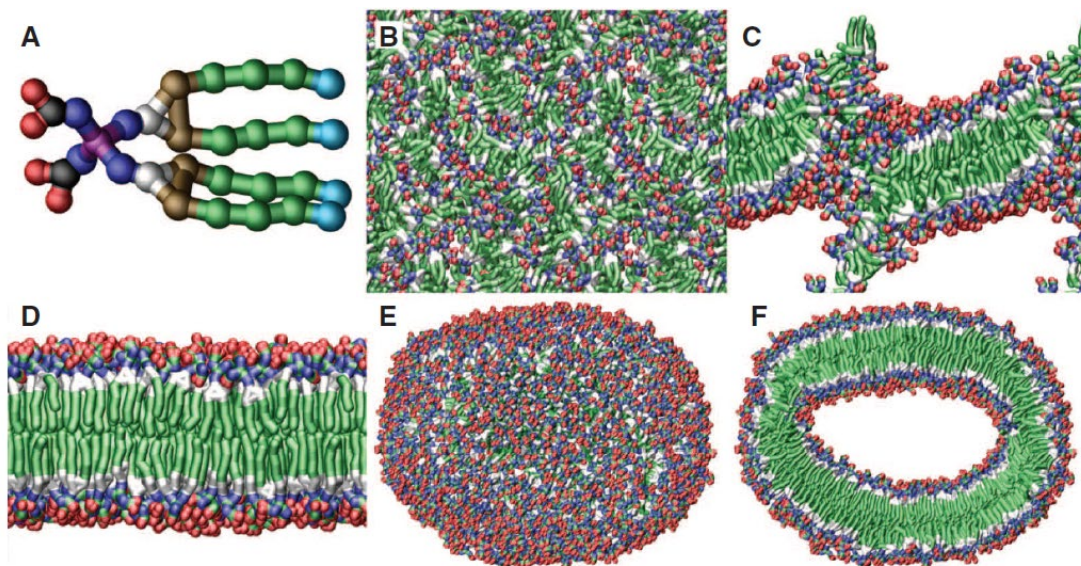


Figure 1.22. Schematic representation of dendrimersomes: (A) Molecular model of Janus dendrimer, (B) interaction potentials derived from fitting to an all-atoms simulation of dendrimer bilayer, (C) snapshot of the continuous formation of dendrimer's bilayer, (D) snapshot of completed formation of bilayer, (E) spontaneous vesicle formation, and (F) complete view of dendrimerosome. Copyright from (Percec, Virgil et al. *Science*, **2010**, 328, 1009-1014.)

The characteristics of dendrimersomes make them ideal vehicles for drug delivery and as diagnostic or theranostic agents as they are monodisperse, stable up to one year in various media and can encapsulate both hydrophilic and/or hydrophobic species.[28, 47] In addition, dendrimersomes contain the stability and the mechanical strength of polymersomes, while maintaining the biological functions of phospholipid liposomes and have been reported to have minimal toxicity both in vitro and in vivo.[71, 101, 113]

The three main techniques with which both polymer- and dendrimer-based self-assembled materials have been prepared are: (i) the nanoprecipitation method, (ii) oil-

in-water method, and (iii) thin-film hydration method.[103] The nanoprecipitation method is performed by dissolving the macromolecules in water miscible organic solvent to form a dilute solution. This dilute solution is then injected into water and vortexed. This is often referred to as a kinetic trapping method because it results in the rapid transition of the molecular building blocks from organic to aqueous media, often affording the kinetically rather than the thermodynamically favored supramolecular assemblies.[103] The oil-in-water method generally involves dissolution of macromolecules in water immiscible organic solvent followed by addition of water. The resulting mixture is stirred rapidly until the organic solvent has completely evaporated.[118] This method, which is significantly slower than the nanoprecipitation method, may result in the thermodynamically favored self-assembly rather than a kinetically trapped structure.[118] Lastly, the thin-film hydration method is performed by dissolving macromolecules in organic solvent, most often highly volatile solvents like CH_2Cl_2 and CHCl_3 , applying a layer of that solution to the bottom of a flask, followed by solvent removal by evaporation in air or under vacuum.[112] Water is then added to the resulting dry film, and hydration occurs usually at moderate temperatures (50–60 °C) for several hours.[112]

1.5 Applications of Self-Assembled Soft Nanomaterials in Nanomedicine:

Nanomedicine is an important area in nanotechnology as it refers to diagnosis, prevention and treatment of diseases to specific medical intervention at the molecular level.[56] One of the most important aspects in nanomedicine is towards site specific drug delivery systems. The concept of designing site specific drug delivery systems is to achieve selective targeting; targeted delivery is an incident where carriers conjugate and/or complex with drugs and deliver them exclusively to preselected and/or target cells in a specific manner (**Figure 1.23**).[56] This means that the drug is targeted

selectively and effectively at pre-identified and/or pre-selected target site in therapeutic concentration, while restricting the movement of drug to normal cells, thus minimizing undesirable effects and maximizing therapeutic concentration at target site.[56]

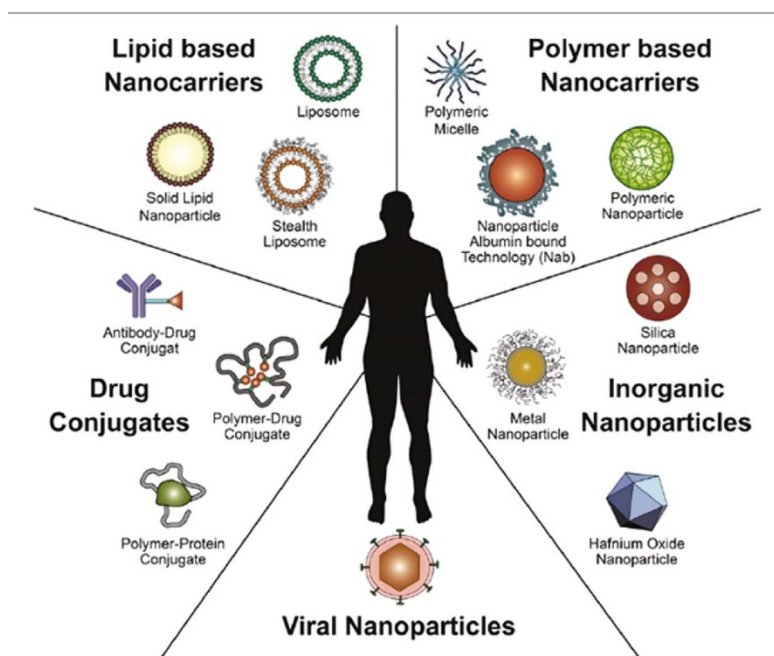


Figure 1.23. Schematic illustration of established nanotherapeutic platforms. Copyright from (Attia, Dalia, (2015), Review article of Nanocarriers Third Generation as Targeted Delivery Systems for Cancer Therapy, DOI: 10.13140/RG.2.1.1397.2320).

In general, the nature of conventional therapeutics, especially their low molecular weight, confers them the capacity to cross various body compartments and access numerous cell types and subcellular organelles. [127] However, this form of indiscriminate distribution leads to the occurrence of side effects and the need for higher doses of the drug to elicit a satisfactory pharmacological response.[127] Overall, conventional therapeutics suffer from major drawbacks; (i) limited water solubility, (ii)

low bioavailability, (iii) toxicity, and (iv) premature degradation.[56] New formulations that ensure a greater pharmacological response, which in turn would lead to lower doses and therefore the minimization of side effects, is a priority.[127] Therefore, research into drug delivery systems is of interest, as it provides advantages of (i) an increase in the drug's hydrophilicity, (ii) prevention of premature drug degradation, (iii) enhancement in cellular uptake, and (iv) reduction in toxicity.[56]

Synthetic macromolecules play an important role in the development of nanocarrier-based cancer drug delivery systems. The word “polymer therapeutics” includes polymer-drug, polymer-protein, and/or polymer-micelles conjugates which are used in nanomedicine.[56] The first report of cancer treatments involves using polymeric micelles. This provided and increased solubility of the drug by encapsulating the drug inside the hydrophobic core of the micelle, as well as increased stability of the encapsulated drug by inactivation and/or hindering enzymatic degradation.[56] Depending on the structure of the polymer, as well as the method of preparation, nanoparticles can be developed to possess different properties and release characteristics for the best delivery or encapsulation of the therapeutic agent; drugs can be absorbed onto the surface, entrapped inside, or dissolved within the matrix of the nanoparticles.[56] While polymers have been studied in detail, dendrimers are highly explored for drug delivery application due to their capability to overcome shortcomings of the current drug delivery systems.[4] The dendritic structure contains two key features that make them of interest as drug carriers. Its interior cavities, which have precise chemical characteristics and allow the encapsulation of drugs with hydrophobic properties.[4, 127] Dendrimers also contain specific surface functional groups that allow attachment of hydrophilic drugs by covalent bonds, electrostatic interactions or hydrogen bonds.[127] The main advantage of dendrimers as drug carriers is the number of potential sites for the attachment of functional surface groups that can grow exponentially generation to generation.[127] The multiple surface groups on a single

entity (multivalency or polyvalency) allow their association with pathogens; they are capable of interacting specifically with tumor cells and they cause apoptosis. These controlled release drugs allow the administration of lower concentration doses and therefore achieve a decrease in toxicity to healthy cells.[127] If one were to decide whether polymers favor dendrimers or vice versa, there is no one right answer. Each macromolecule provides advantages and disadvantages, depending on their molecular structure, degradability, hydrophobicity/hydrophilicity ratio, cytotoxicity, and cellular uptake.[2] In the field of chemistry, the theoretical and practical approaches are very different; the theoretical approach cannot incorporate possible side reactions, half-life of nanoparticles formed, degree of stability and degradability or even how substituted molecules can greatly affect the success or failure of each synthetic reaction, which can only be attained in the practical approach.[2]

Research of amphiphilic macromolecules as building blocks has been essential for the fabrication of nanomaterials, in which the varying morphologies provide widespread applications in science and technology. The objective of this memoire is to synthesize new classes of degradable amphiphilic linear polymers as well as amphiphilic Janus dendrimers (AJDs) with aggregation-induced emission property. The self-assembly behaviour of these two classes of macromolecules will be thoroughly investigated to develop nanomaterials with potential applications in nanomedicine.

CHAPTER II

DEGRADABLE SPIROCYCLIC POLYACETAL-BASED CORE-AMPHIPHILIC ASSEMBLIES FOR ENCAPSULATION AND RELEASE OF HYDROPHOBIC CARGO

Publication: Andrade-Gagnon, Brandon; Bélanger-Bouliga, Marilyne; Trang Nguyen, Phuong; Thi Hong Nguyen, Diep; Bourgault, Steve; Nazemi, Ali, 'Degradable Spirocyclic Polyacetal-Based Core-Amphiphilic Assemblies for Encapsulation and Release of Hydrophobic Cargo' *Nanomaterials*, **2021**, 11, 161 The project described in this chapter was proposed by Dr. Ali Nazemi. Most experimental work was accomplished by the author under the supervision of Dr. Nazemi. Marilyne Bélanger-Bouliga contributed to the monomer synthesis as well as the characterization of particles by AFM. Diep Thi Hong Nguyen performed all the DSC measurements and analyses for the polymers. All cellular studies were accomplished by co-author Phuong Trang Nguyen, under the supervision of Dr. Steve Bourgault. The manuscript was initially drafted by author and Dr. Nazemi provided assistance with editing and final preparation.

2.1 Abstract:

Polymeric nanomaterials that degrade in acidic environments have gained considerable attention in nanomedicine for intracellular drug delivery and cancer therapy. Among various acid-degradable linkages, spirocyclic acetals have rarely been used to fabricate

such vehicles. In addition to acid sensitivity, they benefit from conformational rigidity that is otherwise not attainable by their non-spirocyclic analogs. Herein, amphiphilic spirocyclic polyacetals are synthesized by Cu-catalyzed azide–alkyne “click” polymerization. Unlike conventional block copolymers, which often form core–shell structures, these polymers self-assemble to form core amphiphilic assemblies capable of encapsulating Nile red as a hydrophobic model drug. In vitro experiments show that while release from these materials can occur at neutral pH with preservation of their integrity, acidic pH accelerates efficient cargo release and leads to the complete degradation of assemblies. Moreover, cellular assays reveal that these materials are fully cytocompatible, interact with the plasma membrane, and can be internalized by cells, rendering them as potential candidates for cancer therapy and/or drug delivery.

2.2 Introduction:

Drug delivery systems are a necessity nowadays due to the limitations of most drugs, which often include low water solubility, high toxicity, low metabolic stability, and poor bioavailability. Drug delivery systems can act by one of these mechanisms: (i) increasing the hydrophilicity of drugs, (ii) limiting drug degradation and elimination, and (iii) enhancing their bioavailability and accumulation at the target site.[29, 92] In the past few decades, the emergence of controlled polymerization techniques has enabled the synthesis of polymers of various chemical structures, topologies, and functions.[15, 22, 61, 100, 119] This, coupled with the ability to self-assemble amphiphilic polymers to nano-sized materials with a variety of morphologies, including spherical micelles and vesicles, one dimensional worms and cylinders as well as toroids, has rendered polymer-based nanomaterials promising candidates for applications in nanomedicine.[82, 109] This includes their use as carriers for

hydrophilic and hydrophobic small molecules, proteins, polynucleotides, and imaging contrast agents.[30, 96] In this context, degradable polymeric nanomaterials, in which the release of the encapsulated cargo can be triggered in response to an external stimulus, are of significant interest. To date, materials responsive to almost every conceivable stimulus, including temperature, light, mechanical force, pH, and electron transfer (oxidation-reduction) have been developed.[23, 49, 76] Among these triggers, a change in the acidity, i.e., pH, is particularly interesting for developing responsive/degradable nanomaterials. This is because, when it comes to the delivery of any drug, the pH change from the acidity in the stomach (pH = 2) to the pH in the intestine (pH = 5–8) has to be considered.[111] In addition, it is known that the extracellular pH of tumor tissues is often 0.5–1.0 units lower than that of the blood and normal tissues.[38] Moreover, upon cell uptake via endocytosis [89], the pH drops from neutral to 5.5–6.0 in endosomes and approaches to a value of 4.5–5.0 in late endosomes and lysosomes.[89] Therefore, polymeric materials that could degrade and release their cargo in an acidic environment are attractive candidates for the delivery of therapeutics intracellularly and to cancerous cells.

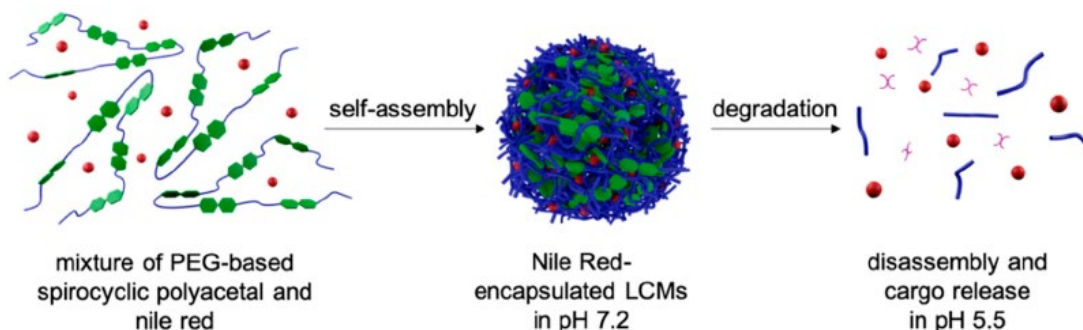
pH-responsive materials are generally divided into two categories. The first class are those containing ionizable functional groups, such as amines and carboxylic acids, which often undergo conformational changes upon (de)protonation without any covalent bond cleavage.[23] The second group is characterized by the presence of linkages, such as acetal, imine, ketal, hydrazine, β -thio ester, and cis-aconityl, that undergo covalent bond cleavage due to pH variations.[10] Among these pH-degradable linkages, acetals have attracted significant attention because their cleavage often results in the formation of charge-neutral and potentially nontoxic products.[54, 75] In fact, a variety of linear and branched polymers as well as dendritic structures with acetal functional groups have been developed. In these materials, the incorporation of acetals within the polymer backbone [48, 58, 107], in their side chain as pendant groups [53,

121, 138] or as branching units **[21, 51, 87]**, has been employed to access scaffolds with tunable degradability.

While it is possible to synthesize both acyclic and cyclic acetals, spirocyclic conformation confers rigidity to the polymer backbone as a result of its restricted conformational flexibility and, hence, results in enhanced polymer thermal stability.**[3, 41, 74]** In this context, spirocyclic polyacetals with various chemical structures have been synthesized via different polymerization methods. This includes direct polyacetalization **[69, 83, 88, 97, 106]** and polytransacetalization **[55]** of carbonyl/acetal and polyol monomers, respectively, as well as polymerization of pre-synthesized spirocyclic acetal monomers via nucleophilic substitution **[86]** and polycondensation reactions.**[67, 73, 74, 110]** In these examples, the focus has been principally on fine-tuning the thermal and rheological properties of the resulting polymers and their potential use as replacements for existing thermoplastic and thermoset commodity polymers. Thus far, hydrophobic, and rigid spirocyclic polyacetals with limited solubilities in organic and aqueous solvents have been obtained. This has posed a significant hurdle in the application of spirocyclic polyacetals in nanomedicine.

Herein, we report the efficient synthesis of poly (ethylene glycol) (PEG)-based spirocyclic polyacetals using copper(I)-catalyzed azide–alkyne cycloaddition (CuAAC) “click” polymerization as an alternative method to the existing approaches to access this class of polymers. Owing to the rigidity and hydrophobicity of the spirocyclic linkages, we demonstrate that these polymers undergo self-assembly to form core-amphiphilic spherical large-compound micelles (LCMs) **[82]** capable of encapsulating the hydrophobic dye Nile red, used as a model drug. These micelles degrade effectively in an acidic environment (pH = 5.5) to release their encapsulated cargo (**Scheme 1**). In addition, these LCMs are fully cytocompatible, interact avidly

with the plasma membrane, and can be uptaken by cells. To our knowledge, this is the first example of an amphiphilic spirocyclic polyacetal capable of forming self-assembled materials with potential application as a drug delivery vehicle.



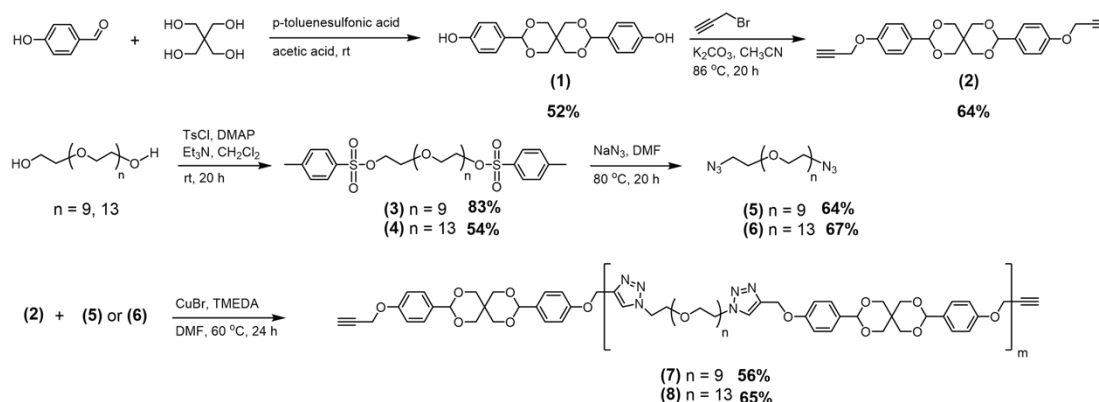
Scheme 1. A schematic illustration of the Nile red-loaded core amphiphilic assembly formation using poly (ethylene glycol) (PEG)-based spirocyclic polyacetals and their pH-triggered disassembly and cargo release.

2.3. Results and Discussion

2.3.1. Synthesis and Characterization of Spirocyclic Polyacetals:

To construct our target polymers via CuAAC “click” polymerization, we envisioned the synthesis of dialkyne-decorated spirocyclic acetal and diazide-functionalized PEG monomers. Our synthetic strategy is shown in **Scheme 2**. The use of starting materials from biorenewable resources is of significant interest as a viable alternative to fossil-based materials due to the ongoing concerns regarding the environmental impact of the latter on the planet. In this context, we chose pentaerythritol and 4-hydroxybenzaldehyde as starting materials for the synthesis of our dialkyne-containing monomer. 4-Hydroxybenzaldehyde is considered as one of the three aromatic 4-hydroxyaldehydes, alongside vanillin and syringaldehyde, derived from lignin, the second most abundant naturally occurring polymer and an excellent source of biobased aromatic feedstocks.[91] Although pentaerythritol is not a bio-sourced compound, it is

produced commercially from formaldehyde and acetaldehyde and is an attractive polyol for the synthesis of spirocyclic acetals because of its low cost.[97] Double protection of this compound using 4-hydroxybenzaldehyde under acidic conditions resulted in the formation of spirocyclic acetal (**1**) with phenol functional groups. The subsequent reaction of (**1**) with propargyl bromide using potassium carbonate as base provided our “clickable” dialkyne-functionalized spirocyclic acetal (**2**) (**Appendix A, Figure A1-A3**) in 64% yield (**Scheme 2**). To render the final polymers and their corresponding particles dispersible in aqueous media, we chose diazide-functionalized PEG as the complementary monomer to (**2**). In order to investigate the effect of hydrophilic segment chain length on the size of the resulting assemblies, PEG with M_n (number average molecular weight) values of 400 and 600 g/mol were selected, corresponding to the degree of polymerization of 10 and 14, respectively. Ditosylation of these PEG molecules (**Appendix A, Figure A4 & A5**) followed by their reaction with sodium azide in DMF afforded the two diazide-decorated PEG (**Appendix A, Figure A6-A9**) target monomers (**7**) and (**8**) (**Scheme 2**).



Scheme 2. The synthesis of the monomers and the spirocyclic polyacetals. TsCl: *p*-toluenesulfonyl chloride.

Having the three monomers in hand, we then synthesized the target spirocyclic polyacetals (**7**) and (**8**) via CuAAC “click” polymerization using CuBr and TMEDA in DMF at 60 °C for 24 h (**Scheme 2**). In all these reactions, a slight excess of dialkyne-

decorated monomer was used to increase the possibility of end-capping the polymers with this functionality and to inhibit the formation of cyclic polymers. However, the formation of the latter cannot be entirely excluded. The resulting polymers were purified by a combination of dialysis against DMF using a 3500 MWCO membrane, to remove any unreacted monomers and low molecular weight oligomers and washed with ammonia to remove the copper catalyst. The $^1\text{H-NMR}$ analysis of **(7)** demonstrated the formation of 1,2,3-triazole rings in the polymer backbone as evidenced by the peak at 7.79 ppm (**Figure 2.1a**). In addition, the peak at 5.37 ppm, corresponding to the two acetal protons, confirms the presence of the spirocyclic acetals in the polymer structure. Similar $^1\text{H NMR}$ spectrum was obtained for **(8)** (**Appendix A, Figure A10**). As shown in **Figure 2.1b**, using SEC, M_n values of 15,900 and 73,000 g/mol with dispersity indices of 2.47 and 3.07 were obtained for **(7)** and **(8)**, respectively. It is noteworthy that CuAAC polymerization is a step-growth polymerization for which relatively high \bar{D} values are expected. Moreover, the chain length distributions of the PEG starting materials carry on and amplify throughout the polymerization, which contributes significantly to \bar{D} broadening of the target polymers. We then used DSC to gain insight into the thermal behaviour of the polymers. The results demonstrate that both **(7)** and **(8)** are amorphous with comparable glass transition temperatures (T_g) at 6 and 0.5 °C, respectively (**Figure 2.1c**). As noted earlier, relatively high T_g values for this class of polymers are often obtained due to the nature of the spacers and the rigidity of the polymer backbone.[55, 97, 106] In **(7)** and **(8)**, the PEG spacers between the spirocyclic acetal moieties impart adequate flexibility to render them amorphous at room temperature.

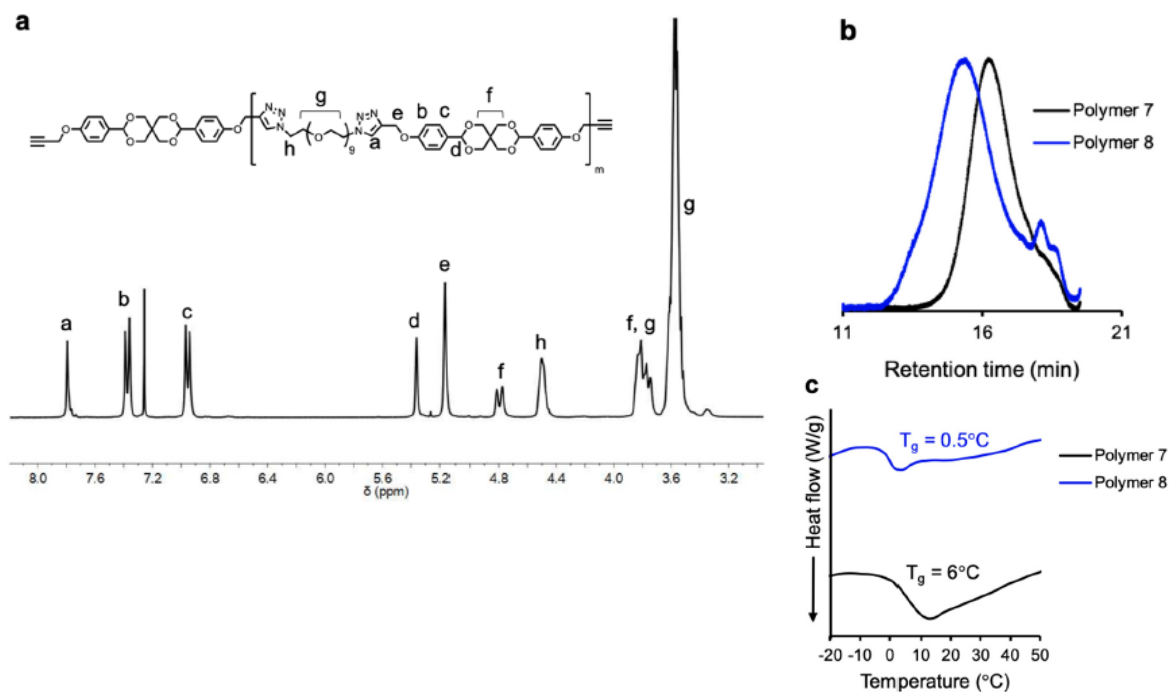


Figure 2.1. (a) ¹H NMR of (7); (b) refractive index (RI) traces in the SEC analysis of (7) and (8) in DMF, which were normalized; (c) DSC analysis of (7) and (8) showing amorphous spirocyclic polyacetals at room temperature.

Before particle formation and pH-triggered degradation and model drug release experiments, we studied the degradation behaviour of polymers (7) and (8) in acidic organic media. To do this, polymers were dissolved (5 mg/mL) in a CDCl₃ solution of trifluoroacetic acid (80 mM, 1 mL) and ¹H-NMR spectra were acquired at specified time points. As shown in **Figure 2.2** for (7), the decrease in intensity of the peak at 5.37 ppm, corresponding to the acetal proton, and the concurrent increase in the intensity of the peak at 9.88 ppm, corresponding to the formation of arylaldehyde derivative, is a strong evidence of the effective breakdown of the polymer backbone. In addition, the initial two sets of doublets at 6.95 and 7.37 ppm, assigned to the aryl groups in the polymer structure, disappear and new doublets appear at 7.11 and 7.83 ppm, which can be attributed to the protons in the resulting arylaldehyde product.

Finally, after complete degradation, which takes place in about 75 h, the singlet at 5.17 ppm, corresponding to the CH₂ between the triazole ring and the spirocyclic moiety, disappears and a new singlet emerges at 5.25 ppm, which is assigned to the same protons now located between the triazole ring and the benzaldehyde derivative in the degradation product. A similar degradation profile was observed for **(8)** under similar conditions (**Appendix A, Figure A11**). A peak corresponding to the formed pentaerythritol was not detectable due to its overlap with those of the PEG backbone. However, the degradation of the spirocyclic backbone is evident by the disappearance of the multiplets at 4.80 and 3.80 ppm assigned to its protons. Performing a similar stability experiment for polymer **(7)** in non-acidic CDCl₃ revealed no degradation of the polymer backbone during the four-day timeframe of the measurements (**Appendix A, Figure A12**). We would like to note that our attempts to carry out this experiment in mixtures of organic solvents, such as dioxane, acetone, dimethyl sulfoxide, and water were met with very limited success as the polymers readily precipitated in such media. SEC analysis of these two samples demonstrated the complete degradation of polymer backbones and the formation of low molecular weight oligomers, further confirming the effective breakdown of **(7)** and **(8)** under acidic condition (**Appendix A, Figure A13**).

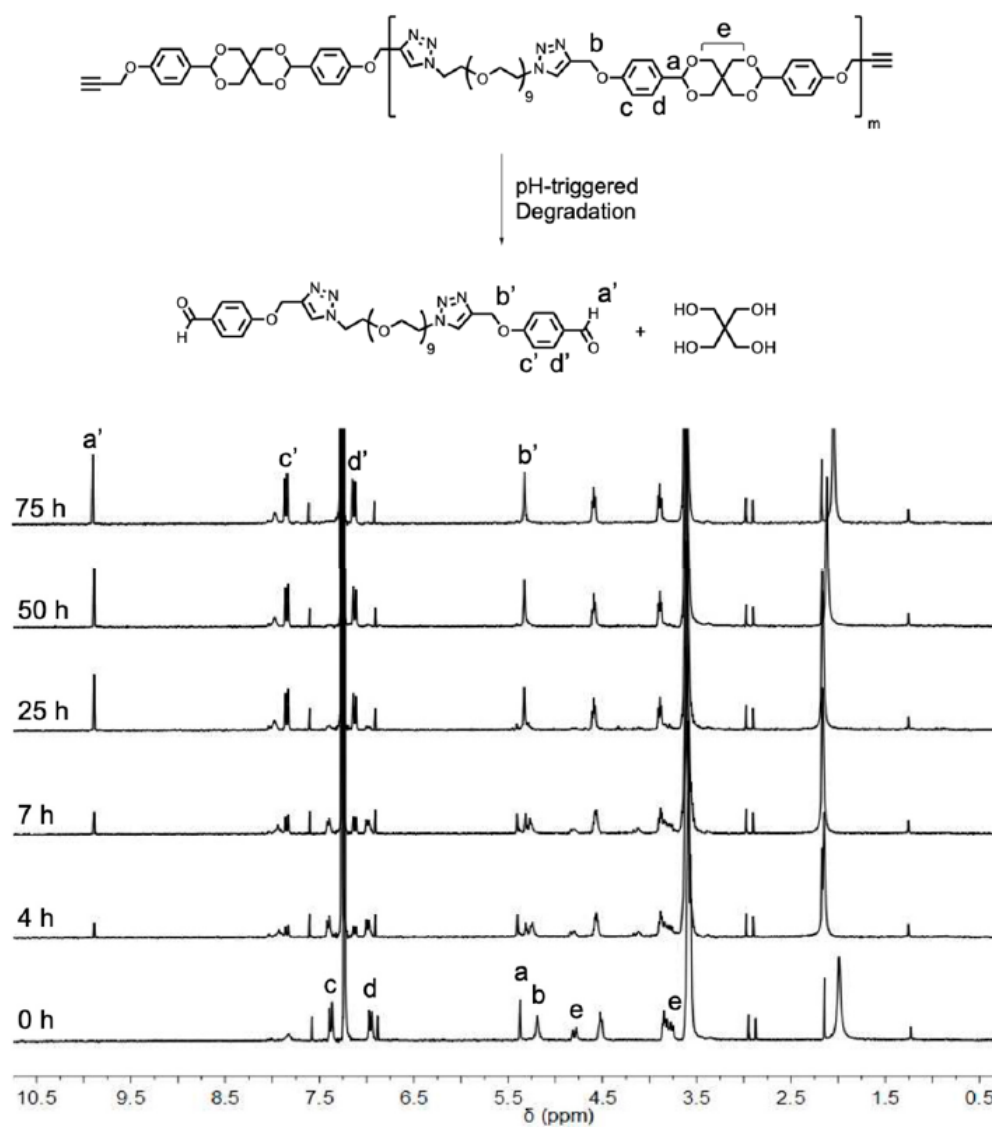


Figure 2.2. A pH-triggered degradation reaction of (7) in acidic media (top) monitored by ¹H-NMR spectroscopy (bottom).

2.3.2. Self-Assembly of Spirocyclic Polyacetals (7) and (8):

Encouraged by these results, we then investigated the self-assembly behaviour of the polymers. In their structures, the PEG chains serve as the hydrophilic segments. On the other hand, the rigidity of the spirocyclic moieties coupled with the phenyl rings of the

4-hydroxybenzaldehyde protecting groups render them hydrophobic. We envisioned that these hydrophobic nodes on the polymer backbone will be able to drive the phase separation of these polymers in an aqueous environment. As a result of this design, polymers **(7)** and **(8)** do not resemble the conventional amphiphilic block copolymers commonly used for the fabrication of soft nanomaterials. To test this hypothesis, polymers (5 mg) were dissolved in DMSO (0.5 mL), and, to these solutions, deionized water (4.5 mL) was added dropwise, with constant stirring. The organic solvent was then removed by dialyzing the solutions against deionized water for 24 h with multiple changes of the dialysate. DLS analysis of the samples obtained from **(7)** and **(8)** (denoted as **P1** and **P2**, respectively) revealed particles with average hydrodynamic diameters of 400 and 460 nm, respectively (**Figure 2.3a, c**, inset). The slightly larger size of **P2** can be potentially attributed to the higher M_n of **(8)** compared to that of **(7)**. Further insight into the morphologies of the structures was obtained by TEM and AFM measurements.

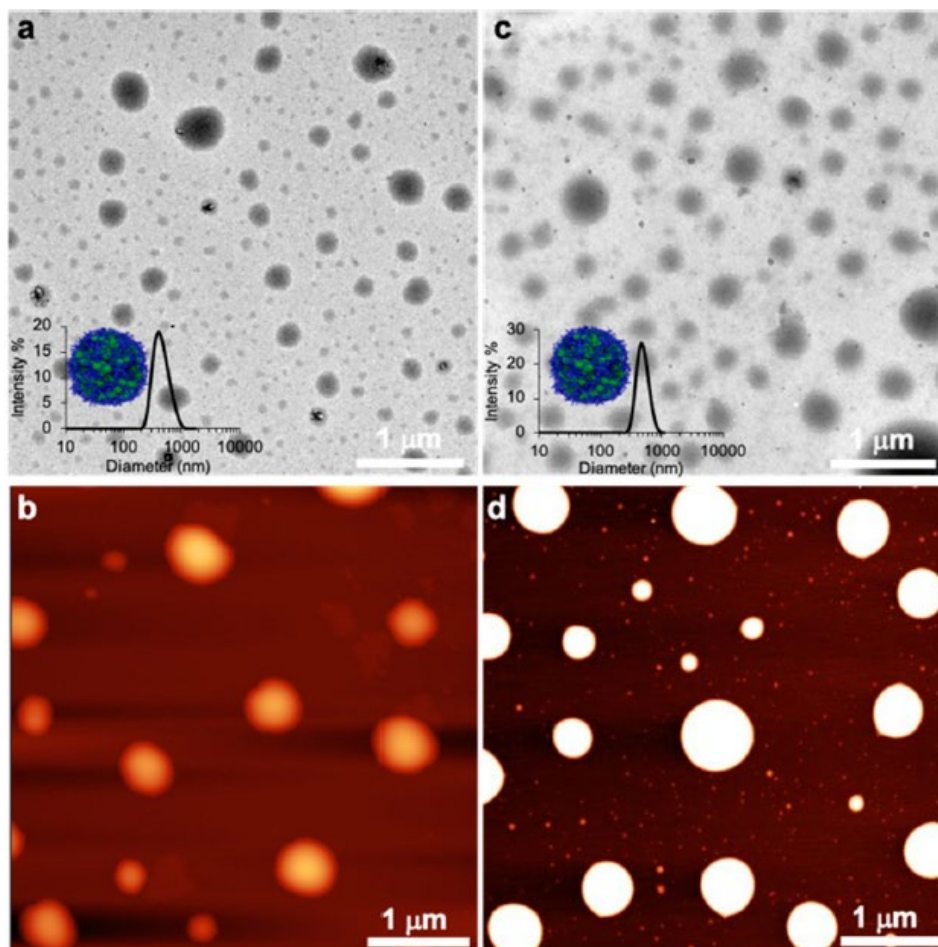


Figure 2.3. (a, b) TEM and AFM images of **P1**. Inset showing the DLS data and a cartoon representation of the particles. (c, d) TEM and AFM images of **P2**. Inset showing the DLS data and a cartoon representation of the particles.

As shown in **Figure 2.3a–d**, these analyses demonstrate that both polymers form polydisperse spherical particles whose size is in good agreement with those obtained by DLS. As noted earlier, although (7) and (8) are amphiphilic, they are not comprised of a block structure, but rather they resemble amphiphilic alternating polymers. As a result of this structural feature, **P1** and **P2** cannot adapt the conventional core-corona morphologies with a hydrophobic core and a hydrophilic corona in an aqueous environment. In contrast, it is conceivable that the self-assembled materials formed are

similar to large compound micelles (LCMs) with an amphiphilic core, comprised of both the hydrophobic spirocyclic acetals and hydrophilic PEG units (**Figure 2.3a, c**, inset). We suggest that it is the association of the hydrophobic spirocyclic nodes on the polymer backbone that act as stitches to form core-amphiphilic LCMs. In addition, we observe the similarity in size and shape with (**Figure 2.3b**) or without (**Figure 2.3d**) Nile red-loaded particles.

2.3.3. Encapsulation and pH-Triggered Release of Nile Red from Particles:

Given the similar morphologies and comparable sizes of **P1** and **P2**, we used **P1** for the rest of the studies to investigate their potential applications as drug delivery vehicles. To do this, we chose Nile red as a model drug that could be encapsulated in the core of particles. It is noteworthy that Nile red is hydrophobic and the amphiphilic core of the micelles, particularly in interactions with the hydrophobic spirocyclic acetal moieties, offer a suitable environment for its encapsulation and minimizes its contact with water. In addition, Nile red is strongly fluorescent when solubilized in a hydrophobic environment such as in the amphiphilic core of our particles. However, its fluorescence is effectively quenched when its solubility is decreased as a result of its exposure to water. Thus, a decrease in the fluorescence intensity of Nile red-loaded particles will be a good indication of model drug release. To form the dye-encapsulated particles, the same self-assembly protocol as before was performed except that Nile red was co-dissolved (1% w/w) with polymer (**7**) in DMSO. DLS analysis of the resulting sample revealed a slight increase in the size of the particles to 458 nm (**Figure 2.4a**). In addition, AFM images of these dye-loaded particles were obtained using a Bruker Multimode 8 nanoscope, using Scanasynt mode. These nanoparticles demonstrated that they preserve their spherical morphology upon encapsulation of Nile red (**Appendix A, Figure A14**). The divergence in both DLS and AFM techniques is a result of a solution or dry state; AFM visualizes nanoparticles in their dry state, where upon

drying, the nanoparticles become deformed, making them appear flat. To examine the efficacy of the particles to release their encapsulated cargo in acidic pH under physiologically relevant conditions, they were transferred to a freshly prepared phosphate buffer (pH = 5.5, 10 mM) in a quartz cuvette preheated at 37 °C. Fluorescence spectra were then acquired at specific time points in order to monitor the change in the fluorescence intensity of Nile red as a consequence of any changes to its surrounding environment. As shown in **Figure 2.4b**, we observed that about 50% of the dye was released during the first 8 h of incubation at 37 °C, with a maximum of 75% release within 48 h, suggesting the degradation of particles and the subsequent release of the dye.

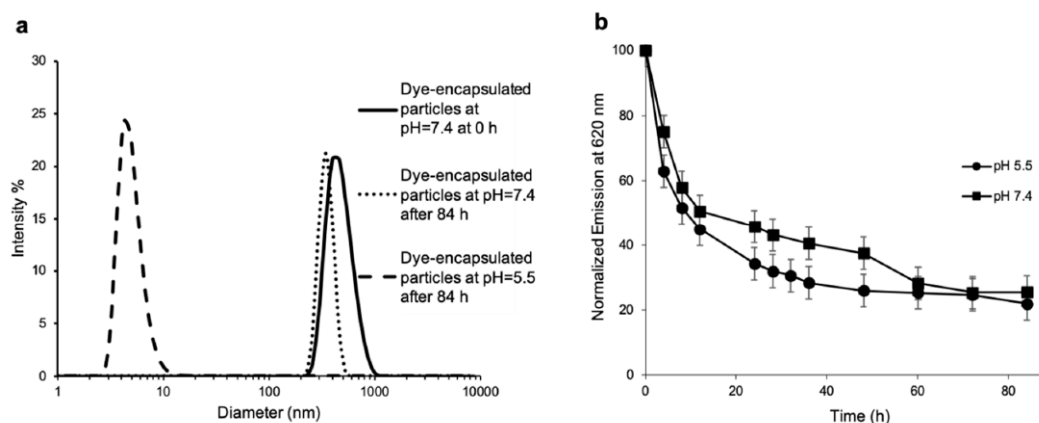


Figure 2.4. (a) DLS data for the Nile red-encapsulated **P1** in water at room temperature as well as those incubated at 37 °C in phosphate buffer at pH 7.4 and 5.5 after 84 h. (b) The release profile of Nile red from **P1** at pH 5.5 and 7.4 at 37 °C.

To investigate the effect of pH in the model drug release, we performed the same experiment at pH = 7.4 (10 mM phosphate buffer) at 37 °C. Surprisingly, a comparable release profile, with slightly slower liberation of Nile red, was observed (**Figure 2.4b**). We hypothesise that due to the amphiphilic nature of the core of the particles, water

has the ability to penetrate inside and come into close contact with Nile red molecules, altering the surrounding environment and quenching their fluorescence. In addition, such burst release is often observed in polymeric nanoparticulate systems in which the cargo is noncovalently encapsulated in their core.[29, 92] In fact, DLS analysis of the dye-loaded particles after 84 h of incubation showed that those in acidic media (pH=5.5) were completely degraded to their small molecule building blocks (**Figure 2.4a**), which is strong evidence of their effective degradation in an acidic aqueous medium, while those at pH = 7.4 kept their integrity, as only minimal change in their size was observed (**Figure 2.4a**). Such a small change in the size of particles in buffer at pH=7.4, compared to deionized water, can be attributed to the presence of salts in the buffer solution. This suggests that while the spirocyclic polyacetal-based assemblies are leaky in their nature, the presence of acetal linkages ensures their effective degradation under acidic conditions, which is highly desirable for any drug delivery vehicle to potentially facilitate its clearance from body.

2.3.4. Cytocompatibility and Interactions of Nile Red-Load Particles with Cells:

Next, we evaluated the cytocompatibility of these particles using ovarian hamster cells (CHO-K1), an epithelial cell line commonly used for the evaluation of the toxicity of particles. CHO-K1 cells were incubated with increasing concentrations of **P1**, ranging from 0.1 to 100 $\mu\text{g/mL}$, for 24 h before measuring cellular viability using the LIVE/DEAD assay and a resazurin-based metabolic activity assay. As observed on fluorescence microscopy images, CHO-K1 cells treated with 100 $\mu\text{g/mL}$ of **P1** showed a similar green/red cell ratio to the vehicle treated cells (PBS) (**Figure 2.5a**). The red fluorescence (ethidium homodimer-1) is associated with loss of plasma membrane integrity whereas the green fluorescence (calcein-AM) correlates with intracellular esterase activity of metabolically active cells. In contrast, treatment with 10 μM saponin, used as positive control of cytotoxicity, led to a sharp increase of red-labelled

cells and a decrease of green fluorescence. Quantitative analysis of the green/red fluorescence ratio, expressed as % of live cells, indicated no significant decrease in cell viability for all **P1** concentrations evaluated (**Figure 2.5b**). Moreover, treatment with **P1** did not reduce the metabolic activity of CHO-K1 cells, as measured by the reduction of resazurin into the highly fluorescent resorufin (**Figure 2.5c**).

Encouraged by these results, using confocal microscopy and flow cytometry, we investigated how the **P1**, loaded with Nile red, interacts with cells and if these particles can be ultimately uptaken by cells. To evaluate plasma membrane adsorption and cell uptake of dye-loaded particles, CHO-K1 cells were incubated with 100 $\mu\text{g}/\text{mL}$ of Nile red-loaded assemblies for 4 h at 37 °C. Confocal fluorescence microscopy analysis showed that **P1** gathered at the cell surface, indicating that they bind to the plasma membrane (**Figure 2.5d**). Moreover, Z-stack projection also revealed that some red fluorescence puncta of **P1** were located inside the cells, indicating that **P1** were internalized by CHO-K1 cells (**Figure 2.5d**). Nonetheless, it is worth mentioning that upon cell uptake likely involving the endosomal-lysosomal pathway, the **P1** undergoes a pH decrease, which could accelerate the release of Nile red and the consequent quenching of its fluorescence. Next, we evaluated the interactions of **P1** with cells by flow cytometry and we observed that, despite extensive washes of cells before analysis, the majority of CHO-K1 cells were highly fluorescent (**Figure 2.5e**). Overall, these studies revealed that spirocyclic polyacetal-based assemblies are fully cytocompatible, interact avidly with the plasma membrane and can be ultimately uptaken by cells.

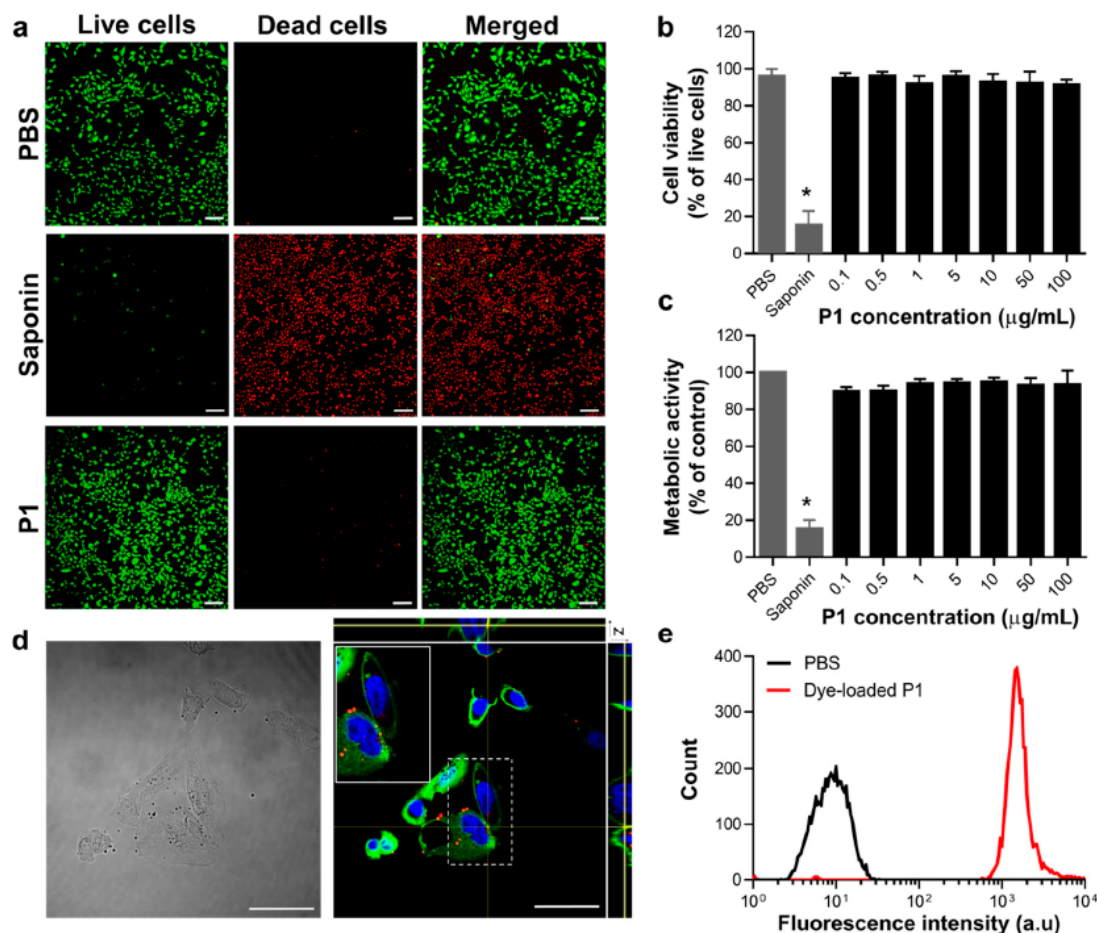


Figure 2.5. (a–c) CHO-K1 cells were treated for 24 h with increasing concentrations of **P1** and cell viability was measured by means of the (a, b) live/dead assay and by (c) resazurin-based metabolic activity. (a) Representative fluorescence microscopy images showing the distribution of lived (green; calcein AM) and dead (red; ethidium homodimer) cells after treatment with PBS saponin (10 $\mu\text{g/mL}$) or particles (100 $\mu\text{g/mL}$). The scale bar is 100 μm . (b, c) The data represent mean \pm S.D. of at least three independent experiments performed in triplicate. The results were analyzed using the student's t-test and the statistical difference (between vehicle-treated control cells (PBS) and treated cells) was established at * $p < 0.01$. (d) Representative differential interference contrast (DIC) and fluorescence confocal microscopy

images of CHO-K1 after 4 h incubation with 100 $\mu\text{g}/\text{mL}$ of dye-loaded particles (red). The plasma membrane is stained in green and the cell nucleus in blue. The scale bar is 50 μm . (e) A flow cytometry diagram showing the plasma membrane adsorption and cellular uptake of dye-loaded **P1**.

2.4 Materials and Methods

All chemicals were purchased from Sigma-Aldrich (St. Louis, MO, USA) or Alfa Aesar (Haverhill, MA, USA) and were used without further purification unless otherwise noted. Anhydrous N, N-dimethylformamide (DMF) was obtained from a solvent purification system using aluminum oxide columns. The reactions were mostly performed in air without the use of air- and moisture-free techniques using reagent grade solvents. The polymerization reactions were performed under argon using Schlenk line techniques and anhydrous DMF. Dialyses were performed using Spectra/Por regenerated cellulose membranes with a 3500 g/mol molecular weight cut-off (MWCO). ^1H - and ^{13}C -NMR spectra were recorded at 300 and 75 MHz, respectively, using CDCl_3 as solvent. Chemical shifts are reported in delta (δ) units, expressed in parts per million (ppm). Coupling constants (J) are expressed in hertz (Hz). The number-average molecular weight (M_n), weight-average molecular weight (M_w), and dispersity indices (\mathcal{D}) of polymers were determined by size exclusion chromatography (SEC) using an EcoSEC HLC-8320 (Tosoh Bioscience, Tokyo, Japan) instrument equipped with two TSKgel Alpha-M, 13 μm columns (7.8 mm ID X 30 cm L) and a TSKgel Alpha Guardcolumn (6.0 mm ID X 4 cm L) calibrated with poly (methyl methacrylate) standards in DMF containing 10 mM LiBr at 60 $^\circ\text{C}$. The samples were prepared at a concentration of 2 mg/mL in DMF and filtered through a 0.22 μm PTFE syringe filter prior to injection. The data were acquired at a flow rate of 1 mL/min at 60 $^\circ\text{C}$. Dynamic light scattering (DLS) data were obtained using a Zetasizer Nano ZS instrument from Malvern Instruments (Malvern, UK) at a polymer

concentration of 0.05 mg/mL. Fluorescence spectroscopy was performed with a Perkin Elmer LS45 Spectrofluorometer (Waltham, MA, USA). Samples were analyzed at a polymer concentration of 0.05 mg/mL. The excitation wavelength for acquiring the emission spectra was set at 552 nm. Differential scanning calorimetry (DSC) data were obtained using a DSC1 Mettler Toledo instrument (Columbus, OH, USA) with a heating/cooling rate of 10 °C/min between -30 and 100 °C under nitrogen atmosphere. The midpoint glass transition temperature (T_g) values were extracted from the second heating cycle. Atomic force microscopy (AFM) data were obtained using a Veeco/Bruker Multimode AFM (Billerica, MA, USA). One drop of the sample (0.05mg/mL) was deposited on a clean mica surface (12 mm diameter) and was left to dry overnight. They were then used for imaging the next day. Lastly, the samples for the transmission electron microscopy (TEM) were prepared by drop casting one drop (ca. 20 μ L) of the colloidal particle solution (1 mg/mL) onto a formvar carbon-coated copper grid rested on a piece of filter paper, which were left to dry overnight. The measurements were performed on a Joel JEM-2100F instrument (Tokyo, Japan) at 80kV. High-resolution mass spectrometry (HRMS) was performed using a Liquid Chromatography Mass Spectrometry Time of Flight (LC-MS TOF) mass analyzer (Agilent Technologies Santa Clara, CA, USA) in the electrospray mode.

2.4.1 Synthesis of Compound 2:

Compound **1** [**126**] (1.6 g, 4.5 mmol, 1.0 equiv.) was dissolved in acetonitrile (60 mL) in a 100 mL round bottom flask. Potassium carbonate (6.2 g, 45 mmol, 10 equiv.) was added slowly to the stirring solution over 10 min. Propargyl bromide (5.4 g, 45 mmol, 10 equiv.) was then added slowly and the solution was stirred under reflux (86 °C) for 20 h. After the removal of the round bottom flask from the oil bath, the solution was cooled down, after which acetonitrile was removed on a rotary evaporator. The residue was dissolved in equal in water/dichloromethane and transferred to a separatory funnel.

The aqueous phase was extracted with dichloromethane (3 x 30 mL). The combined organic layers were washed with brine (1 x 30 mL), dried over magnesium sulfate, filtered, and concentrated. The product was a light-yellow solid (1.2 g, yield = 64%). ¹H-NMR (300 MHz, CDCl₃, δ): 7.46 (d, J = 9 Hz, 2H, ArH), 7.00 (d, J = 9 Hz, 2H, ArH), 5.44 (s, 2H, CH–O₂), 4.86 (d, 2H, J = 9 Hz, O–CH₂–C), 4.70 (d, J = 3 Hz, 4H, CH₂C≡CH), 3.87–3.80 (m, 4H, O–CH₂–C), 3.64 (m, 2H, O–CH₂–C), 2.54 (t, 3H, J = 3 Hz, CH₂C≡CH). ¹³C-NMR (75 MHz, CDCl₃, δ): 158.1, 131.4, 127.4, 114.7, 102.0, 78.4, 75.7, 71.1, 70.6, 55.8, and 32.4. HRMS (EI, m/z): [M + H]⁺. Calculated for, C₂₅H₂₅O₆ 421.1651; found, 421.1643.

2.4.2. Synthesis of Compound 3:

This compound was synthesized according to a previously published procedure.^[130] Polyethylene glycol (M_n = 400 g/mol, 5.0 g, 12 mmol, 1.0 equiv.) was dissolved in dichloromethane (100 mL). Triethylamine (5.0 g, 50 mmol, 4.0 equiv.) was added slowly to the stirring solution, followed by 4-dimethylaminopyridine (3.0 g, 25 mmol, 2.0 equiv.) and *p*-toluenesulfonyl chloride (7.1 g, 38 mmol, 3.0 equiv.). The reaction was stirred at room temperature overnight. The organic layer was washed with HCl (2M, 2 x 30 mL), water (1 x 30 mL), brine (1 x 30 mL), dried over magnesium sulfate, filtered, and concentrated to remove dichloromethane. The product was a dark orange viscous oil (7.4 g, yield = 83%). ¹H-NMR (300 MHz, CDCl₃, δ): 7.77 (d, J = 6 Hz, 2H, ArH), 7.33 (d, J = 6 Hz, 2H, ArH), 4.14 ppm (t, J = 6 Hz, 4H, CH₂–OTs), 3.76–3.56 (m, 36H, O–CH₂–CH₂), 2.43 (s, 6H, CH₃).

2.4.3 Synthesis of Compound 4:

This compound was synthesized according to a previously published procedure.^[130] Polyethylene glycol (M_n = 600, 5.0 g, 8.3 mmol, 1.0 equiv.) was dissolved in a 250 mL

round bottom flask in dichloromethane (100 mL). Triethylamine (3.4 g, 33 mmol, 4.0 equiv.) was added slowly to the stirring solution, followed by 4-dimethylaminopyridine (2.0 g, 17 mmol, 2.0 equiv.) and p-toluenesulfonyl chloride (4.8 g, 25 mmol, 3.0 equiv.). The reaction was stirred at room temperature overnight. The organic layer was washed with HCl (2M, 2 x 30 mL), water (1 x 30 mL), brine (1 x 30 mL), dried over magnesium sulfate, filtered, and concentrated to remove dichloromethane. The product was a dark orange viscous oil (4.1 g, yield = 54%). ¹H-NMR (300 MHz, CDCl₃, δ): 7.75 (d, J = 6, 2H Hz, ArH), 7.31 (d, J = 6 Hz, 2H, ArH), 4.12 (t, J = 6 Hz, 4H, CH₂-OTs), 3.66–3.54 (m, 56H, O-CH₂-CH₂), 2.41 (s, 6H, CH₃).

2.4.4. Synthesis of Compound 5:

Compound 3 (7.4 g, 10 mmol, 1.0 equiv.) was dissolved in a 100 mL round bottom flask in DMF (70 mL). Sodium azide (14 g, 2.1 x 10² mmol, 20 equiv.) was added slowly to the stirring solution. The reaction mixture was stirred at 80 °C overnight. After the solution was cooled down, DMF was removed using a rotary evaporator. Portions of water/dichloromethane were added to the round bottom flask and transferred to a separatory funnel. Aqueous layer was extracted with dichloromethane (3 x 30 mL). The organic layers were combined and washed with brine (1 x 30 mL), dried over magnesium sulfate, filtered, and concentrated to remove dichloromethane. Product was obtained as a light orange viscous oil (3.2 g, 68% yield). ¹H-NMR (300 MHz, CDCl₃, δ): 3.80–3.54 (m, 32H, O-CH₂-CH₂), 3.27 ppm (t, J = 6 Hz, 4H, CH₂-N₃). ¹³C-NMR (75 MHz, CDCl₃, δ): 70.7, 70.7, 70.6, 70.6, 70.0, 50.7 ppm.

2.4.5. Synthesis of Compound 6:

Compound 4 (4.1 g, 4.5 mmol, 1.0 equiv.) was dissolved in a 100 mL round bottom flask in DMF (60 mL). Sodium azide (5.8 g, 90 mmol, 20 equiv.) was added slowly to

the stirring solution. The reaction mixture was stirred at 80 °C overnight. After the solution was cooled down, the DMF was removed using a rotary evaporator. Equal portions of water/ dichloromethane were added to the round bottom flask and transferred to a separatory funnel. The aqueous layer was extracted with dichloromethane (3 x 30 mL). The organic layers were combined and washed with brine (1 x 30 mL), dried over magnesium sulfate, filtered, and concentrated to remove dichloromethane. The product was obtained as a light orange viscous solid (2.0 g, yield= 67%). ¹H-NMR (300 MHz, CDCl₃, δ): 3.84–3.57 (m, 52H, O–CH₂–CH₂), 3.31 ppm (t, J = 6 Hz, 4H, CH₂–N₃). ¹³C-NMR (75 MHz, CDCl₃, δ): 70.7, 70.7, 70.6, 70.6, 70.0, 50.7 ppm.

2.4.6. Synthesis of Polymer 7:

A dry Schlenk flask was first purged with argon. Compound **5** (0.24 g, 0.53 mmol, 1.0 equiv.) was then added directly to the Schlenk flask, followed by compound **2** (0.24 g, 0.56 mmol, 1.05 equiv.), and anhydrous DMF (5 mL). While the mixture was stirring under argon, N, N, N', N'-tetramethylethylenediamine (TMEDA) (16 mg, 0.13 mmol, 0.25 equiv.) was added. The solution was saturated with argon. Copper(I) bromide (19 mg, 0.13 mmol, 0.25 equiv.) was added and the solution was freeze-pump-thawed three times to remove oxygen. The reaction mixture was placed in an oil bath pre-heated at 60 °C and stirred for 24 h. After the solution was cooled down, it was dialyzed against DMF for 24 h using a 3.5 K MWCO membrane where the dialysate was changed every 6 h. Afterwards, the DMF was removed under reduced pressure and the product was dissolved in chloroform. The solution was placed in an Erlenmeyer flask, where ammonia was added and stirred for 10 min (to remove the residual Cu catalyst). Both layers were transferred to a separatory funnel, where the organic layer was removed. The organic layer was repetitively placed in ammonia until the color remained constant. The organic layer was washed with brine (3 x 30 mL) dried over magnesium sulfate,

filtered, and concentrated to remove chloroform. Product was obtained as a light-yellow sticky solid (0.26 g, yield = 56%). ¹H-NMR (300 MHz, CDCl₃, δ): 7.79 (s, 2H, triazole ring) 7.38 (d, J = 9 Hz, 2H, ArH), 6.95 (d, J = 9 Hz, 2H, ArH), 5.37 (s, 2H, CH-O₂), 5.17 ppm (s, 4H, C-CH₂-O), 4.78 ppm (br. D, 2H, O-CH₂-C), 4.50 (br. S, 4H, O-CH₂-CH₂-N), 3.83-3.51 (m, 40H, CH₂ in PEG backbone and the rest of protons in spirocyclic skeleton). SEC: M_n = 15,900 g/mol, Đ = 2.47.

2.4.7. Synthesis of Polymer **8**:

A dry Schlenk flask was first purged with argon. Compound **6** (0.31 g, 0.48 mmol, 1.0 equiv.) was then added directly to the Schlenk flask, followed by compound **2** (0.21 g, 0.51 mmol, 1.05 equiv.) and anhydrous DMF (5 mL). While the mixture was stirring under argon, TMEDA (14 mg, 0.12 mmol, 0.25 equiv.) was added. The solution was saturated with argon. Copper(I) bromide (17 mg, 0.12 mmol, 0.25 equiv.) was added and the solution was freeze-pump-thawed three times to remove oxygen. The reaction mixture was placed in an oil bath pre-heated at 60 °C and stirred for 24 h. After the solution was cooled down, it was dialyzed against DMF for 24 h using a 3.5 K MWCO membrane in, where the dialysate was changed every 6 h. Afterwards, DMF was removed under reduced pressure and the product was dissolved in chloroform. The solution was placed in an Erlenmeyer flask, where ammonia was added and stirred for 10 min (to remove the residual Cu catalyst). Both layers were transferred to a separatory funnel, where the organic layer was removed. The organic layer was repetitively placed in ammonia until the color remained constant. The organic layer was washed with brine (3 x 30 mL) dried over magnesium sulfate, filtered, and concentrated to remove chloroform. The product was obtained as a light-yellow sticky solid (0.34 g, yield = 65%). ¹H-NMR (300 MHz, CDCl₃, δ): 7.81 (s, 2H, triazole ring), 7.37 (d, J = 9 Hz, 2H, ArH), 6.95 (d, J = 9 Hz, 2H, ArH), 5.37 (s, 2H, CH-O₂), 5.17 ppm (s, 4H, C-CH₂-O), 4.78 ppm (br. D, 2H, O-CH₂-C), 4.50 (br. S, 4H, O-CH₂-

CH₂-N), 3.83–3.51 (m, 58H, CH₂ in PEG backbone and the rest of protons in spirocyclic skeleton). SEC: M_n = 73,000 g/mol, Đ = 3.07.

2.4.8. Procedure for the Self-Assembly of (7) and (8):

To obtain 1 mg/mL solutions of the self-assembled materials, 5 mg of polymers (7) and (8) were separately dissolved in dimethyl sulfoxide (DMSO) (0.5 mL) and sonicated for 5 min to ensure their complete dissolution. To this solution, filtered nanopure water (4.5 mL) was added dropwise while stirring. Following the formation of particles, the samples were dialyzed against deionized (DI) water using a 3500 MWCO membrane for 24 h with multiple changes of the dialysate. The resulting assemblies were then used for characterization by DLS, AFM, and TEM.

2.4.9. Procedure for the Encapsulation of Nile Red by Particles Formed by Polymer (7):

To encapsulate Nile red in the assemblies formed from polymer (7), the above-mentioned procedure for the particle formation was employed except that the initial solution of (7) in DMSO contained 1% w/w Nile red.

2.4.10. Procedure for the Degradation Study of Polymers (7) and (8) by ¹H-NMR:

To study the degradation of (7) and (8) by ¹H-NMR, these polymers were separately dissolved in trifluoroacetic acid (TFA)-containing deuterated chloroform (CDCl₃) (80mM, 1 mL) and NMR spectra were obtained at the specified time points. We would like to note that our attempts to carry out this experiment in mixtures of organic solvents, such as dioxane, acetone, and DMSO, and water were met with very limited success as the polymers readily precipitated in such media.

2.4.11. Procedure for Nile Red Release Study:

To study the release of Nile red from particles formed by (7), as detailed above, the preformed dye-encapsulated assemblies (150 μL , 1 mg/mL) were added to phosphate buffer (2.85 mL, 10 mM) at pH 5.5 and 7.4 in quartz cuvettes preheated at 37 °C in a water bath. Fluorescence spectra were acquired at the specified time points, with an excitation wavelength of 552 nm, and the samples were rapidly placed back in water bath to minimize any significant drop in temperature. At the end of the release studies, the same samples were used to measure the size of particles by DLS.

2.4.12. Procedure for Cell Viability Assays:

Chinese hamster ovary cells K1 (CHO K1; from ATCC, Manassas, VA, USA) were maintained in Ham's F12 medium supplemented with 10% fetal bovine serum (FBS), 2 mM L-glutamine and antibiotic antimycotic (10,000 UI/mL penicillin, and 10,000 UI/mL streptomycin). The cells were maintained as a monolayer at 37 °C in a humidified atmosphere of 5% CO₂ and 95% air and passaged by trypsinization when the cells reached around 80% confluence. For the LIVE/DEAD assay, CHO K1 were seeded in 12-well plates at a density of 60,000 cells/well and incubated overnight at 37 °C. The cells were then treated with the direct addition of particle solutions (diluted in PBS) to reach the final desired concentrations. After 24 h incubation, the medium was removed and LIVE/DEAD reagent solution (4 μM ethidium homodimer-1; 2 μM calcein-AM) in sterile PBS was added in each well. After incubation for 45 min, the samples were analyzed using a fluorescent microscope with a 20x objective lens. At least three images per well were taken and processed using ImageJ software. The percentage of cell viability was calculated as the viable cells (green labelled) over the total number of cells (green + red). For the metabolic assay, CHO K1 cells were seeded in black-wall clear-bottom 96-well plates at a density of 30,000 cells/well and

incubated overnight at 37 °C in a 5% CO₂. The cells were treated by the direct addition of particle solutions (diluted in PBS) to reach the final desired concentrations. After 24h incubation, cellular viability was measured by the resazurin reduction assay. Cell viability (in %) was calculated from the ratio of the fluorescence of the treated sample to the vehicle-treated control cells (PBS). The data of at least three independent experiments were averaged and expressed as the mean \pm S.D. The results were analyzed using the student's t-test and statistical difference was established at $p < 0.01$. Statistical analysis was performed using Prism 6.0 software.

2.4.13. Procedure for Evaluation of Cellular Uptake:

CHO K1 cells were cultured on coverslips for 24 h at 60,000 cells/well in 8-well cell culture chamber. The cells were washed with PBS and incubated with particles (100 μ g/mL) at 37 °C for 4 h. The cells were then washed three times with PBS, fixed with 4% paraformaldehyde (Santa Cruz) and stained with 1 μ g/mL DAPI (40,6-Diamidino-2-phenylindole dihydrochloride) for the nucleus and FAST DiO for the plasma membrane. The cover glasses were mounted, and the fluorescence was analyzed with a confocal microscope using a 60x oil immersion lens. The images were analyzed using ImageJ software. For flow cytometry analysis, the cells were seeded in 12-well plates at a density of 60,000 cells/well overnight. The cells were treated by the direct addition of dye-loaded particles (diluted in PBS) to reach a final concentration of 100 μ g/mL. After incubation for 4 h, the cells were washed 3 times with PBS buffer and harvested. Cells were suspended in PBS buffer prior to flow cytometry analysis.

2.5 Conclusion:

In summary, we demonstrated a Cu-catalyzed azide-alkyne “click” polymerization approach to synthesize amphiphilic spirocyclic polyacetals using diazide-

functionalized PEG and dialkyne-decorated spirocyclic acetal monomers. The resulting polymers exhibit low T_g values rendering them amorphous at ambient temperature. Degradation of these polymers in acidic $CDCl_3$ showed a gradual decomposition of the starting polymers and formation of their starting constituents as evidenced by 1H -NMR. In addition, it was shown that these amphiphilic spirocyclic polyacetals are able to undergo self-assembly in DMSO/ H_2O mixture to form particles with diameters of ~ 400 nm. Furthermore, by means of Nile red encapsulation and in vitro release experiments, we demonstrated that these materials possess an amphiphilic core, rendering them leaky at neutral pH with the preservation of particle integrity, as evidenced by DLS measurements. Nevertheless, efficient Nile red release and the complete degradation of these materials were achieved at $pH = 5.5$. To show the potential application of this system in nanomedicine, cellular assays demonstrated the nontoxic nature of these self-assembled materials. Moreover, these particles bind to the cell surface and can be taken up by CHO-K1 cells and ultimately transport their encapsulated cargo into cells. Our results show that the spirocyclic polyacetal-based particles are promising candidates for biomedical applications.

CHAPTER III

SYNTHESIS AND SELF-ASSEMBLY OF AMPHIPHILIC JANUS DENDRIMERS WITH AGGREGATION-INDUCED EMISSION PROPERTY TO POTENTIAL THERANOSTICS

Publication of interest: The manuscript resulting from the work described in the Chapter is currently in preparation and will be submitted to Chemical Communications. “Size-tunable fluorescent dendrimersomes” Bélanger-Bouliga, Marilyne[‡]; Andrade-Gagnon, Brandon[‡]; Thi Hong Nguyen, Diep; Nazemi, Ali ([‡]These authors have contributed equally to this work). The project described in this chapter was proposed by Dr. Ali Nazemi. The synthesis of the dendrimers was accomplished by the author under the supervision of Dr. Nazemi. All self-assembly studies as well as the characterization of the dendrimersomes by DLS and TEM were accomplished by Marilyne Bélanger-Bouliga under the supervision of Dr. Nazemi. Diep Thi Hong Nguyen performed the DSC measurements and analyses of the dendrons and dendrimers. The manuscript was drafted by Dr. Nazemi with input from the coauthors.

3.1 Abstract:

Janus dendrimers, unlike conventional dendrimers, provide asymmetry and can impart significantly different chemical and/or physical properties. The broken symmetry offers new and efficient characteristic properties to form complex self-assembled materials, such as cubosomes, tubular vesicles, helical ribbons and bilayered vesicles (dendrimersomes), which provide monodispersity and stability of up to one year in

various media. This has provided applications towards:(i) dendritic conjugation of a drug to a Janus dendrimer, (ii) self-assembly to form various nanostructures as drug delivery vehicles and (iii) as biologically active molecules and excipients, such as antibacterial and penetration enhancers. The dendritic peripheral groups can be used to attach various functional molecules to Janus dendrimers. Here, we present the synthesis of amphiphilic Janus dendrimers with aggregation-induced emission (AIE) properties via the attachment of tetraphenylethylene (TPE) moieties, a known molecule to efficiently undergo AIE, to dendritic backbone. The self-assembly behaviour of three generations of these Janus dendrimers to various structures will be discussed. The amphiphilic nature of our Janus dendrimers and their AIE properties can lead to potential investigation of applying therapeutic drugs with their inherent diagnostic capabilities to form a theranostic system.

3.2 Introduction:

Natural and synthetic macromolecules have been used as vehicles for the delivery of drugs and gene therapy, as well as diagnostic agents.[71] Macromolecules are hypothesized to protect the molecule of interest from undesirable interactions with biological components, along with improving its solubility in aqueous medium. Several carriers have been studied: linear polymers, micellar assemblies, liposomes, polymersomes, and, more recently, dendritic structures (dendrimers and dendrons).[1] The ideal carrier should facilitate high drug loading, long blood circulation time, high accumulation in the desired tissue, low toxicity, low immunogenicity, simplicity in its preparation, and, preferably, adequate biodegradability.[1, 5, 71] Dendrimers are a class of highly branched polymers that are synthesized through a step-by-step growth, affording a perfectly defined and highly reproducible 3-dimensional architecture.[16] A dendrimer's uniform and well-defined size and shape are of interest in biomedical

applications because of their ability to cross cellular membranes, reduce the risk of primitive clearance from the body, and because of high level of control over their architecture.[62] Traditional dendrimers are symmetrical and possess a single type of terminal group due to their ease of synthesis. However, it has been shown that having two (or more) types of terminal groups is highly desirable to combine several properties within a single molecule.[17] In order for the dendritic structure to contain two or more terminal groups, it would have to be composed of at least two halves, each having different sizes and/or number of terminal groups. These types of dendrimers are referred to as Janus dendrimers, representing the two-faced Roman God.[17]

Amphiphilic Janus dendrimers are promising candidates for developing drug carriers. Different from conventional dendrimers, they provide asymmetry and can impart significantly different chemical and/or physical properties within a single molecule.[105] The broken symmetry is composed of a polar (hydrophilic) and non-polar (hydrophobic) dendritic blocks, where the hydrophobic block is the driving force for the spontaneous self-assembly of Janus dendrimers in water to form complex structures that are presently unattainable for conventional dendrimers. These include cubosomes, tubular vesicles, helical ribbons and bilayered vesicles (also termed dendrimersomes).[28] These self-assembled materials provide monodispersity, stability of up to one year in various media and encapsulation of both hydrophilic and hydrophobic species. [28, 99] These sophisticated structures have allowed the drug delivery field to expand, where it has been subdivided into three main categories: (i) dendritic conjugation of a drug to a Janus dendrimer, (ii) self-assembly to form drug delivery systems and (iii) as biologically active molecules and excipients, such as antibacterial and penetration enhancers.[94, 101, 114, 131] Of all the various morphologies, the characteristics of dendrimersomes make them ideal vehicles for drug delivery, as they contain the stability and the mechanical strength of polymersomes, while maintaining the biological functions of phospholipid liposomes.[28, 99] In

addition, the hydrophobic membrane of the dendrimersomes are capable of trapping hydrophobic drugs while their aqueous interior can be used to encapsulate hydrophilic molecules at the same time.

The dendrimer's surface groups, besides determining predominantly their physicochemical properties, will also determine their biological activity and biocompatibility.[71] This can provide an opportunity for advances in cancer diagnostics due to their versatility, size, and physicochemical characteristics.[32] The peripheral surface groups allow flexible functionalization to have therapeutic and diagnostic agents to be covalently conjugated to the surface, providing customized detection of cancer-specific biomarkers. The combination of using one radioactive drug to identify (diagnose) and a second radioactive drug to deliver therapy to treat specific metastatic cancerous cells is termed as theranostic materials.[32] Theranostics have the potential to improve treatment efficiency and reduce the side effects caused by image-guided therapy.[32] To date, various imaging methods have been adopted for cancer diagnosis, including ultrasound, computed tomography (CT), positron emission tomography (PET), and magnetic resonance imaging (MRI).[132] However, these imaging techniques have some drawbacks, including (i) poor resolution, (ii) potential radiation damage, and (iii) high equipment costs.[132] To overcome these challenges, fluorescence imaging has been introduced as it has significant advantages of high spatial resolution, good biocompatibility, low cost, and easy accessibility.[132] Traditional fluorophores, such as green fluorescent proteins, which are held together by non-covalent interactions, suffer from aggregation-caused fluorescence quenching (ACQ).[122, 132] This occurs due to the intermolecular π - π stacking interactions, leading to high background noise in dilute solution, poor photostability, and difficulties associated with combining them with therapeutic functions. In contrast to conventional fluorophores, luminogens with aggregation-induced emission (AIE) characteristics emit weakly in solution but show bright emission in their aggregated/solid state.[36,

64] AIE luminogens have significant advantages in terms of excellent photostability and the lack of self-quenching. One structural feature required for a fluorophore to show AIE characteristics is based on the presence of several aromatic rings, typically connected to a central core, containing very low rotational energy barrier.[**36, 64, 98, 122, 132]** A well studied AIE luminogen is tetraphenylethylene (TPE), which has rich electrochemical and excited state properties, along with extensive usage as an electron transfer catalyst in a variety of polymerization reactions.[**52, 57]** Structural relaxations are effective upon photoexcitation, causing deactivation of the excited states of TPE molecules, making them almost non-emissive in solution. However, in its aggregated state, TPE fluorescence becomes significantly enhanced, inhibiting the internal rotation and torsion that are responsible for non-radiative pathways.[**52, 57]** It is also possible to inhibit the internal rotation and torsion by modifying the TPE framework or by linking appropriate groups to the TPE core. One such example is when the phenyl rings are connected through shorter hydrocarbon bonds, the framework becomes more rigid.[**52, 57]**

Luminescent dendrimers fall into two classes: (i) fully conjugated dendrimers and (ii) non-conjugated dendrimers functionalized with chromophores.[**37, 52, 64]** The first dendrimer class provides an advantage in its conjugation by forming a rigid framework, enabling easily understood structure-property relationships. Nevertheless, dendrimers with π -extended structures are associated with growth and stability problems.[**37, 52, 64]** The non-globular, planar shapes of these systems often bring about π -stacking of molecules with loss of the luminescent properties. The second dendrimer class has flexible branches and photo- and/or electroactive units in the different regions of the structure, where these units can be bonded in a covalent or non-covalent approach.[**37, 52, 64]** Dendrimers of this type have been modified mainly in the periphery. However, it should be noted that structure-property relationships are more difficult to determine and predict in materials with flexible branches.[**37, 52, 64]** Most reported luminescent

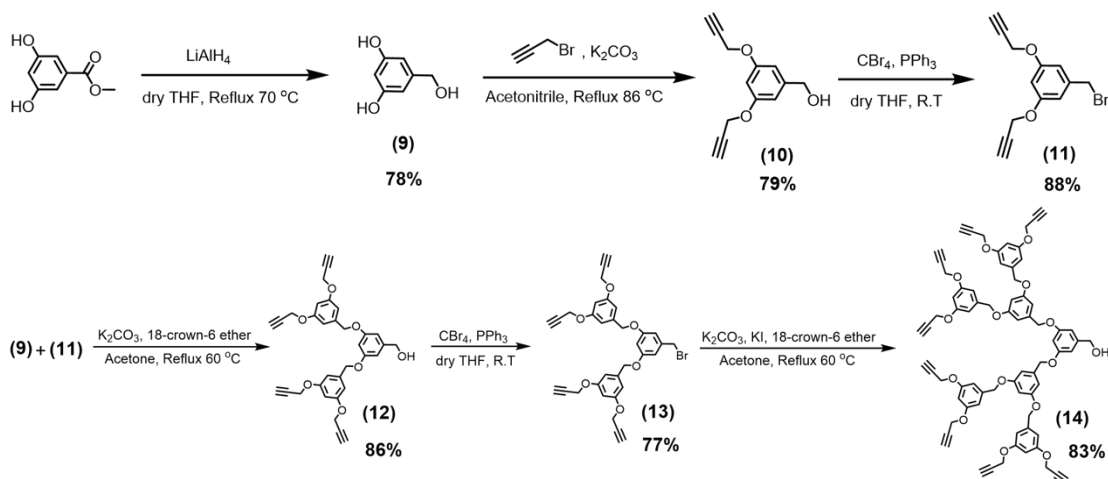
dendrimers involve the conjugation of two-photon absorption (TPA), pyrene and carbazole and their derivatives.[108] Reports with dendrimers conjugated to TPE mainly involve TPE compounds acting as the core, capped with dendrons of different generations.[37, 52, 64] Luminescent Janus dendrimers have been rarely reported. Two main articles have been the initial reports of Janus dendrimers conjugated to TPE, in which only 2-dimensional sheets were obtained from the self-assembly of TPE-functionalized Janus dendrimers. These studies mainly focused on the application of such sheets as supports for the immobilization of gold nanoparticles and for the capture and agglutination of Escherichia Coli (E. Coli).[65, 66] Herein, we report the synthesis of three generations of TPE-conjugated amphiphilic aryl ether-based Janus dendrimers using copper-(II)-catalyzed alkyne-azide cycloaddition (CuAAC) “click” reaction as an alternative method to the existing approaches. These amorphous monodisperse amphiphilic Janus dendrimers contain AIE properties that demonstrate an increase in luminescent intensity with each generation. The π - π stacking of the aromatic rings of the highly conjugated TPE molecules will drive the self-assembly of the amphiphilic Janus dendrimers, which can not only encapsulate a target drug but render the assemblies emissive, leading to a potential image-guided therapy material.

3.3 Results and Discussion:

3.3.1 Synthesis of Hydrophobic Aryl Ether-Based Dendrons:

The main component for the synthesis of the amphiphilic Janus dendrimers is the aryl ether-based dendrons (**Scheme 3**). These dendrons have already been synthesized and fully characterized according to literature; therefore the compounds will be characterized only by proton nuclear magnetic resonance ($^1\text{H-NMR}$).[85] Initially, methyl-3,5-dihydroxybenzoate is reduced to its benzyl alcohol derivative (**9**) using lithium aluminium hydride. Based on $^1\text{H-NMR}$, the main peaks of interest are the

disappearance of the methoxy group at 3.76 ppm and the appearance of a triplet at 4.98ppm corresponding to the benzyl hydroxy group, as well as the doublet at 4.29ppm corresponding to the methylene group adjacent to the benzyl hydroxy group (**Appendix B, Figure B1**). From there, the peripheral phenolic hydroxy groups of (**9**) were reacted with propargyl bromide under basic condition to give the first generation hydrophobic dendron (**10**). Successful attachment of the alkynes is presented in the $^1\text{H-NMR}$ by the appearance of a doublet at 4.68 ppm corresponding to the methylene group adjacent to the alkyne, and the triplet at 2.53 ppm for the terminal proton on the alkyne (**Appendix B, Figure B2**). The benzylic hydroxyl dendron (**10**) was brominated at the focal point using carbon tetrabromide and triphenyl phosphine to synthesize the brominated benzylic dendron (**11**). Based on $^1\text{H-NMR}$, attachment of bromine at the focal point is based on the disappearance of the singlet at 4.65 ppm corresponding to the benzylic hydroxyl group, and the appearance of the singlet at 4.42 ppm for the benzylic brominated focal point (**Appendix B, Figure B3**). To synthesize the second generation dendron (**12**), (**11**) was reacted with (**9**) under basic condition. The $^1\text{H-NMR}$ showed disappearance of benzylic bromide and provided two sets of doublets and triplets in the aromatic region between 6.68-6.50 ppm, a singlet at 4.98 ppm for the interior benzylic groups and the singlet at 4.63 ppm corresponding to the benzylic hydroxyl focal point (**Appendix B, Figure B4**). The bromination of (**12**) was repeated under the same conditions as (**11**) to synthesize (**13**), with the same observation of shift in the singlet peak for the benzylic focal point (**Appendix B, Figure B5**). Lastly, the third generation dendron (**14**) was synthesized using (**13**) reacting with (**9**) under basic condition. The $^1\text{H-NMR}$ showed disappearance of benzylic bromide and provided three sets of doublets and triplets in the aromatic region between 6.67-6.47 ppm, two singlets at 4.98ppm and 4.95 ppm for the interior benzylic groups and the singlet peak at 4.61 ppm corresponding to the benzylic hydroxyl focal point (**Appendix B, Figure B6**).

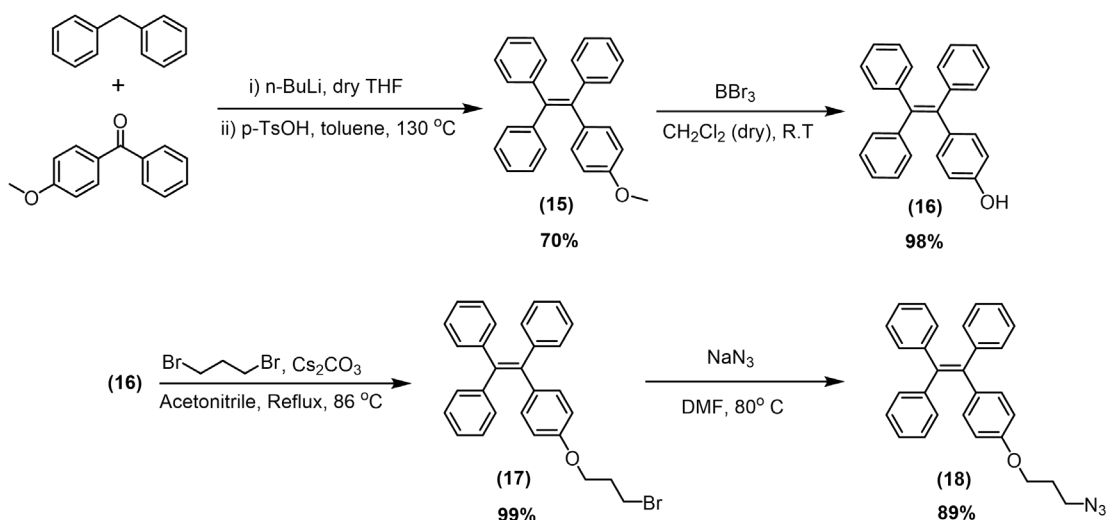


Scheme 3. Synthetic approach to three generations of hydrophobic aryl ether-based dendrons.

3.3.2 Synthesis of the Azido-Functionalized Tetraphenylethylene:

Azido-propoxy tetraphenylethylene (TPE) (**Scheme 4**) has already been synthesized according to the literature; therefore the compounds will be characterized only by $^1\text{H-NMR}$.^[7, 115] The synthesis of the methoxy-functionalized TPE (**15**) is divided into two synthetic steps. Initially, the lithiation product of diphenylmethane is reacted with 4-methoxybenzophenone to afford the corresponding alcohol. This is followed by dehydration using an acid catalyst (para-toluenesulfonic acid) to produce the methoxy-functionalized TPE. Successful synthesis of the methoxy-functionalized TPE (**15**), based on $^1\text{H-NMR}$, is the presence of multiplets between 7.11-7.02 ppm, the two sets of doublets at 6.93 ppm and 6.63 ppm corresponding to the para-substituted aromatic ring, and the singlet at 3.74 ppm corresponding to the methoxy group (**Appendix B, Figure B7**). The synthesis of hydroxy-functionalized TPE (**16**) is accomplished via the deprotection of (**15**) using boron tribromide. Main peak of interest by $^1\text{H-NMR}$ for successful deprotection is the disappearance of the methoxy peak and the appearance

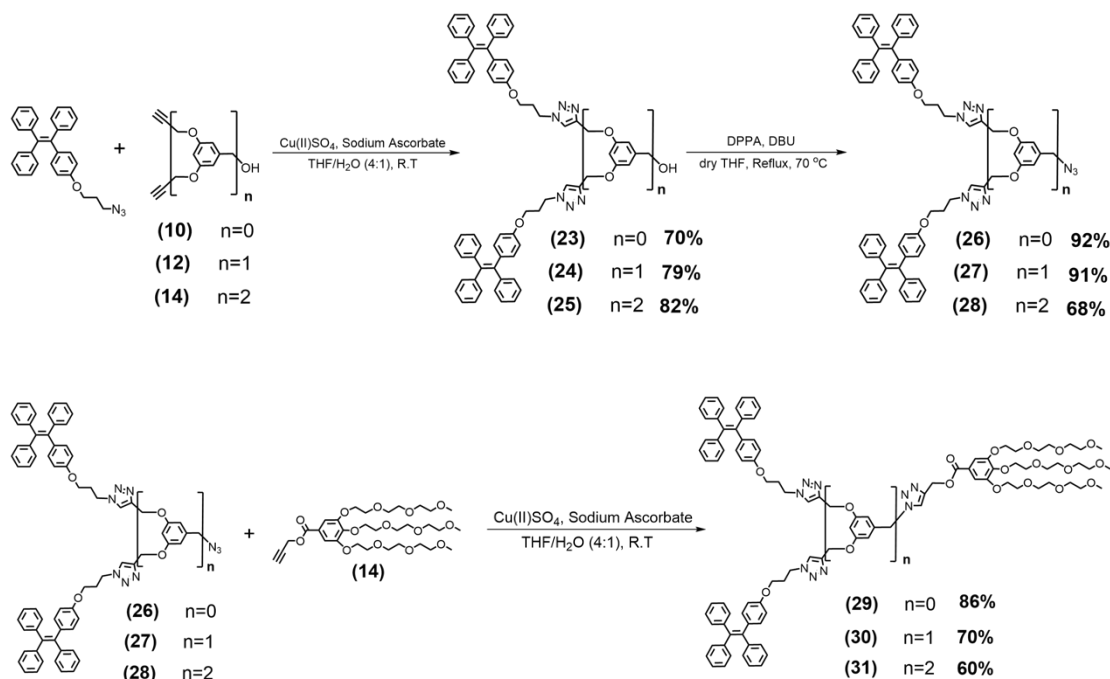
of a singlet at 9.34 ppm, corresponding to the hydroxy peak (**Appendix B, Figure B8**). Using the hydroxy-functionalized TPE (**16**), it was reacted with 1,3-dibromopropane to synthesize the bromo-propoxy TPE (**17**). Main peaks of interest by $^1\text{H-NMR}$ for successful alkylation are the triplet at 4.02 ppm corresponding to the methylene peak adjacent to the oxygen, the triplet at 3.58 ppm for the methylene adjacent to the bromide and quintet at 2.28 ppm for the methylene group in between the oxygen and bromide (**Appendix B, Figure B9**). Lastly, the bromo-propoxy TPE (**17**) was reacted with sodium azide to synthesize the desired azido-propoxy TPE (**18**). Main peaks of interest by $^1\text{H-NMR}$ for successful azido group attachment is the shift in the triplet from 4.02 ppm to 4.00 ppm, shift in triplet from 2.58 ppm to 3.52 ppm, and the shift in quintet from 2.28 ppm to 2.04 ppm (**Appendix B, Figure B10**).



Scheme 4. Synthetic approach to azido-functionalized tetraphenylethylene derivative **18**.

3.3.3 Synthesis of Hydrophilic Alkyne-Functionalized Oligo(ethylene Glycol)-decorated Gallate:

The hydrophilic alkyne-functionalized oligo(ethylene glycol)-decorated gallate was synthesized and fully characterized according to the literature; therefore, the compounds will be characterized only by $^1\text{H-NMR}$. [129, 133, 141] Initially, triethylene glycol (TEG) monomethyl ether was reacted with tosyl chloride under basic condition to form the tosylated TEG (**19**). $^1\text{H-NMR}$ indicated the presence of tosyl group based on the two sets of doublets at 7.77 ppm and 7.31 ppm corresponding to the aromatic ring, as well as the singlet at 2.42 ppm corresponding to the methyl group (**Appendix B, Figure B11**). From there, 3,4,5-trihydroxybenzoate was reacted with (**19**) under basic condition to synthesize the oligoethylene glycol gallate (**20**). Main peaks of interest, determined by $^1\text{H-NMR}$, were the disappearance of the aromatic peaks for the tosyl group, along with the methyl group, and the appearance of a singlet at 7.29 ppm corresponding to the gallate aromatic protons, and the singlet at 3.90 ppm to indicate the methoxy peak (**Appendix B, Figure B12**). The gallate derivative (**20**) was then hydrolyzed using sodium hydroxide to synthesize the gallic acid derivative (**21**). Based on $^1\text{H-NMR}$, the only observation to indicate successful hydrolysis is the removal of the methoxy peak at 3.90 ppm (**Appendix B, Figure B13**). Lastly, (**21**) was reacted with propargyl bromide under basic condition to synthesize the desired hydrophilic alkyne-functionalized oligo(ethylene glycol) gallate (**22**). Main peaks of interest based on $^1\text{H-NMR}$ are the presence of the doublet at 4.88 ppm corresponding to the methylene group adjacent to the alkyne and the triplet at 2.50 ppm corresponding to the alkyne proton (**Appendix B, Figure B14**).



Scheme 6. Synthesis of TPE-functionalized dendrons (**top**) and the amphiphilic Janus dendrimers (**bottom**).

We initially began with the attachment of the azido-propoxy TPE (**18**) to the periphery of each hydrophobic aryl ether-based dendron (**10**), (**12**), and (**14**) via CuAAC. The CuAAC reaction was successful using copper (II) sulfate and sodium ascorbate, where the $^1\text{H-NMR}$ s for each TPE-conjugated dendron demonstrated the appearance of the triazole rings, represented as a singlet at 7.60 ppm, with the respected number of protons for each generation. In addition, there is the appearance of a singlet at 5.14ppm, corresponding to the methylene group adjacent to the triazole rings (**Appendix B, Figures B15, B17, and B19**). Since these dendrons have not been reported before, they were fully characterized by $^{13}\text{C-NMR}$ and infra-red (IR) spectroscopies, size exclusion chromatography (SEC), high-resolution mass spectrometry (HR-MS), thermogravimetric analysis (TGA), differential scanning calorimetry (DSC), and UV-Vis and fluorescence spectroscopies. To obtain the desired dendrons before attachment to the hydrophilic segment, dendrons (**23**), (**24**), and (**25**) were reacted with diphenyl

phosphoryl azide (DPPA) under basic condition to attach the azide units to the focal point of each dendron. Successful synthesis of azide-functionalized TPE-conjugated dendrons **(26)**, **(27)**, and **(28)** was initially shown by $^1\text{H-NMR}$, where the benzylic hydroxyl group at 4.60 ppm was eliminated, and the appearance of a singlet at 4.25 ppm corresponding to the benzylic azido group (**Appendix B, Figures B21, B23, and B25**). Since these dendrons have also not been synthesized before, they were fully characterized by $^{13}\text{C-NMR}$ and IR spectroscopies, HR-MS, TGA, DSC, SEC analysis, and UV-Vis and fluorescence spectroscopies. To render the final dendrimers and their corresponding assemblies dispersible in aqueous media, we chose to synthesize an alkyne-functionalized oligo(ethylene glycol) gallate as the complementary hydrophilic segment.**[65, 66]** Both segments were conjugated under the same CuAAC condition as for the dendrons conjugated to TPE. In these reactions, a slight excess of the hydrophobic segment was used to maximize the possibility of purified high yielding dendrimers, as it was noticed that the hydrophilic segment would be challenging to successfully separate through thin-layer chromatography. The amphiphilic Janus dendrimers **(29)**, **(30)**, and **(31)** were fully characterized by $^1\text{H-}$ and $^{13}\text{C-NMR}$ spectroscopy, HR-MS, IR, TGA, DSC, SEC analysis and UV-Vis and fluorescence spectroscopies. While each dendrimer has been fully characterized, the third generation Janus dendrimer **(31)** shall be discussed as it is considered the unknown compound and similar synthesis has been done on the first and second generation. The successful conjugation of both segments was initially proven by $^1\text{H-NMR}$ (**Figure 3.1**), where the 1,4-disubstituted 1,2,3-triazole rings overlapped with the triazole rings shown for the peripheries of the hydrophobic segment at 7.62 ppm (**shown in blue**). In addition, the presence of a singlet at 5.38 ppm corresponds to the methylene protons adjacent to both sides of the triazole ring (**shown in green**), along with the disappearance of the alkyne doublet at 4.88 ppm and the triplet at 2.51 ppm of the hydrophilic segment. Similar patterns were observed for **(29)** and **(30)**, where each generation corresponded to a certain number of protons for the triazole peaks (**Appendix B, Figures B27 and B29**).

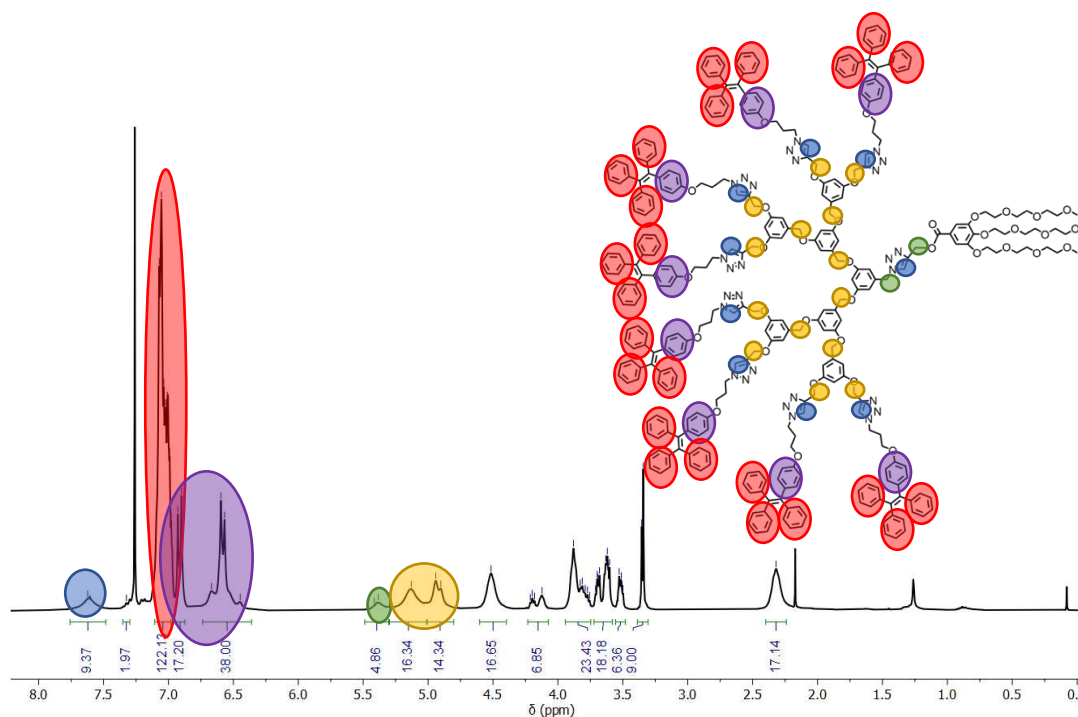


Figure 3.1. ^1H NMR of the third generation amphiphilic Janus dendrimer (**31**). Triazole rings are represented in blue, non-substituted TPE aromatic rings represented in red, para-substituted TPE aromatic rings represented in purple, methylene groups adjacent to junction triazole ring represented in green and methylene benzylic groups represented in yellow.

For IR spectroscopy, the main peaks of interest to confirm successful synthesis of the dendrimers were the disappearance of the dendron's azide peak at 2094 cm^{-1} , along with the C-O stretching of the ester peaks at 1178 cm^{-1} . In all the spectra, we observed the alkane C-H stretching ranging from 3048 cm^{-1} to 2622 cm^{-1} , the C-H bending at 1460 cm^{-1} , the C-O stretching of alkyl aryl ether peaks at 1239 cm^{-1} , and the aromatic C=C of disubstituted and trisubstituted stretching peaks at 1046 cm^{-1} and 697 cm^{-1} , respectively (**Appendix B, Figures B32, B33 and B34**).

3.3.5 Characterization of the Amphiphilic Janus Dendrimers:

To confirm dendrimers were obtained with monodisperse molecular weights, SEC analysis was performed on each corresponding dendron, and dendrimer represented by their refractive index (RI) trace (**Figure 3.2**). As observed, the shift in SEC traces for each dendron going to its respective dendrimer indicates complete consumption of dendrons and successful synthesis of dendrimers. It is important to note that while the traces for dendrons **(23)**, **(24)** and **(25)** are not shown below as there is little shift in comparison to dendrons **(26)**, **(27)** and **(28)**, their important values are indicated in the preceding table.

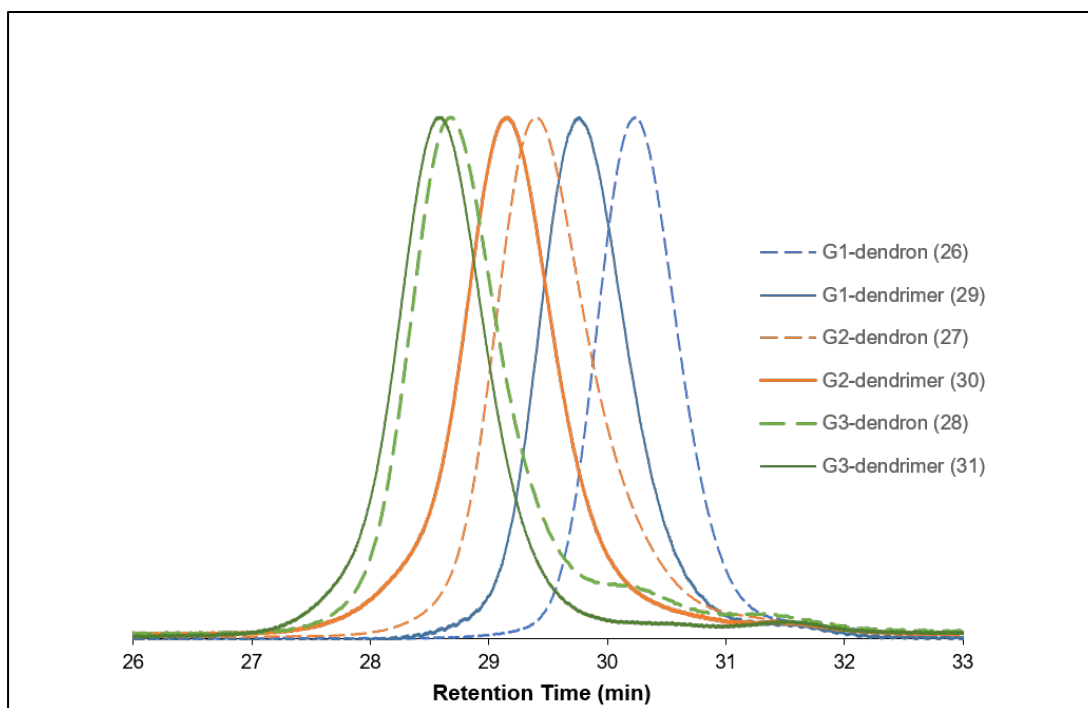


Figure 3.2. SEC refractive index of TPE-conjugated dendrons (**dashed lines**) and Janus dendrimers (**solid lines**).

For more details, **Table 3.1** indicates that the first generation dendron/dendrimer **(23)**, **(26)**, & **(29)** contain number average molecular weight (M_n) values of 1600 g/mol, 1600

g/mol and 2200 g/mol, respectively, with dispersity indices (D) between 1.05-1.07. Similar pattern is shown for the second generation (**24**, **27**, & **30**) where M_n values of 2300 g/mol, 2500 g/mol and 3300 g/mol were obtained respectively, with dispersity indices between 1.01-1.16. The third generation (**25**, **28**, & **31**) provided M_n values of 3900 g/mol, 4400 g/mol and 4700 g/mol, respectively, and dispersity indices between 1.07-1.13. The dispersity values for all TPE-conjugated dendrons and Janus dendrimers indicated monodispersity, which is expected, considering they possess defined molecular weights.

Table 3.1: Summary of SEC analysis for each dendron/dendrimer.

Dendron/Dendrimer	M_n (g/mol)	D
G1-OH (23)	1600	1.06
G1-N ₃ (26)	1600	1.07
G1-amphiphilic (29)	2200	1.08
G2-OH (24)	2300	1.17
G2-N ₃ (27)	2500	1.12
G2-amphiphilic (30)	3300	1.01
G3-OH (25)	3900	1.11
G3-N ₃ (28)	4400	1.14
G3-amphiphilic (31)	4700	1.08

Further characterization was performed on the dendrons and dendrimers through differential scanning calorimetry (DSC) to gain insight into the thermal behaviour (glass transition temperature) of each TPE-conjugated dendron and the effect of the hydrophilic segment attachment on their thermal behaviour. The thermal properties of the obtained dendrons and dendrimers (**Table 3.2**) can be correlated directly to their structure, and, to some extent, their molecular weight. When comparing the respective dendrons, we observed that going from the first to the second to the third generation,

there is an increase in their glass transition temperature (T_g). This is directly affected by the increase in conformational rigidity. However, it is observed that the T_g for the third generation provides a slight decrease in temperature; this is a result of the spatial disposition and the folding of the peripheries.[90] A similar trend occurs for the comparison of the respective dendrimers. What is of particular interest is the change in glass transition temperature going from each dendron to its respective dendrimer, where there is a substantial decrease (**Appendix B, Figures B35, B36 and B37**). Conjugation of the hydrophilic segment to the focal point of the TPE-conjugated dendrons leads to an enhanced solubility of the dendrimers, allowing spatial disposition and folding of the peripheries, directly influencing the glass transition temperature.[55, 90, 97, 106]

Table 3.2: Summary of DSC analysis for each dendron/dendrimer.

Generations	Glass Transition Temperature (measured by DSC)	
	Dendron	Dendrimer
G1	72 °C	25 °C
G2	102 °C	58 °C
G3	99 °C	77 °C

3.3.6 AIE Absorption and Emission Properties:

The optical properties of each TPE-conjugated dendrimer were investigated by UV-Vis absorption and fluorescence emission spectroscopies, which were studied at the same concentration of 17 μM in CH_2Cl_2 . **Figure 3.3** depicts the UV-Vis absorption spectra for each amphiphilic Janus dendrimer. We observe for all three generations that there is a prominent band centered at 312 nm, corresponding to $\pi - \pi^*$ transitions of TPE, with poorly resolved vibrational structure. It is also observed that there is a trend of the absorption spectrum; the absorption intensity increases with each generation. This is a result of the addition of the hydrophilic segment to the TPE-conjugated dendrons, where the enhancement of the dendrimer's solubility allows the spacers

between the TPE molecules to be more distant, which in turn, increases the absorption intensity.[7] Similar absorption trends occur when comparing each generation's TPE conjugated dendrons and dendrimers (**Appendix B, Figures B38, B39 and B40**).

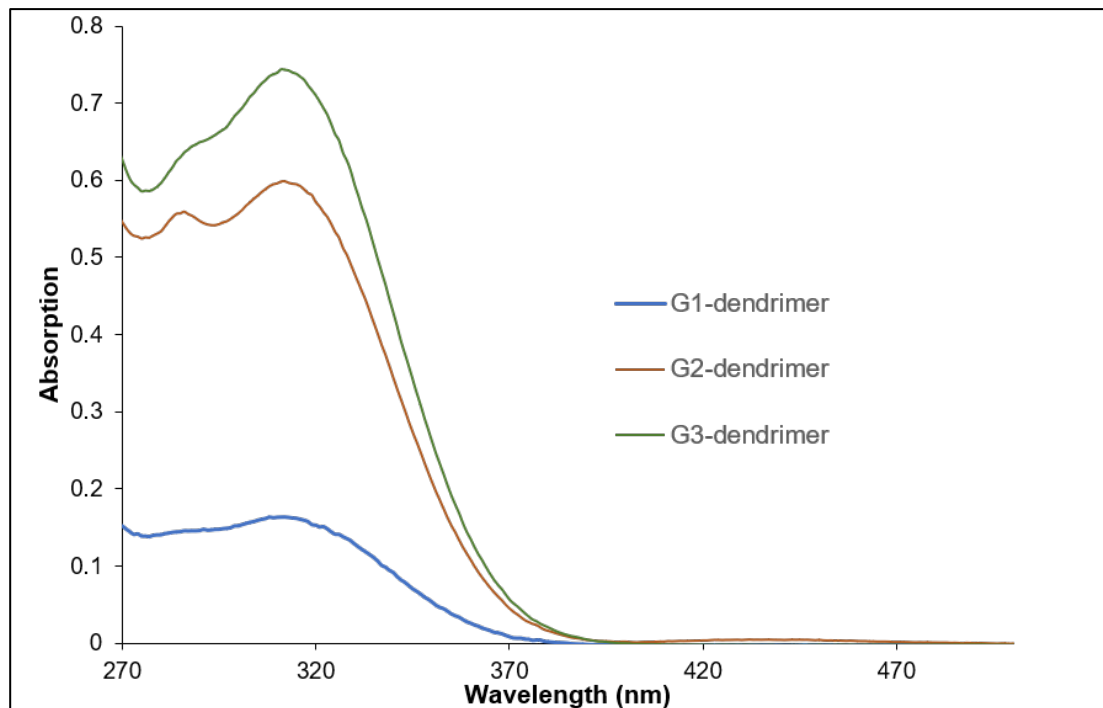


Figure 3.3. UV-Vis absorption spectra for Janus dendrimers (**29**), (**30**), and (**31**).

From these spectra, we were able to obtain an excitation wavelength at 317 nm, which is essential for monitoring the aggregation behaviour of the amphiphilic Janus dendrimers. As a result, the AIE behaviour of the dendrimers were monitored by fluorescence spectroscopy by introducing filtered nanopure water into DMSO solutions of each generation. The fluorescence spectra for each generation were studied at various water contents (0–90 vol %). The fluorescence spectrum (**Appendix B, Figure B41**) for dendrimer (**29**), shows that at 0% water content, no emission was detected. As the water fraction increased to 30%, a weak emission maximum was obtained at

480 nm. Further increment to 60% and 90% led to an enhancement in intensity, showing little to no change between them. Lastly, 99% water content provided the highest fluorescent intensity. Overall, this indicated that the fluorescence emission of dendrimer (**29**) due to the formation of self-assembled intermolecular π - π stacking from TPE started from a minimum water content of 30% to a maximum emission at 99%. The fluorescence spectrum (**Appendix B, Figure B42**) for dendrimer (**30**) exhibits a similar trend with the increase in water content with an emission maximum at 482 nm; however, the initial water content of 30% already exhibited a high fluorescent intensity. Even as the water content was increased from 30% to 60% to 90%, and 99%, there was a slight increase in intensity, showing a narrow gap between each water content. The fluorescence spectrum (**Appendix B, Figure B43**) for dendrimer (**31**) followed the same pattern as dendrimer (**30**), with the exception of having an emission maximum at 478 nm, where the fluorescence intensity at 60%, 90% and 99% water content are similar. When comparing the fluorescence emission profile for each generation (**Figure 3.4**), we observe that going from the first generation to the second, there is an overall increase in fluorescence, and a similar increase going from the second to the third generation. However, we observe that for the third generation, there is a faster fluorescence saturation obtained, which is a result of the larger hydrophobic volume than the first two generations, allowing it to self-assemble faster.

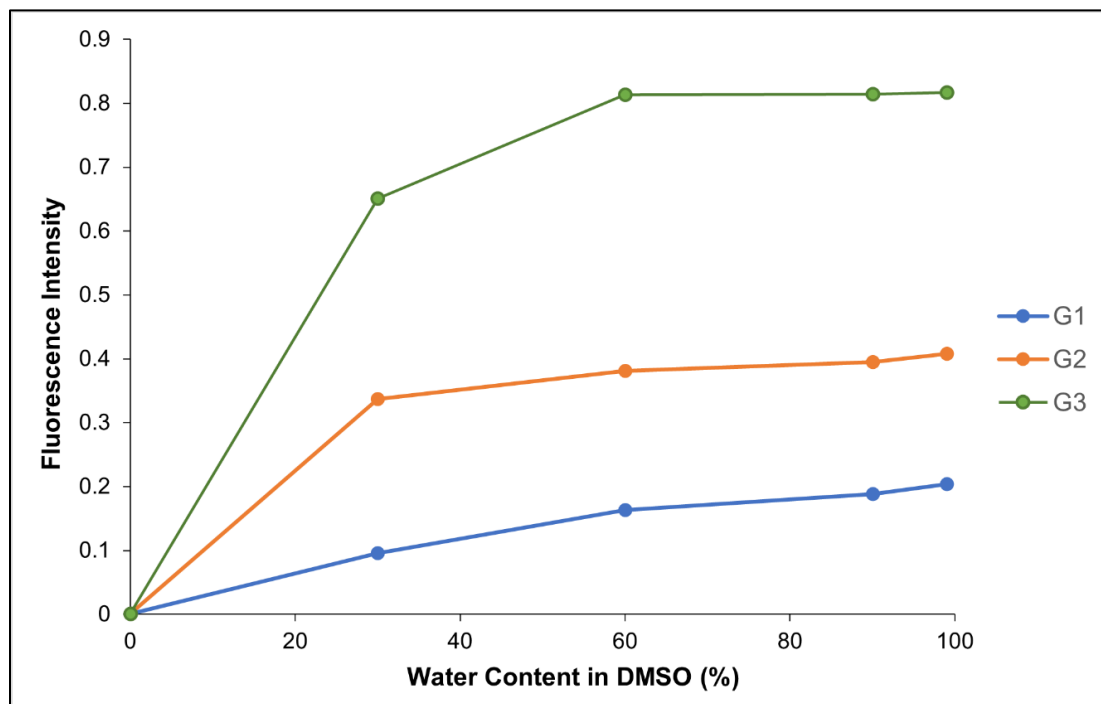


Figure 3.4. Fluorescence emission profile for Janus dendrimers **(29)**, **(30)**, and **(31)**.

3.3.7 Self-Assembly of Amphiphilic Janus Dendrimers:

The fluorescence emission profile provided the starting point for the conditions necessary to study their self-assembly. Based on previous reports of similar TPE-conjugated Janus dendrimers, self-assembly formed high aspect ratio two-dimensional (2D) crystalline nanosheets, indicating that the π - π stacking of the highly conjugated TPE as well as the restricted flexibility, made it difficult to form a closed system.[65, 66] However, other Janus dendrimers studied with non-conjugated TPE units provided a hydrophilic weight fraction is considerably smaller than in the first two generations, which appear to form dendrimersomes.[93] The self-assembly of dendrimers **(29)**, **(30)**, and **(31)** was investigated using two different methods, where each dendrimer was dissolved in DMSO. The first method is where the dendrimer solutions (250 μ L) are

added rapidly to filtered nanopure water (2.75 mL) as a means to study their self-assembly under kinetic control. The second method is where filtered nanopure water (2.75 mL) is added dropwise to each dendrimer solution (250 μ L) as a means to study their self-assembly under thermodynamic control. Both methods had the DMSO removed through dialysis to provide accurate values from the measurements. Studies initially occurred by dynamic light scattering (DLS) to determine the size of the nanoparticles. As shown in **Table 3.3**, under kinetic control, the first-generation dendrimer provided small sized particles averaging 50 nm. The second and third generation dendrimers were substantially different; after removal of DMSO, two sets of sizes were presented. For the second generation, sizes were averaging at 80 nm and 450 nm, while for the third generation, the sizes were averaging at 50 nm and 250 nm. For stable particles, the removal of the organic solvent leads to a decrease in size, indicating presence of swelling. In this scenario, having larger particles after dialysis can indicate various morphologies present. The DLS data under thermodynamic control revealed larger sized particles, averaging between 140-190 nm, where one set of sizes was provided for each generation.

Table 3.3: Summary of DLS data for the self-assembly of amphiphilic Janus dendrimers under two conditions, before and after removal of DMSO.

Self-Assembly Janus Dendrimer Generation	DMSO into Water		Water into DMSO	
	Before Dialysis	After Dialysis	Before Dialysis	After Dialysis
G1	60 nm	50 nm	225 nm	190 nm
G2	122 nm	80 nm, 450 nm	220 nm	160 nm
G3	60 nm	50 nm, 250 nm	190 nm	140 nm

Given these initial results, further insight into the morphology of the structures was obtained by transmission electronic microscopy (TEM) measurements. For the self-assembled materials under kinetic control, analysis of Janus dendrimer **(29)** (**Figure 3.5a**) revealed the presence of bilayered vesicles (dendrimerosomes) based on the contrast of the black rim with the gray interior, where the sizes observed were averaging 70 nm, which is in good accordance with DLS size of 50 nm (**Figure 3.5b**). The Janus dendrimers **(30)** (**Figure 3.5c**) and **(31)** (**Figure 3.5e**), on the other hand, provided gyroid morphologies. The gyroids for Janus dendrimer **(30)** provided sizes averaging between 100 nm-500 nm, which agrees with DLS sizes of 80 nm and 450 nm (**Figure 3.5d**). The gyroids for Janus dendrimer **(31)** provided sizes averaging between 100 nm-300 nm, which agrees with DLS sizes of 50 nm and 250 nm (**Figure 3.5f**). Overall, gyroids are continuous and triple periodic cubic morphology which possess a mean constant curvature surface.[45] The vials shown with each TEM image (**Figure 3.5a, c & e**) indicated that during self-assembly, the TPE units aggregated, leading to a bright blue illumination.

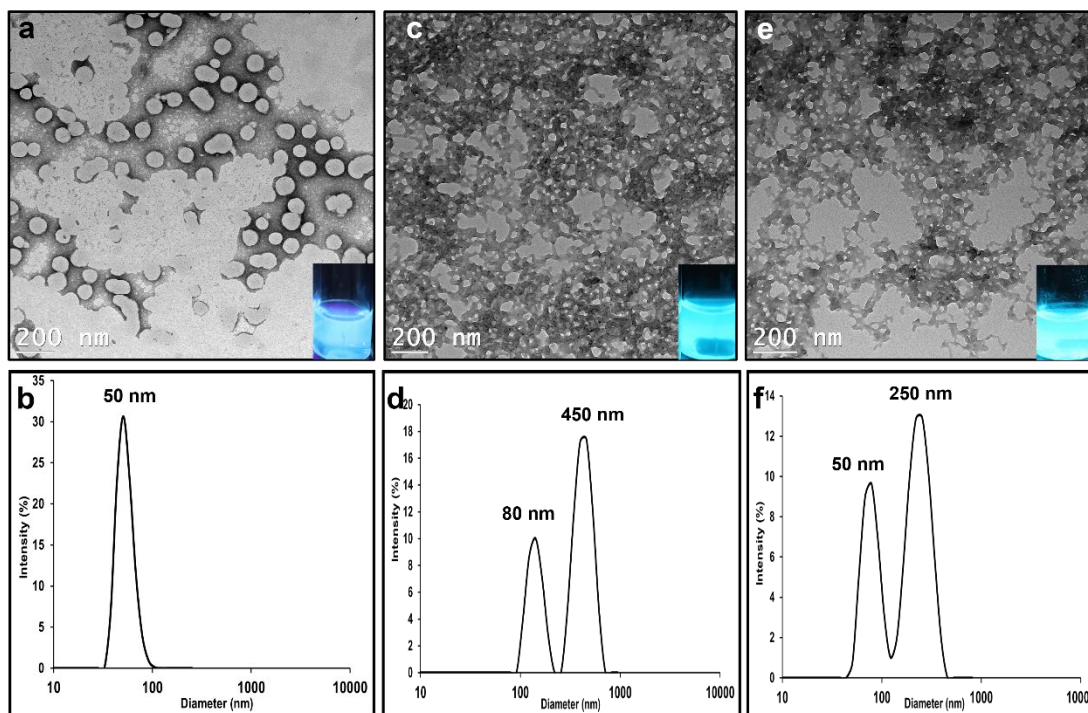


Figure 3.5: Amphiphilic Janus dendrimers under kinetic control: **(a)** first generation TEM image and **(b)** DLS curve, **(c)** second generation TEM image and **(d)** DLS curve, and **(e)** third generation TEM image and **(f)** DLS curve. Note: Illuminated vials in **(a)**, **(c)** and **(e)** correspond to the fluorescent self-assembled amphiphilic Janus dendrimers at an excitation wavelength of 317 nm.

For the self-assembled materials under thermodynamic control, TEM images for all three Janus dendrimers indicated monodisperse bilayered vesicles (dendrimerosomes), based on the contrast of the black rim with the gray interior. Janus dendrimer **(29)** (**Figure 3.6a**) provided dendrimerosomes averaging at 200 nm in size, which is in good accordance with the DLS size of 190 nm (**Figure 3.6b**). Janus dendrimer **(30)** (**Figure 3.6c**) has a decrease in size in comparison to **(29)**, where the sizes of the dendrimerosomes are averaging at 170 nm, which is in good agreement with the DLS size of 160 nm (**Figure 3.6d**). Janus dendrimer **(31)** (**Figure 3.6e**) has even smaller

dendrimersomes, where the sizes are averaging at 125 nm, which is in good agreement with the DLS size of 140 nm (**Figure 3.6e**). Similar to the self-assembly under kinetic control, the vials shown with each TEM image (**Figure 3.6a, c & e**) indicated that during self-assembly, the TPE units aggregated, leading to a bright blue illumination.

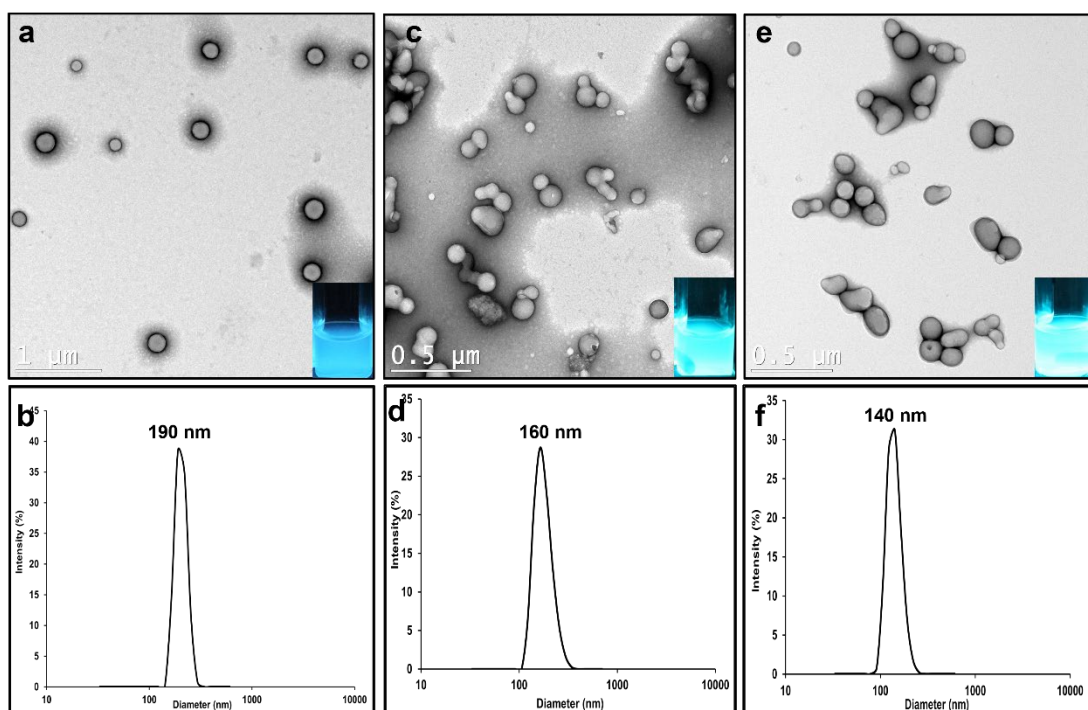


Figure 3.6: Amphiphilic Janus dendrimers under thermodynamic control: **(a)** first generation TEM and **(b)** DLS curve, **(c)** second generation TEM and **(d)** DLS curve, and **(e)** third generation TEM and **(f)** DLS curve. Note: Illuminated vials in **(a)**, **(c)** and **(e)** corresponds to the fluorescent self-assembled amphiphilic Janus dendrimers at an excitation wavelength of 317 nm.

When comparing the TEM images from both kinetic and thermodynamic control, we obviously observe a difference in size and morphology. While the kinetic control provides mostly variable sized gyroids (**Appendix B, Figure B44**), thermodynamic control provides stable, controlled dendrimersomes (**Appendix B, Figure B45**). Based

on these results, it can be suggested that if applied to drug delivery systems, the formation of dendrimersomes through thermodynamic control is favoured, being able to encapsulate hydrophobic/hydrophilic drugs, whereas gyroid morphology is always continuous, meaning no truly defined stable shape, making them inefficient towards any applications.

3.4 Materials and Methods:

All chemicals were purchased from Sigma-Aldrich or Alfa Aesar and were used without further purification unless otherwise noted. Anhydrous tetrahydrofuran (THF) and anhydrous dichloromethane (CH_2Cl_2) were obtained from a solvent purification system using aluminum oxide columns. The reactions were mostly performed under argon using Schlenk line techniques and anhydrous THF/ CH_2Cl_2 . ^1H - and ^{13}C -NMR spectra were recorded at 300 and 150 MHz, respectively, using CDCl_3 and DMSO-d_6 as solvents. Chemical shifts are reported in delta (δ) units, expressed in parts per million (ppm). Coupling constants are expressed in hertz (Hz). The number-average molecular weight (M_n), weight-average molecular weight (M_w), and dispersity indices (D) of polymers were determined by size exclusion chromatography (SEC) using an EcoSEC HLC-8320 (Tosoh Bioscience, Tokyo, Japan) instrument equipped with two TSKgel Alpha-M, 13 μm columns (7.8 mm ID x 30 cm L) and a TSKgel Alpha Guardcolumn (6.0 mm ID x 4 cm L) calibrated with poly (methyl methacrylate) standards in DMF at 50 °C. The samples were prepared at a concentration of 2 mg/mL in DMF and filtered through a 0.22 μm PTFE syringe filter prior to injection. The data were acquired at a flow rate of 0.6 mL/min at 50 °C. Dynamic light scattering (DLS) data were obtained using a Zetasizer Nano ZS instrument from Malvern Instruments (Malvern, UK) at a dendrimer concentration of 0.05 mg/mL. Fluorescence spectroscopy was performed with a Perkin Elmer LS45 Spectrofluorometer (Waltham,

MA, USA). Samples were analyzed at a dendrimer concentration of 5×10^{-5} M. The excitation wavelength for acquiring the emission spectra was set at 317 nm. Differential scanning calorimetry (DSC) data were obtained using a DSC1 Mettler Toledo instrument (Columbus, OH, USA) with a heating/cooling rate of 10 °C/min between -50 and 200 °C under nitrogen atmosphere. The midpoint glass transition temperature (T_g) values were extracted from the second heating cycle. Transmission electron microscopy (TEM) were prepared by drop casting one drop (ca. 20 μ L) of the colloidal particle solution (17 μ M) onto a formvar carbon-coated copper grid rested on a piece of filter paper, which were left to dry overnight. The measurements were performed on a Joel JEM-2100F instrument (Tokyo, Japan) at 80 kV. High-resolution mass spectrometry (HRMS) was performed using a Liquid Chromatography Mass Spectrometry Time of Flight (LC-MS TOF) mass analyzer (Agilent Technologies Santa Clara, CA, USA) in the electrospray mode.

3.4.1 Experimental Section:

3.4.2 Synthesis of reduced benzoate (**9**):

In a dry Schlenk flask (undergone vacuum-Argon cycle 3x), LiAlH_4 (5.5 g, 0.15 mol, 7.0 equivalents) was dissolved in 70 mL anhydrous tetrahydrofuran (THF) and placed in an ice bath for a few minutes. 30 mL of dissolved methyl-3,5-dihydroxybenzoate (3.4 g, 21 mmol, 1.0 equivalent) in THF was added slowly to the stirred solution for a duration of 40 minutes. Solution was then warmed to room temperature, where it was then refluxed for 7 hours under argon. After being cooled down to room temperature, solution was quenched slowly with addition of ethyl acetate (EtOAc), 2.0 M HCl, and ethanol until bubbles stopped forming. Solution was then placed under vacuum filtration, where the filtrate was rotary evaporated to remove THF. Product was washed

with water/ethyl acetate, extracted with ethyl acetate (3 x 50 mL), and the accumulated organic layer was dried with magnesium sulfate, filtered, and rotary evaporated. Crude product was purified by column (1:1, EtOAc: CH₂Cl₂). Pure product was a white solid (2.3 g, yield= 78%). ¹H-NMR (300 MHz, DMSO-d₆, δ): 9.06 (s, 2H, Ar-OH), 6.16 (d, J= 2.2 Hz, 2H, Ar-H), 6.04 (t, J= 2.2 Hz, 1H, Ar-H), 4.98 (t, J= 6.0 Hz, 1H, Ar-CH₂-OH), 4.29 (d, J= 6.0 Hz, 2H, Ar-CH₂-OH).

3.4.3 Synthesis of first-generation alkyne (**10**):

In a 250 mL round bottom flask, **9** (1.3 g, 9.0 mmol, 1.0 equivalent) was dissolved in 100 mL acetonitrile. Potassium carbonate (6.4 g, 47 mmol, 5.0 equivalents) was slowly added to the stirred solution. After letting the solution stir for 10 minutes, propargyl bromide (3.6 mL, 47 mmol, 5.0 equivalents) was added and the solution was under reflux for 24 hours. After solution was cooled down, acetonitrile was removed by rotary evaporation. Product was dissolved in water/dichloromethane (CH₂Cl₂), extracted with CH₂Cl₂ (3 x 50 mL), and the accumulated organic layer was dried with magnesium sulfate, filtered, and rotary evaporated. Crude product was purified by column (98:2, CH₂Cl₂: EtOAc). Pure product was a light-yellow solid (1.6 g, yield= 79%). ¹H-NMR (300 MHz, CDCl₃, δ): 6.63 (d, J= 2.3 Hz, 2H, Ar-H), 6.55 (t, J= 2.3 Hz, 1H, Ar-H), 4.68 (d, J= 2.4 Hz, 4H, Ar-CH₂-C≡C-H), 4.65 (s, 2H, Ar-CH₂-OH), 2.53 (t, J= 2.4 Hz, 2H, Ar-CH₂-C≡C-H).

3.4.4 Synthesis of brominated first-generation alkyne (**11**):

In a dry Schlenk flask (undergone vacuum-Argon cycle 3x), **10** (1.4 g, 7.0 mmol, 1.0 equivalent) was dissolved in 70 mL anhydrous THF. Carbon tetrabromide (3.3 g, 10mmol, 1.5 equivalents), was added to the stirred solution, followed by the slow

addition of triphenylphosphine (2.6 g, 10 mmol, 1.5 equivalents). Solution (opaque) was stirred at room temperature, where after 24 hours, an extra 1.5 equivalent of carbon tetrabromide and triphenylphosphine were added. Solution was monitored by thin layer chromatography (tlc), where it came to completion after 48 hours. Solution was quenched with water (went from opaque to transparent), followed by removal of THF by rotary evaporation. Product was dissolved in water/CH₂Cl₂, extracted with CH₂Cl₂ (3 x 30 mL), and the accumulated organic layer was dried with magnesium sulfate, filtered, and rotary evaporated. Crude product was purified by column (3:1, hexane: CH₂Cl₂). Pure product was a light-brown solid (1.7 g, yield=88%). ¹H-NMR (300 MHz, CDCl₃, δ): 6.65 (d, J= 2.3 Hz, 2H, Ar-**H**), 6.56 (t, J= 2.3 Hz, 1H, Ar-**H**), 4.68 (d, J= 2.4 Hz, 4H, Ar-**CH**₂-C≡C-H), 4.42 (s, 2H, Ar-**CH**₂-Br), 2.54 (t, J= 2.4 Hz, 2H, Ar-**CH**₂-C≡C-H).

3.4.5 Synthesis of second-generation alkyne (**12**):

In a 250 mL round bottom flask, **9** (0.25 g, 2.0 mmol, 1.0 equivalent) was dissolved in 70 mL acetone. Potassium carbonate (0.73 g, 5.0 mmol, 3.0 equivalents) and 18-crown-6 ether (93 mg, 0.40 mmol, 0.20 equivalent) were slowly added to the stirred solution. After letting the solution stir for 10 minutes, **11** (1.2 g, 4.0 mmol, 2.5 equivalents) was added and placed under reflux for 24 hours. After solution was cooled down, acetone was removed by rotary evaporation. Product was dissolved in water/CH₂Cl₂, extracted with CH₂Cl₂ (3 x 30 mL), and the accumulated organic layer was dried with magnesium sulfate, filtered, and rotary evaporated. Crude product was purified by column (1:1, EtOAc: hexane). Pure product was a light-yellow solid (0.81 g, yield= 86%). ¹H-NMR (300 MHz, CDCl₃, δ): 6.67 (d, J= 2.3 Hz, 4H, Ar-**H**), 6.60 (d, J= 2.3 Hz, 2H, Ar-**H**), 6.57 (t, J= 2.3 Hz, 2H, Ar-**H**), 6.51 (t, J= 2.3 Hz, 1H, Ar-**H**), 4.99 (s, 4H, Ar-O-**CH**₂-

Ar), 4.67 (d, $J = 2.4$ Hz, 8H, Ar-**CH₂-C≡C-H**), 4.63 (s, 2H, Ar-**CH₂-OH**), 2.52 (t, $J = 2.4$ Hz, 4H, Ar-**CH₂-C≡C-H**).

3.4.6 Synthesis of brominated second-generation alkyne (**13**):

In a dry Schlenk flask (undergone vacuum-Argon cycle 3x), **12** (0.42 g, 0.80 mmol, 1.0 equivalent) was dissolved in 70 mL anhydrous THF. Carbon tetrabromide (0.39 g, 1.0 mmol, 1.5 equivalents), was added to the stirred solution, followed by the slow addition of triphenylphosphine (0.31 g, 1.0 mmol, 1.5 equivalents). Solution (opaque) was monitored by thin layer chromatography (tlc), where an extra 1.5 equivalent of carbon tetrabromide and triphenylphosphine was added every 24 hours, where it came to completion after 72 hours. Solution was quenched with water (went from opaque to transparent), followed by removal of THF by rotary evaporation. Product was dissolved in water/CH₂Cl₂, extracted with CH₂Cl₂ (3 x 30 mL), and the accumulated organic layer was dried with magnesium sulfate, filtered, and rotary evaporated. Crude product was purified by column (3:1, hexane: CH₂Cl₂). Pure product was a light-brown solid (0.36g, yield= 77%). ¹H-NMR (300 MHz, CDCl₃, δ): 6.67 (d, $J = 2.3$ Hz, 4H, Ar-**H**), 6.62 (d, $J = 2.3$ Hz, 2H, Ar-**H**), 6.57 (t, $J = 2.3$ Hz, 2H, Ar-**H**), 6.50 (t, $J = 2.3$ Hz, 1H, Ar-**H**), 4.98 (s, 4H, Ar-O-**CH₂-Ar**), 4.68 (d, $J = 2.4$ Hz, 8H, Ar-**CH₂-C≡C-H**), 4.40 (s, 2H, Ar-**CH₂-Br**), 2.52 (t, $J = 2.4$ Hz, 4H, Ar-**CH₂-C≡C-H**).

3.4.7 Synthesis of third-generation alkyne (**14**):

In a 250 mL round bottom flask, **9** (17 mg, 0.10 mmol, 1.0 equivalent) was dissolved in 20 mL acetone. Potassium carbonate (51 mg, 0.40 mmol, 3.0 equivalents), potassium iodide (11 mg, 6.1×10^{-2} mmol, 0.50 equivalent) along with 18-crown-6 ether (6.4 mg,

2.4×10^{-2} mmol, 0.20 equivalent) was slowly added to the stirred solution. After letting the solution stir for 10 minutes, **13** (0.18 g, 0.30 mmol, 2.5 equivalents) was added and placed under reflux for 24 hours. After solution was cooled down, acetone was removed by rotary evaporation. Product was dissolved in water/ CH_2Cl_2 , extracted with CH_2Cl_2 (3 x 30 mL), and the accumulated organic layer was dried with magnesium sulfate, filtered, and rotary evaporated. Crude product was purified by column (1:1, EtOAc: hexane). Pure product was a light-yellow solid (0.12 g, yield= 83%). $^1\text{H-NMR}$ (300 MHz, CDCl_3 , δ): 6.66 (d, $J= 2.3$ Hz, 8H, Ar-**H**), 6.63 (d, $J= 2.3$ Hz, 4H, Ar-**H**), 6.57 (d, $J= 2.3$ Hz, 2H, Ar-**H**), 6.55 ppm (t, $J= 2.3$ Hz, 4H, Ar-**H**), 6.52 (t, $J= 2.3$ Hz, 2H, Ar-**H**), 6.48 (t, $J= 2.3$ Hz, 1H, Ar-**H**), 4.98 (s, 8H, Ar-O-**CH**₂-Ar), 4.95 (s, 4H, Ar-O-**CH**₂-Ar), 4.65 (d, $J= 2.4$ Hz, 16H, Ar-**CH**₂-C \equiv C-H), 4.61 (s, 2H, Ar-**CH**₂-OH), 2.51 (t, $J= 2.4$ Hz, 8H, Ar-**CH**₂-C \equiv C-**H**).

3.4.8 Synthesis of methoxy-functionalized tetraphenylethylene (**15**):

In a dry Schlenk flask (undergone vacuum-Argon cycle 3x), diphenylmethane (5.0 g, 30 mmol, 1.0 equivalent) was dissolved in 100 mL anhydrous THF. Solution was placed in an ice bath, where *n*-butyllithium (**2.5 M Hexane solution**) (14 mL, 36 mmol, 1.2 equivalent) was added slowly. Reaction was stirred in an ice bath for 30 minutes (solution went from orange to light yellow). In a separate dry flask, 4-methoxybenzophenone (5.7 g, 27 mmol, 0.90 equivalent) was dissolved in 40 mL anhydrous THF. When diphenylmethane solution was cooled to room temperature, 4-methoxybenzophenone was transferred to the Schlenk flask and the reaction was stirred for 6 hours. The reaction was then quenched with saturated ammonium chloride, followed by removal of THF via rotary evaporation. Product was dissolved in water/ CH_2Cl_2 , extracted with CH_2Cl_2 (3 x 50 mL), and the accumulated organic layer was dried with magnesium sulfate, filtered, and rotary evaporated. In a 250 mL round bottom flask, crude product was then dissolved in 100 mL toluene. To the stirred

solution, *p*-toluenesulfonic acid monohydrate (0.85 g, 4.0 mmol, 0.20 equivalent) was added, and placed under reflux, using a Dean-Stark trap, for 4 hours, where water was being continuously accumulated. Once the solution was cooled down, toluene was removed by rotary evaporation. Product was dissolved in water/CH₂Cl₂, extracted with CH₂Cl₂ (3x 30mL), and the accumulated organic layer was dried with magnesium sulfate, filtered, and rotary evaporated. Crude product was purified via column (98:2, hexane: EtOAc), where the pure product was a white solid (7.6 g, yield=70%). ¹H-NMR (300 MHz, CDCl₃, δ): 7.11-6.98 (m, 15H, Ar-H), 6.93 (d, J= 8.8 Hz, 2H, O-Ar-H), 6.63 (d, J= 8.8 Hz, 2H, O-Ar-H), 3.74 (s, 3H, O-CH₃).

3.4.9 Synthesis of hydroxy-functionalized TPE (**16**):

In a dry Schlenk flask (undergone vacuum-Argon cycle 3x), **15** (2.0 g, 6.0 mmol, 1.0 equivalent) was dissolved in 40 mL anhydrous CH₂Cl₂, where the solution was then cooled down to -20° C. Boron tribromide (1.0 M CH₂Cl₂ solution) (11 mL, 11 mmol, 3.0 equivalents) was added slowly to stirred solution. The solution was then returned to room temperature, where it stirred for 7 hours. The reaction was then quenched with saturated sodium bicarbonate, and the combined organic layer was dried with magnesium sulfate, filtered and rotary evaporated to obtain the pure product as a light brown solid (1.9 g, yield=98%). ¹H-NMR (300 MHz, DMSO-d₆, δ): 9.34 (s, 1H, TPE-OH), δ 7.17-6.91 (m, 15H, Ar-H), 6.73 (d, J= 8.8 Hz, 2H, O-Ar-H), 6.50 (d, J= 8.8 Hz, 2H, O-Ar-H).

3.4.10 Synthesis of bromo-propoxy TPE (**17**):

In a 250 mL round bottom flask, **16** (1.9 g, 5.0 mmol, 1.0 equivalent) was dissolved in 100 mL acetonitrile. Cesium carbonate (3.5 g, 11 mmol, 2.0 equivalents) was added slowly to the stirred solution. After letting the reaction stir for 10 minutes, 1,3-dibromopropane (14 mL, 0.14 mol, 25 equivalents) was added, where the solution was under reflux for 24 hours. After solution was cooled down, acetonitrile was removed by rotary evaporation. Product was dissolved in water/CH₂Cl₂, extracted with CH₂Cl₂ (3 x 30 mL), and the accumulated organic layer was dried with magnesium sulfate, filtered, and rotary evaporated. Crude product was purified by column (2:1, EtOAc: hexane). Pure product was a light-yellow viscous solid (2.6 g, yield= 99%). ¹H-NMR (300 MHz, CDCl₃, δ): 7.17-6.98 (m, 15H, Ar-H), 6.93 (d, J= 8.8 Hz, 2H, O-Ar-H), 6.63 (d, J= 8.8 Hz, 2H, O-Ar-H), 4.02 (t, J= 5.8 Hz, 2H, Ar-O-CH₂), 3.58 ppm (t, J= 6.4 Hz, 2H, Ar-O-CH₂-CH₂-CH₂-Br), 2.28 ppm (q, J= 12 Hz, 2H, Ar-O-CH₂-CH₂).

3.4.11 Synthesis of azido-propoxy TPE (**18**):

In a 250 mL round bottom flask, **17** (2.6 g, 5.0 mmol, 1.0 equivalent) was dissolved in 100 mL N, N-dimethylformamide (DMF). Sodium azide (3.6 g, 55 mmol, 10 equivalents) was added to the solution, where it underwent reflux for 24 hours. After solution was cooled down, DMF was removed by rotary evaporation. Product was dissolved in water/CH₂Cl₂, extracted with CH₂Cl₂ (3 x 30 mL), and the accumulated organic layer was dried with magnesium sulfate, filtered, and rotary evaporated, where the pure product was obtained as an orange viscous solid (2.2 g, yield=89%). ¹H-NMR (300 MHz, CDCl₃, δ): 7.14-7.00 (m, 15H, Ar-H), 6.98 (d, J= 8.8 Hz, 2H, O-Ar-H), 6.67 (d, J= 8.8 Hz, 2H, O-Ar-H), 4.00 (t, J= 5.9 Hz, 2H, Ar-O-CH₂), 3.52 (t, J= 6.6 Hz, 2H, Ar-O-CH₂-CH₂-CH₂-N₃), 2.04 (q, J= 12 Hz, 2H, Ar-O-CH₂-CH₂).

3.4.12 Synthesis of tosylated TEG (**19**):

In a 250 round bottom flask, triethylene glycol monomethyl ether (15 g, 9.1 mmol, 1.0 equivalent) was dissolved in 100 mL CH₂Cl₂. To the stirred solution, triethylamine (9.7g, 9.6 mmol, 1.1 equivalent), 4-dimethylamino pyridine (5.6 g, 4.6 mmol, 0.50 equivalent) and *p*-toluenesulfonyl chloride (19 g, 10 mmol, 1.1 equivalent) were added in that order and the reaction stirred at room temperature for 24 hours. Solution was washed with 4.0 M HCl (3 x 50 mL), washed with Brine (1 x 50 mL), dried with magnesium sulfate, filtered and rotary evaporated to give the pure product as a light-yellow liquid (24 g, yield=83%). ¹H-NMR (300 MHz, CDCl₃, δ): 7.78 (d, J= 8.3 Hz, 2H, Ar-**H**), 7.33 (d, J= 8.3 Hz, 2H, Ar-**H**), 4.15 (t, J= 4.9 Hz, 2H, Ts-O-**CH**₂), 3.69-3.50 (m, 10 H, (**CH**₂)₅), 3.36 (s, 3H, O-**CH**₃), 2.44 (s, 3H, Ts-**CH**₃).

3.4.13 Synthesis of oligo(ethylene glycol)-functionalized gallate (**20**):

In a 250 mL round bottom flask, methyl gallate (0.69 g, 4.0 mmol, 1.0 equivalent) was dissolved in dry DMF (60 mL). To the stirred solution, **19** (4.8 g, 15 mmol, 4.0 equivalents), potassium iodide (0.50 g, 3.0 mmol, 0.80 equivalent), and potassium carbonate (5.2 g, 38 mmol, 10 equivalents) were added and stirred at 80 °C for 24 h under argon. After solution cooled down, DMF was rotary evaporated. Product was dissolved in water/CH₂Cl₂, extracted with CH₂Cl₂ (3 x 30 mL), and the accumulated organic layer was dried with magnesium sulfate, filtered, and rotary evaporated. After evaporating the solvent, the residue was purified by column chromatography (20:1, CH₂Cl₂: MeOH). Pure product was a colorless liquid (2.2 g, yield= 93%). ¹H-NMR (300 MHz, CDCl₃, δ): 7.29 (s, 2H, Ar-**H**), 4.20 (m, 6H, Ar-**CH**₂-TEG), 3.87 (m, 7H, Ar-COO**CH**₃, **CH**₂-TEG), 3.79 (m, 2H, **CH**₂-TEG), 3.74-3.61 (m, 21H, **CH**₂-TEG), 3.55 (m, 6H, **CH**₂-TEG), 3.37 (s, 9H, TEG-O**CH**₃).

3.4.14 Synthesis of oligo(ethylene glycol)-functionalized gallic acid (**21**):

In a 250 mL round bottom flask, **20** (1.4 g, 2.0 mmol, 1.0 equivalent), was dissolved in 20 ml deionized water. To the stirred solution, sodium hydroxide (0.65 g, 16 mmol, 8.0 equivalents) was added slowly and reflux for 5 hours. After solution was cooled down, HCl was added to quench the reaction (until pH reached 2-3). Solution was then extracted with CH₂Cl₂ (3 x 20 mL), and the accumulated organic layer was dried with magnesium sulfate, filtered, and rotary evaporated. Pure product was a yellow oil (0.90g, yield= 86%). ¹H-NMR (300 MHz, CDCl₃, δ): 7.35 (s, 2H, Ar-**H**), 4.22 (m, 6H, Ar-**CH**₂-TEG), 3.86 (m, 4H, **CH**₂-TEG), 3.81-3.61 (m, 21H, **CH**₂-TEG), 3.55 (m, 6H, **CH**₂-TEG), 3.37 (s, 9H, TEG-O**CH**₃).

3.4.15 Synthesis of hydrophilic alkyne-functionalized oligoethylene glycol gallate (**22**):

Compound **21** (0.90 g, 2.0 mmol, 1.0 equivalent) was dissolved in dry DMF (20 mL), and vigorously stirred. Potassium carbonate (1.0 g, 7.0 mmol, 5.0 equivalents) was added. After 10 minutes of the solution stirring, propargyl bromide (0.87 g, 7.0 mmol, 5.0 equivalents, 80% wt in toluene) was injected dropwise into the mixture and refluxed for 24 hours under argon. After solution was cooled down, DMF was removed by rotary evaporation. Product was dissolved in water/CH₂Cl₂, extracted with CH₂Cl₂ (3 x 20mL), and the accumulated organic layer was dried with magnesium sulfate, filtered, and rotary evaporated. Crude product was purified by column chromatography (10% MeOH in CH₂Cl₂). Pure product was a brown oil (0.88 g, yield= 92%). ¹H-NMR (300 MHz, CDCl₃, δ): 7.31 (s, 2H, Ar-**H**), 4.88 (d, J= 2.4 Hz, 2H, Ar-**CH**₂-C≡C-**H**), 4.21 (m, 6H, Ar-**CH**₂-TEG), 3.86 (m, 4H, **CH**₂-TEG), 3.77 (m, 2H, **CH**₂-TEG), 3.74-3.61 (m, 19H, **CH**₂-TEG), 3.53 (m, 6H, **CH**₂-TEG), 3.37 (s, 9H, TEG-O**CH**₃), 2.50 (t, J= 2.4 Hz, 1H, **CH**₂-C≡C-**H**).

3.4.16 Synthesis of first-generation TPE-conjugated dendron (**23**):

In a vial, **10** (0.41 g, 2.0 mmol, 1.0 equivalent) was dissolved in 10 mL THF. Separately, **18** (2.0 g, 5.0 mmol, 2.4 equivalents) was dissolved in THF and added to the stirred solution. Sodium ascorbate (0.76 g, 4.0 mmol, 2.0 equivalents) was dissolved in 2 mL water and transferred to the solution. Lastly, copper sulfate (0.48 g, 2.0 mmol, 1.0 equivalent) was separately dissolved in water and transferred to the solution (changing colors from opaque green to opaque orange to opaque yellow), where the reaction stirred at room temperature for 24 hours. After the reaction was completed, THF was removed by rotary evaporation. Product was dissolved in water/CH₂Cl₂, extracted with CH₂Cl₂ (3 x 30 mL), and the accumulated organic layer was dried with magnesium sulfate, filtered, and rotary evaporated. Crude product was purified by column (5% MeOH in CH₂Cl₂). Pure product is a white fluffy solid (1.4 g, yield= 70%). ¹H-NMR (300 MHz, CDCl₃, δ): 7.59 (s, 2H, triazole-**H**), 7.14-6.98 (m, 30H, Ar-**H**), 6.91 (d, J= 8.8 Hz, 4H, O-Ar-**H**), 6.62-6.55 (m, 7H, O-Ar-**H**, Ar'-**H**, Ar''-**H**), 5.16 (s, 4H, triazole-**CH**₂-**O**), 4.60 (d, J= 6.1 Hz, 2H, **CH**₂-**OH**), 4.54 (t, J= 6.9 Hz, 4H, Ar-O-**CH**₂), 3.90 (t, J= 5.7 Hz, 4H, Ar-O-**CH**₂-**CH**₂-**CH**₂-**N**₃), 2.35 (q, J= 12 Hz, 4H, Ar-O-**CH**₂-**CH**₂), 1.76 (t, J= 6.0 Hz, 1H, **CH**₂-**OH**). ¹³C-NMR (150 MHz, CDCl₃, δ): 159.4, 156.9, 144.3, 143.9, 143.8, 140.3, 140.2, 136.6, 132.6, 131.3, 127.7, 127.6, 126.4, 126.3, 123.4, 113.6, 105.7, 101.1, 64.6, 63.9, 61.8, 47.2, 29.9.

HRMS (EI, *m/z*): [M+H]⁺ calculated for C₇₁H₆₂N₆O₅: 1079.4782, found 1079.4854.

3.4.17 Synthesis of second-generation TPE-conjugated dendron (**24**):

In a vial, **12** (0.20 g, 0.40 mmol, 1.0 equivalent) was dissolved in 10 mL THF. Separately, **18** (0.77 g, 2.0 mmol, 4.8 equivalents) was dissolved in THF and added to the stirred solution. Sodium ascorbate (0.30 g, 2.0 mmol, 4.0 equivalents) was

dissolved in 2 mL water and transferred to the solution. Lastly, copper sulfate (0.19 g, 0.80 mmol, 2.0 equivalents) was separately dissolved in water and transferred to the solution (changing colors from opaque green to opaque orange to opaque yellow), where the reaction stirred at room temperature for 48 hours. After the reaction was completed, THF was removed by rotary evaporation. Product was dissolved in water/CH₂Cl₂, extracted with CH₂Cl₂ (3 x 30 mL), and the accumulated organic layer was dried with magnesium sulfate, filtered, and rotary evaporated. Crude product was purified by column (5% MeOH in CH₂Cl₂). Pure product is a white fluffy solid (0.67g, yield= 79%). ¹H-NMR (300 MHz, CDCl₃, δ): 7.58 (s, 4H, triazole-**H**), 7.14-6.98 (m, 60H, Ar-**H**), 6.92 (d, J= 8.8 Hz, 8H, O-Ar-**H**), 6.67 (d, J= 2.2 Hz, 4H, Ar-**H**) 6.61-6.58 (m, 12H, O-Ar-**H**, Ar'-**H**, Ar''-**H**), 6.46 (t, J= 2.2 Hz, 1H, Ar-**H**), 5.14 (s, 8H, triazole-**CH**₂-**O**), 4.96 (s, 4H, Ar-**CH**₂-**O**), 4.60 (d, J= 5.9 Hz, 2H, **CH**₂-**OH**), 4.52 (t, J= 6.9 Hz, 8H, Ar-**O-CH**₂), 3.89 (t, J= 5.7 Hz, 8H, Ar-**O-CH**₂-**CH**₂-**CH**₂-**N**₃), 2.33 (q, J= 12 Hz, 8H, Ar-**O-CH**₂-**CH**₂). ¹³C-NMR (150 MHz, CDCl₃, δ): 159.8, 159.6, 156.9, 144.1, 144.0, 143.9, 143.8, 140.4, 140.3, 136.6, 132.6, 131.3, 127.8, 127.7, 126.4, 126.4, 123.4, 113.6, 106.5, 105.8, 101.5, 101.2, 69.7, 64.8, 64.0, 62.0, 47.3, 30.0.

HRMS (EI, *m/z*): [M+H]⁺ calculated for C₁₄₉H₁₂₈N₁₂O₁₁: 2260.9826, found 2260.9809.

3.4.18 Synthesis of third generation TPE-conjugated dendron (**25**):

In a vial, **14** (0.16 g, 0.10 mmol, 1.0 equivalent) was dissolved in 10 mL THF. Separately, **18** (0.55 g, 1.0 mmol, 9.6 equivalents) was dissolved in THF and added to the stirred solution. Sodium ascorbate (0.21 g, 1.0 mmol, 8.0 equivalents) was dissolved in 2 mL water and transferred to the solution. Lastly, copper sulfate (0.13 g, 0.50 mmol, 4.0 equivalents) was separately dissolved in water and transferred to the solution (changing colors from opaque green to opaque orange to opaque yellow), where the reaction stirred at room temperature for 72 hours. After the reaction was

completed, THF was removed by rotary evaporation. Product was dissolved in water/CH₂Cl₂, extracted with CH₂Cl₂ (3 x 30 mL), and the accumulated organic layer was dried with magnesium sulfate, filtered, and rotary evaporated. Crude product was purified by column (2% MeOH in CH₂Cl₂). Pure product is a white fluffy solid (0.50g, yield= 82%). ¹H-NMR (300 MHz, CDCl₃, δ): 7.59 (s, 8H, triazole-**H**), 7.07-6.97 (m, 120H, Ar-**H**), 6.91 (d, J= 8.8 Hz, 16H, O-Ar-**H**), 6.64-6.42 (m, 37H, O-Ar-**H**, Ar'-**H**, Ar''-**H**), 5.12 (s, 16H, triazole-CH₂-O), 4.93 (s, 12H, Ar-CH₂-O), 4.56 (d, J= 5.9 Hz, 2H, CH₂-OH), 4.49 (t, J= 6.9 Hz, 16H, Ar-O-CH₂), 3.87 (t, J= 5.7 Hz, 16H, Ar-O-CH₂-CH₂-CH₂-N₃), 2.30 (q, J= 12 Hz, 16H, Ar-O-CH₂-CH₂). ¹³C-NMR (150 MHz, CDCl₃, δ): 159.9, 159.5, 156.9, 144.2, 143.9, 143.8, 140.3, 140.2, 139.6, 136.5, 132.6, 131.3, 130.9, 127.7, 127.6, 126.4, 126.3, 113.6, 106.4, 101.4, 64.0, 47.4, 29.9, 29.7.

HRMS (EI, *m/z*): [M+H]⁺ calculated for C₃₀₅H₂₆₀N₂₄O₂₃: 4625.9913, found 4625.9921.

3.4.19 Synthesis of first-generation azido-functionalized TPE-conjugated dendron (**26**):

In a Schlenk flask, **23** (1.4 g, 1.3 mmol, 1.0 equivalent) was dissolved in 20 mL anhydrous THF and stirred under argon. 1,8-diazabicyclo [5.4.0] undec-7-ene (DBU) was added (0.33 g, 2.2 mmol, 1.7 equivalent), followed by diphenyl phosphoryl azide (DPPA) (0.57 g, 2.2 mmol, 1.7 equivalent). Solution was placed under reflux at 65°C overnight. The reaction completion was confirmed by TLC, quenched with saturated ammonium chloride, and extracted with CH₂Cl₂ (3 x 20 mL), and the accumulated organic layer was dried with magnesium sulfate, filtered, and rotary evaporated. Crude product was purified by column (2% MeOH in CH₂Cl₂). Pure product is a brown fluffy solid (1.3 g, yield= 92%). ¹H-NMR (300 MHz, CDCl₃, δ): 7.61 (s, 2H, triazole-**H**), 7.11-6.99 (m, 30H, Ar-**H**), 6.92 (d, J= 8.8 Hz, 4H, O-Ar-**H**), 6.61-6.56 (m, 7H, O-Ar-**H**, Ar'-**H**, Ar''-**H**), 5.18 (s, 4H, triazole-CH₂-O), 4.55 (t, J= 6.9 Hz, 4H, Ar-O-CH₂),

4.24 (s, 2H, **CH₂-N₃**), 3.91 (t, J= 5.7 Hz, 4H, Ar-O-CH₂-CH₂-**CH₂-N₃**), 2.36 (q, J= 12 Hz, 4H, Ar-O-CH₂-**CH₂**). ¹³C-NMR (150 MHz, CDCl₃, δ): 159.6, 156.2, 143.8, 143.7, 140.2, 140.1, 137.7, 136.5, 132.4, 131.1, 131.0, 127.6, 127.4, 127.3, 126.2, 126.1, 126.0, 113.4, 107.3, 101.6, 67.7, 63.8, 61.8, 54.4, 47.0, 29.7, 25.4.

HRMS (EI, *m/z*): [M+H]⁺ calculated for C₇₁H₆₁N₉O₄: 1104.4847, found 1104.4927.
IR (cm⁻¹): 3048, 2933, 2869, 2094, 1595, 1505, 1442, 1239, 1152, 1043, 697.

3.4.20 Synthesis of second-generation azido-functionalized TPE-conjugated dendron (**27**):

In a Schlenk flask, **24** (0.67 g, 0.30 mmol, 1.0 equivalent) was dissolved in 20 mL anhydrous THF and stirred under argon. DBU was added (76 mg, 0.50 mmol, 1.7 equivalent), followed by DPPA (0.14 g, 0.50 mmol, 1.7 equivalent). Solution was placed under reflux at 65°C overnight. The reaction completion was confirmed by TLC, quenched with saturated ammonium chloride, and extracted with CH₂Cl₂ (3 x 20mL), and the accumulated organic layer was dried with magnesium sulfate, filtered, and rotary evaporated. Crude product was purified by column (2% MeOH in CH₂Cl₂). Pure product is a brown fluffy solid (0.62 g, yield= 91%). ¹H-NMR (300 MHz, CDCl₃, δ): 7.67 (s, 4H, triazole-**H**), 7.11-6.98 (m, 60H, Ar-**H**), 6.92 (d, J= 8.8 Hz, 8H, O-Ar-**H**), 6.68-6.53 (m, 17H, O-Ar-**H**, Ar'-**H**, Ar''-**H**), 5.19 (s, 8H, triazole-**CH₂-O**), 5.00 (s, 4H, Ar-**CH₂-O**), 4.59 (t, J= 6.9 Hz, 8H, Ar-O-**CH₂**), 4.27 (s, 2H, **CH₂-N₃**), 3.93 (t, J= 5.7 Hz, 8H, Ar-O-CH₂-CH₂-**CH₂-N₃**), 2.38 (q, J= 12 Hz, 8H, Ar-O-CH₂-**CH₂**). ¹³C-NMR (150 MHz, CDCl₃, δ): 159.9, 159.5, 156.8, 143.8, 143.7, 143.5, 140.2, 140.1, 139.2, 136.4, 132.4, 131.2, 131.1, 127.6, 127.5, 126.2, 126.1, 123.2, 113.5, 107.2, 106.4, 101.7, 101.4, 69.7, 63.9, 61.9, 54.5, 47.1, 29.8.

HRMS (EI, m/z): $[M+H]^+$ calculated for $C_{149}H_{127}N_{15}O_{10}$: 2289.9890, found 2289.9889.
IR(cm^{-1}): 3050, 2950, 2870, 2096, 1594, 1505, 1444, 1241, 1154, 1045, 698.

3.4.21 Synthesis of third generation azido-functionalized TPE-conjugated dendron (28):

In a Schlenk flask, **25** (0.45 g, 9.7×10^{-2} mmol, 1.0 equivalent) was dissolved in 20 mL anhydrous THF and stirred under argon. DBU was added (25 mg, 0.20 mmol, 1.7 equivalent), followed by DPPA (46 mg, 0.20 mmol, 1.7 equivalent). Solution was placed under reflux at 65°C overnight. The reaction completion was confirmed by TLC, quenched with saturated ammonium chloride, and extracted with CH_2Cl_2 (3 x 20mL), and the accumulated organic layer was dried with magnesium sulfate, filtered, and rotary evaporated. Crude product was purified by column (2% MeOH in CH_2Cl_2). Pure product is a brown fluffy solid (0.31 g, yield= 68%). 1H -NMR (300 MHz, $CDCl_3$, δ): 7.60 (s, 8H, triazole-**H**), 7.09-6.97 (m, 120H, Ar-**H**), 6.92 (d, $J = 8.8$ Hz, 16H, O-Ar-**H**), 6.66-6.51 (m, 37H, O-Ar-**H**, Ar'-**H**, Ar''-**H**), 5.18 (s, 16H, triazole-**CH₂-O**), 4.96 (s, 12H, Ar-**CH₂-O**), 4.53 (t, $J = 6.9$ Hz, 16H, Ar-O-**CH₂**), 4.22 (s, 2H, **CH₂-N₃**), 3.90 (t, $J = 5.7$ Hz, 16H, Ar-O-**CH₂-CH₂-CH₂-N₃**), 2.34 (q, $J = 12$ Hz, 16H, Ar-O-**CH₂-CH₂**). ^{13}C -NMR (150 MHz, $CDCl_3$, δ): 159.9, 159.5, 156.8, 143.9, 143.8, 143.6, 140.3, 140.2, 136.4, 132.5, 131.2, 131.1, 129.8, 127.7, 127.5, 126.3, 126.2, 126.1, 123.2, 120.0, 113.5, 106.4, 101.4, 69.7, 63.9, 61.9, 47.1, 29.8.

HRMS (EI, m/z): $[M+H]^+$ calculated for $C_{305}H_{259}N_{27}O_{22}$: 4650.9978, found 4650.9982.
IR(cm^{-1}): 3100, 2970, 2868, 2096, 1592, 1508, 1440, 1237, 1155, 1046, 699.

3.4.22 Synthesis of first-generation amphiphilic Janus dendrimer (**29**):

In a vial, **22** (0.23 g, 0.40 mmol, 1.0 equivalent) was dissolved in 10 mL THF. Separately, **26** (0.50 g, 0.50 mmol, 1.3 equivalents) was dissolved in THF and added to the stirred solution. Sodium ascorbate (83 mg, 0.40 mmol, 1.2 equivalents) was dissolved in 2 mL water and transferred to the solution. Lastly, copper sulfate (61 mg, 0.20 mmol, 0.70 equivalent) was separately dissolved in water and transferred to the solution, where the reaction stirred at room temperature for 24 hours. After the reaction was completed, THF was removed by rotary evaporation. Product was dissolved in water/ CH₂Cl₂, extracted with CH₂Cl₂ (3 x 10 mL), and the accumulated organic layer was dried with magnesium sulfate, filtered, and rotary evaporated. Crude product was purified by column (10% MeOH in EtOAc). Pure product is a fluffy solid (0.53 g, yield= 86%). ¹H-NMR (300 MHz, CDCl₃, δ): 7.72 (s, 3H, triazole-**H**), 7.28 (s, 2H, Ar-**H**), 7.14-6.98 (m, 30H, Ar-**H**), 6.92 (d, J= 8.6 Hz, 4H, O-Ar-**H**), 6.60 (d, J= 8.6 Hz, 7H, Ar-**H**), 5.42 (s, 4H, triazole-**CH**₂-O), 5.12 (t, J= 6.0 Hz, 4H, triazole-**CH**₂), 4.57 (t, J= 6.7 Hz, 4H, Ar-O-**CH**₂), 4.20 (m, 6H, Ar-**CH**₂-TEG), 3.91 (t, J= 5.4 Hz, 3H, Ar-**CH**₂-TEG), 3.84 (t, J= 9.8 Hz, 4H, Ar-O-**CH**₂-**CH**₂-**CH**₂-N₃), 3.74-3.61 (m, 21H, **CH**₂-TEG), 3.53 (m, 6H, **CH**₂-TEG), 3.36 (s, 9H, TEG-O**CH**₃), 2.39 (q, J= 12 Hz, 4H, Ar-O-**CH**₂-**CH**₂). ¹³C-NMR (150 MHz, CDCl₃, δ): 165.6, 159.6, 156.7, 152.0, 143.7, 143.6, 142.6, 140.1, 140.0, 136.7, 136.3, 132.3, 131.1, 131.0, 127.5, 127.4, 126.2, 126.1, 126.0, 124.3, 113.4, 108.9, 107.2, 101.7, 72.2, 71.6, 70.5, 70.4, 70.3, 70.2, 70.1, 69.3, 68.7, 63.8, 61.6, 58.7, 57.8, 47.1, 29.6.

HRMS (EI, *m/z*): [M+H]⁺ calculated for C₁₀₂H₁₁₁N₉O₁₈: 1749.8047, found 1749.8086.
IR(cm⁻¹): 2800, 2642, 2621, 1461, 1344, 1255, 1178, 991, 852, 447.

3.4.23 Synthesis of second-generation amphiphilic Janus dendrimer (**30**):

In a vial, **22** (0.11 g, 0.20 mmol, 1.0 equivalent) was dissolved in 10 mL THF. Separately, **27** (0.50 g, 0.20 mmol, 1.3 equivalents) was dissolved in THF and added to the stirred solution. Sodium ascorbate (40 mg, 0.20 mmol, 1.2 equivalents) was dissolved in 2 mL water and transferred to the solution. Lastly, copper sulfate (29 mg, 0.10 mmol, 0.70 equivalent) was separately dissolved in water and transferred to the solution, where the reaction stirred at room temperature for 24 hours. After the reaction was completed, THF was removed by rotary evaporation. Product was dissolved in water/CH₂Cl₂, extracted with CH₂Cl₂ (3 x 10 mL), and the accumulated organic layer was dried with magnesium sulfate, filtered, and rotary evaporated. Crude product was purified by column (10% MeOH in EtOAc). (0.34 g, yield= 70%). ¹H-NMR (300 MHz, CDCl₃, δ): 7.69 (s, 5H, triazole-**H**), 7.35 (s, 2H, Ar-**H**), 7.12-7.01 (m, 60H, Ar-**H**), 6.94 (d, J= 8.6 Hz, 8H, O-Ar-**H**), 6.62 (d, J= 8.6 Hz, 17H, Ar-**H**), 5.46 (s, 4H, triazole-**CH**₂-O), 5.19 (t, J= 6.0 Hz, 8H, triazole-**CH**₂), 4.96 (s, 4H, Ar-O-**CH**₂), 4.59 (t, J= 6.7 Hz, 8H, Ar-O-**CH**₂), 4.22 (m, 6H, Ar-**CH**₂-TEG), 3.93 ppm (t, J= 5.4 Hz, 3H, Ar-**CH**₂-TEG) 3.87 (t, J= 9.8 Hz, 8H, Ar-O-**CH**₂-**CH**₂-**CH**₂-N₃), 3.85-3.63 (m, 21H, **CH**₂-TEG), 3.54 (m, 6H, **CH**₂-TEG), 3.39 (s, 9H, TEG-O**CH**₃), 2.43 ppm (q, J= 12 Hz, 8H, Ar-O-**CH**₂-**CH**₂). ¹³C-NMR (150 MHz, CDCl₃, δ): 165.7, 160.0, 159.4, 156.7, 152.1, 143.7, 143.6, 143.0, 140.2, 140.0, 139.0, 136.3, 132.4, 131.1, 131.0, 127.6 ppm, 127.5, 127.4, 126.2, 126.1, 126.0, 124.3, 114.0, 109.0, 107.1, 106.3, 102.1, 100.9, 72.2, 71.7, 70.6, 70.5, 70.4, 70.3, 69.4, 68.7, 63.8, 58.8, 47.4, 29.7.

HRMS (EI, *m/z*): [M+H]⁺ calculated for C₁₈₀H₁₇₇N₁₅O₂₄: 2932.3091, found 2932.3069. IR(cm⁻¹): 3047, 2919, 2867, 1594, 1508, 1446, 1243, 1148, 1044, 695.

3.4.24 Synthesis of third-generation amphiphilic Janus dendrimer (**31**):

In a vial, **22** (23 mg, 3.6×10^{-2} mmol, 1.0 equivalent) was dissolved in 10 mL THF. Separately, **28** (0.22 g, 4.7×10^{-2} mmol, 1.3 equivalents) was dissolved in THF and added to the stirred solution. Sodium ascorbate (8.6 mg, 4.3×10^{-2} mmol, 1.2 equivalents) was dissolved in 2 mL water and transferred to the solution. Lastly, copper sulfate (6.3 mg, 2.5×10^{-2} mmol, 0.70 equivalent) was separately dissolved in water and transferred to the solution, where the reaction stirred at room temperature for 24 hours. After the reaction was completed, THF was removed by rotary evaporation. Product was dissolved in water/ CH_2Cl_2 , extracted with CH_2Cl_2 (3 x 10 mL), and the accumulated organic layer was dried with magnesium sulfate, filtered, and rotary evaporated. Crude product was purified by column (10% MeOH in EtOAc). (0.11 g, yield= 60%). $^1\text{H-NMR}$ (300 MHz, CDCl_3 , δ): 7.62 (s, 9H, triazole-**H**), 7.32 (s, 2H, Ar-**H**), 7.09-6.90 (m, 120H, Ar-**H**), 6.63 (d, $J= 8.6$ Hz, 16H, O-Ar-**H**), 6.49 (d, $J= 8.6$ Hz, 37H, Ar-**H**), 5.40 (s, 4H, triazole-**CH}_2\text{-O}**), 5.13 (t, $J= 6.0$ Hz, 16H, triazole-**CH}_2**), 4.92 (d, $J= 11$ Hz, 12H, Ar-O-**CH}_2**), 4.51 (t, $J= 6.7$ Hz, 16H, Ar-O-**CH}_2**), 4.22 (m, 6H, Ar-**CH}_2\text{-TEG}**), 3.88 (t, $J= 5.4$ Hz, 3H, Ar-**CH}_2\text{-TEG}**) 3.83 (t, $J= 9.8$ Hz, 16H, Ar-O-**CH}_2\text{-CH}_2\text{-CH}_2\text{-N}_3**), 3.81-3.60 (m, 21H, **CH}_2\text{-TEG}**), 3.52 (m, 6H, **CH}_2\text{-TEG}**), 3.35 (s, 9H, TEG-O**CH}_3**), 2.32 (q, $J= 12$ Hz, 16H, Ar-O-**CH}_2\text{-CH}_2**). $^{13}\text{C-NMR}$ (150 MHz, CDCl_3 , δ): 165.9, 160.2, 160.0, 159.6, 156.9, 151.9, 143.9, 143.8, 140.3, 140.2, 136.5, 132.6, 131.4, 131.3, 127.7, 127.6, 127.5, 126.4, 126.3, 126.2, 113.6, 109.1, 107.3, 106.5, 102.0, 101.7, 101.4, 72.4, 71.9, 70.8, 70.6, 70.5, 70.4, 69.6, 68.9, 64.0, 62.3, 59.0, 47.4, 29.9.

HRMS (EI, m/z): $[\text{M}+\text{H}]^+$ calculated for $\text{C}_{336}\text{H}_{309}\text{N}_{27}\text{O}_{36}$: 5297.3179, found 5297.3188. IR(cm^{-1}): 3048, 2921, 2874, 1598, 1500, 1441, 1238, 1147, 1040, 700.

3.4.25 Procedure for the self-assembly of Janus dendrimers (29), (30), and (31):

To obtain 17 μM solutions of the self-assembled materials, an initial DMSO solution of 5 mg/mL for dendrimers (29), (30), and (31) were prepared in accordance with their molecular weight and sonicated for 5 minutes to ensure their complete dissolution. Under kinetic control, 250 μL of each solution was added rapidly to filtered nanopure water (2.75 mL). Under thermodynamic control, filtered nanopure water (2.75 mL) was added dropwise while stirring. Following the formation of particles, the samples were dialyzed against deionized (DI) water using a 3500 MWCO membrane for 24 h with multiple changes of the dialysate. The resulting assemblies were then used for characterization by DLS and TEM.

3.4.26 Procedure for TEM images of Janus dendrimers (29), (30), and (31):

5.0 μL of each Janus dendrimer's solution is cast on a TEM grid, being held by a tweezler, and set to dry for 45-60 minutes. After grid is dry, 5.0 μL of the uranyl formate staining solution is cast on the grid. After waiting 60 seconds, the solution was blotted off with filter paper.

3.5 Conclusion:

In summary, we demonstrated a CuAAC convergent approach to synthesize amphiphilic Janus dendrimers using alkyne-functionalized oligo(ethylene glycol)-functionalized gallate and azide-functionalized TPE-conjugated dendrons. The attachment of the hydrophilic segment to the dendrons lead to a substantial decrease in glass transition temperature for the Janus dendrimers and to have a correlating fluorescence incremental profile as the generation and water contents increase. In addition, our results show that these amphiphilic Janus dendrimers are able to undergo

self-assembly in DMSO/H₂O mixture, particularly under thermodynamic control, to form fluorescent dendrimersomes for all three generations, with diameters averaging from 125-200 nm. This is highly sought as it can provide potential applications towards theranostics, especially that control over nanoparticle size is quite difficult and in order to be useful for biomedical applications, they should be smaller than 300 nm.**[14]** Applications of these dendrimersomes are currently under investigation.

CONCLUSION AND FUTURE PERSPECTIVE

Macromolecular materials have been essential throughout our daily life; clothes, furniture, industry, and medicine. Polymeric nanomaterials have been the main source of benefit for all these applications based on their enormous potential of being flexible, viscous, and resistant. In the field of nanomedicine, polymers are continuously being studied and pursued towards intracellular drug delivery and cancer therapy. Amphiphilic polymers investigated with acid-cleavable spirocyclic acetals demonstrated successful synthesis under copper-catalyzed azide-alkyne “click” polymerization, where they were able to undergo self-assembly to form spherical particles with diameters averaging 400 nm. Degradation of these polyacetals into their hydroxy and aldehyde units resulted in gradual decomposition over several days. In addition, efficient Nile red encapsulation and release from complete degradation of these nanomaterials was achieved within several days. Cellular assay concluded their non-toxic nature and ability to bind to the cell surface of ovarian hamster cells, capable of transporting encapsulated cargo into cells. These polymers are promising candidates for further applications as cleavable products must degrade within a range of a few days to possibly be used in clinical trials. Cleavable compounds that degrade too quickly (several hours) are inefficient towards drug delivery systems as the encapsulated cargo would not reach its target site. Cleavable compounds that degrade slowly (few weeks) are also inefficient as the cancerous cells would spread faster within the body than the desired drugs reaching their target site.

The amphiphilic Janus-based dendrimers investigated demonstrated successful synthesis under copper-catalyzed azide-alkyne “click” reactions, where they were able to undergo self-assembly to form bilayered vesicles (dendrimersomes), with diameters averaging from 130 nm to 200 nm. In addition, upon aggregation, bright blue illumination of the solution was present, where at the same molar concentration, the

increase in generation lead to increase in fluorescence intensity as a result of augmentation of TPE moles. The increase in generation also lead to a decrease in the size of the dendrimersomes as a result of the compact factor from the TPE molecules. These dendrimers are promising candidates as their dendrimersomes are highly sought for their capability of encapsulating both hydrophobic and hydrophilic drugs, leading to potential investigations into theranostic applications.

Despite the progress in the design of dendritic structures with improved features for biomedical application, one of the main drawbacks of the most currently used dendrimers is their non-degradability under physiological conditions that can result in cytotoxicity and accumulation of nondegradable synthetic materials inside cells or in tissues.[71] In vitro studies have shown that dendrimer cytotoxicity is mainly associated with cell membrane disruption and subsequent necrosis/non-apoptotic cell death. Apart from membrane destabilization, toxicity may also arise from impaired oxidative metabolism resulting from mitochondrial dysfunction and changes in endogenous gene expression that ultimately lead to apoptotic cell death.[71] Dendrimer chemistry, charge, and size are features that will also have an impact on in vivo biodistribution and pharmacokinetics. The use of biodegradable materials that can degrade into smaller fragments and be eliminated through metabolic pathways is expected to overcome the risk of long-term complications.[71] In accordance with these preliminary results, we have the potential to envision and research three new avenues of Janus dendrimer applications: (i) degradable amphiphilic Janus dendrimers and their assemblies for controlled drug release, (ii) light responsive azo-containing amphiphilic Janus dendrimers and their assemblies for controlled drug release, as well as investigation of cis-trans transformation upon illumination, and (iii) development of linear-dendritic block copolymers and their assemblies with aggregation induced emission properties for controlled drug release and theranostic applications.

APPENDIX A

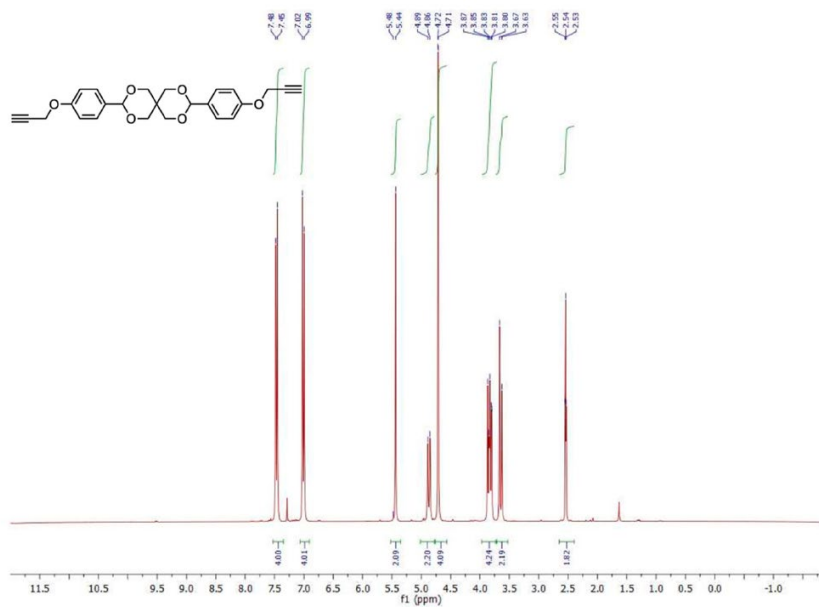


Figure A1. ¹H-NMR spectrum of compound 2 (300 MHz, CDCl₃).

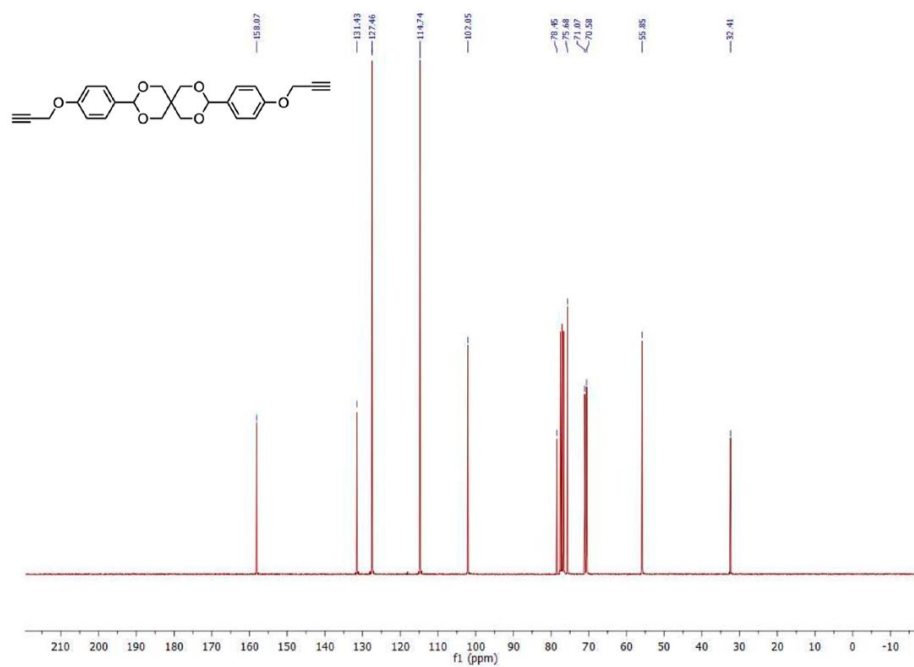


Figure A2. ¹³C-NMR spectrum of compound 2 (75 MHz, CDCl₃).

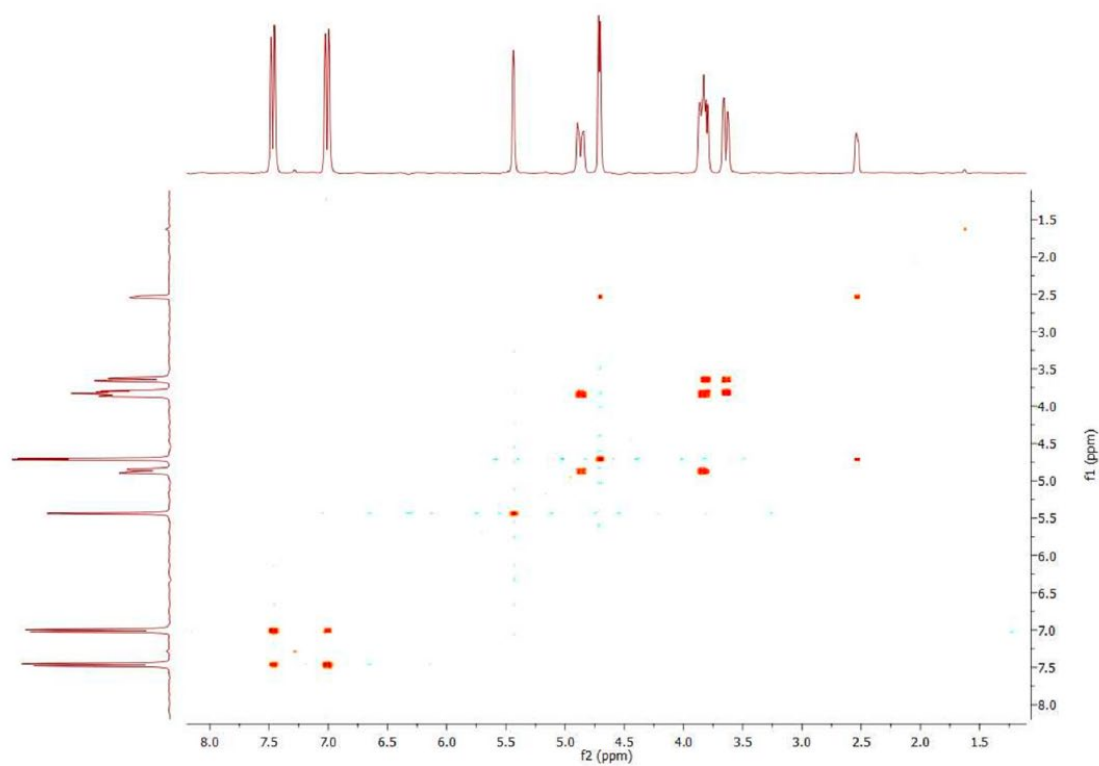


Figure A3. ^1H - ^1H COSY spectrum of compound **2** (300 MHz, CDCl_3).

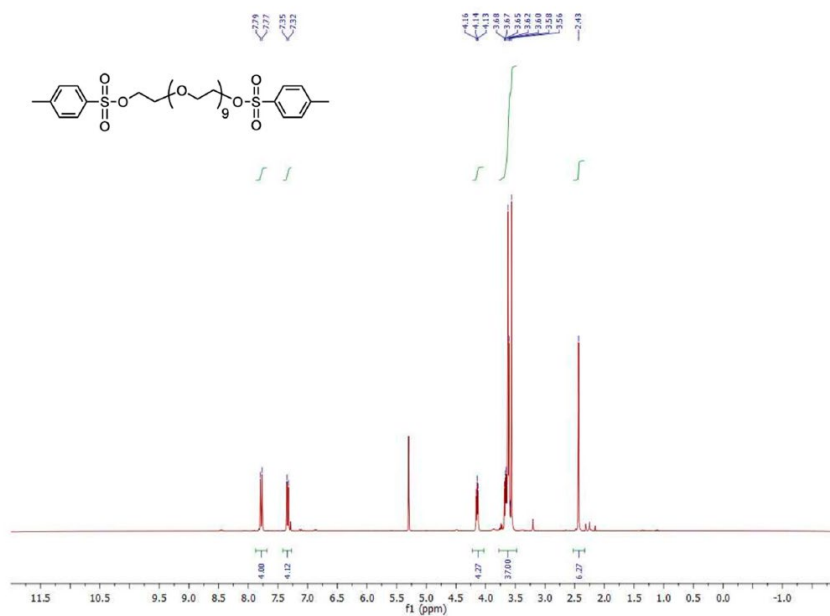


Figure A4. ^1H -NMR spectrum of compound **3** (300 MHz, CDCl_3).

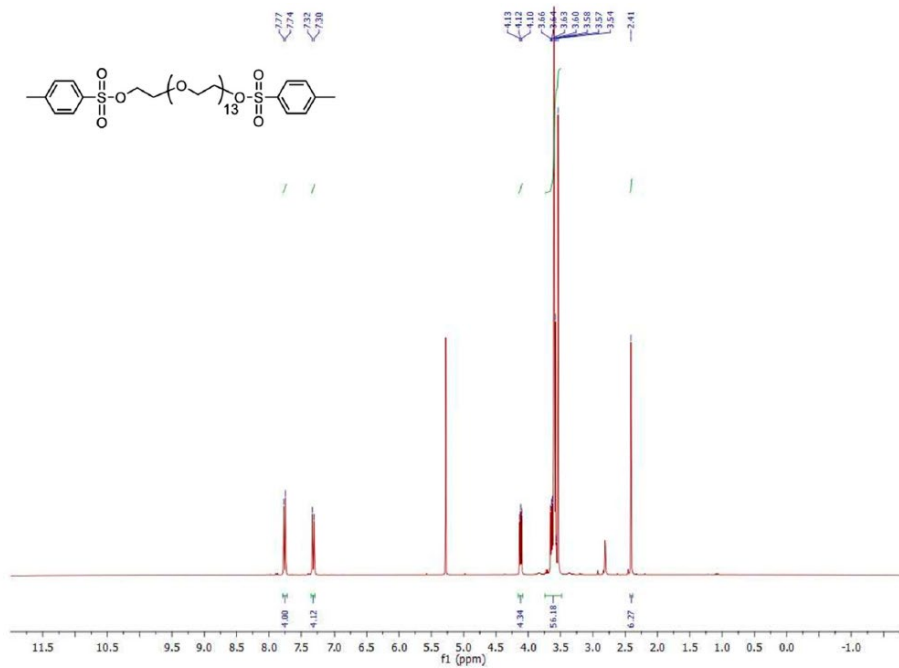


Figure A5. ¹H-NMR spectrum of compound 4 (300 MHz, CDCl₃).

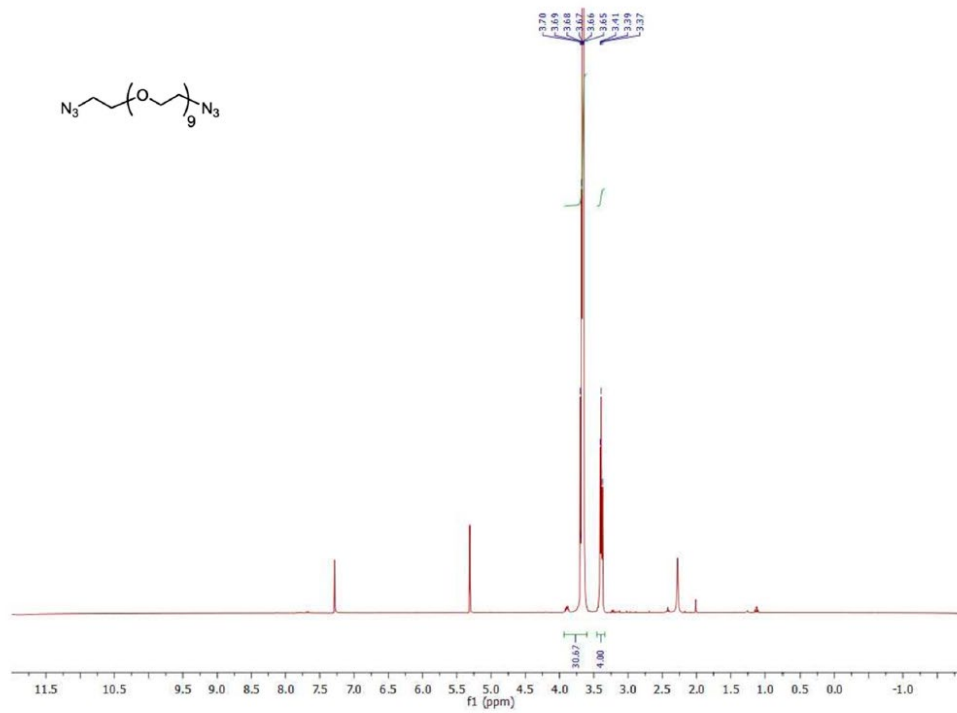


Figure A6. ¹H-NMR spectrum of compound 5 (300 MHz, CDCl₃).

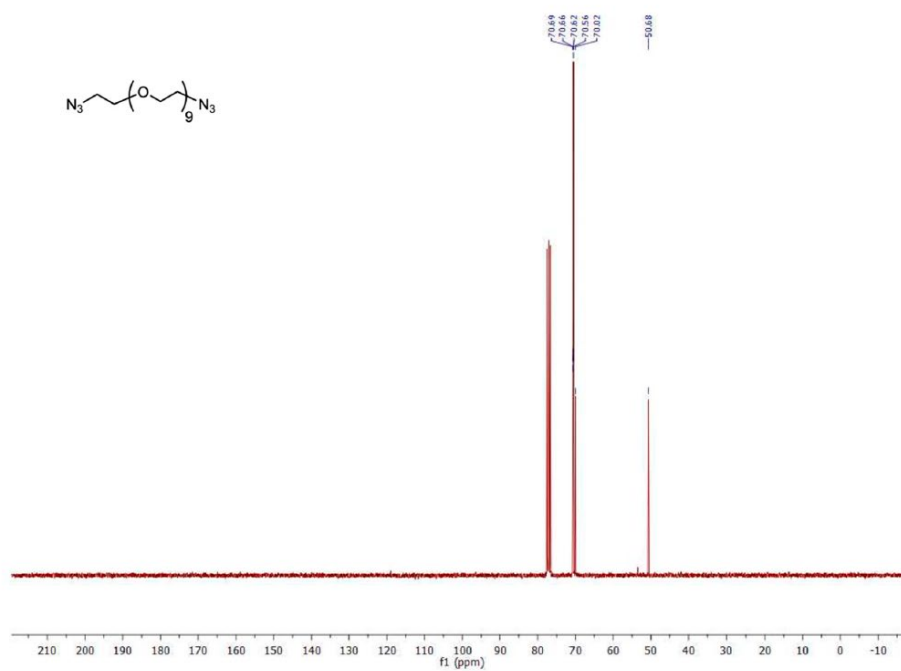


Figure A7. ¹³C-NMR spectrum of compound **5** (75 MHz, CDCl₃).

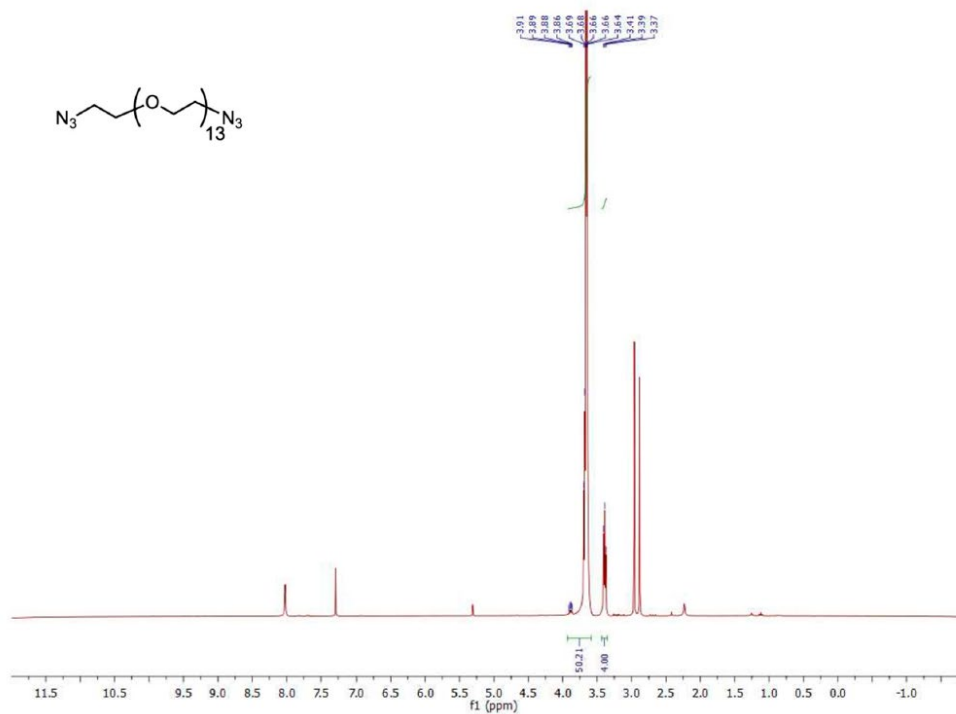


Figure A8. ¹H-NMR spectrum of compound **6** (300 MHz, CDCl₃).

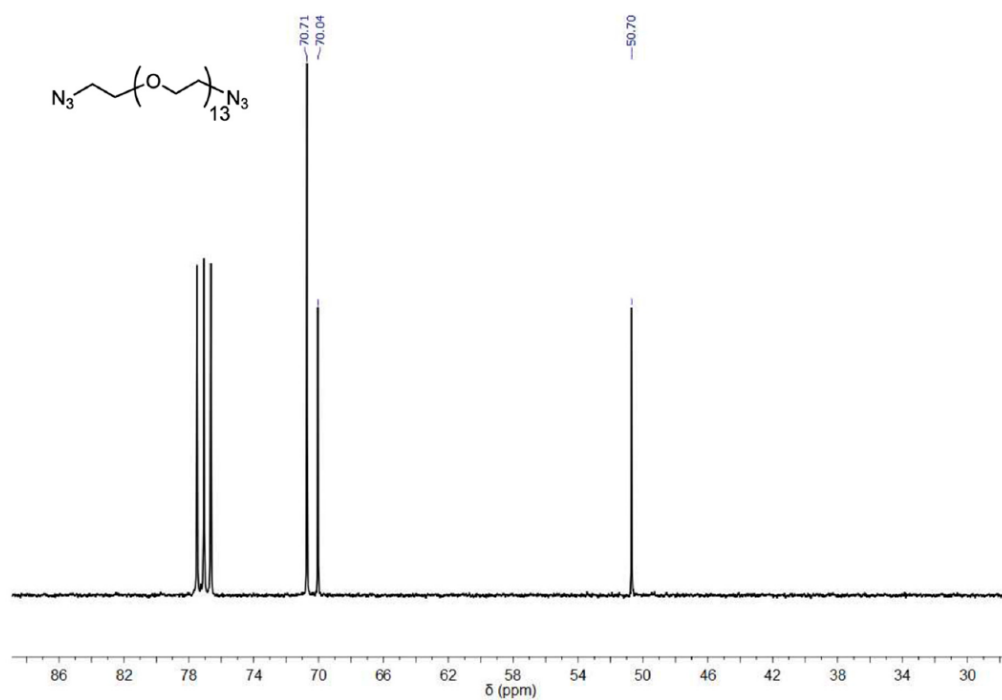


Figure A9. $^{13}\text{C-NMR}$ spectrum of compound **6** (75 MHz, CDCl_3).

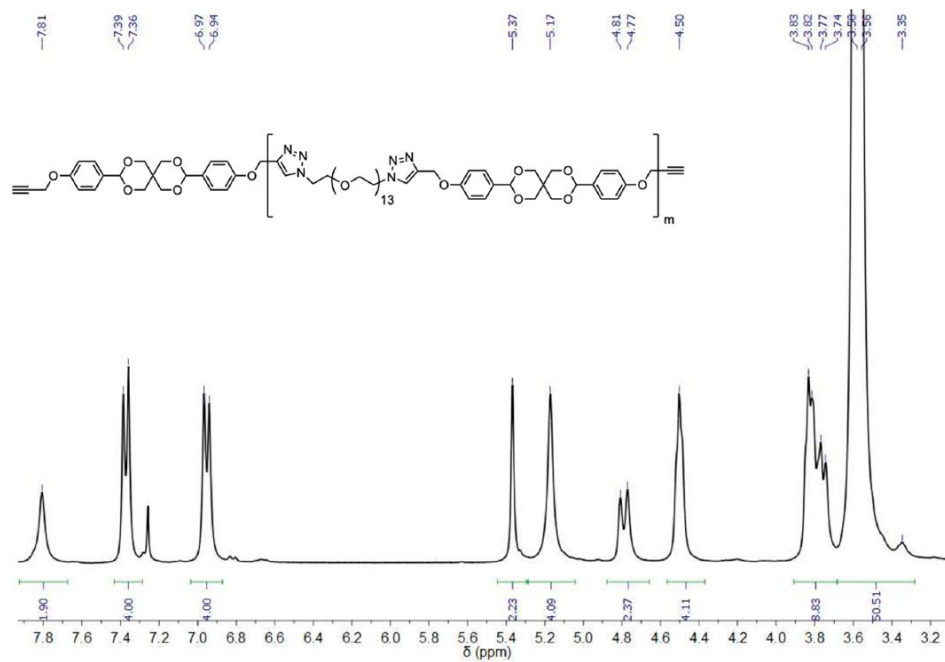


Figure A10. $^1\text{H-NMR}$ spectrum of polymer **8** (300 MHz, CDCl_3).

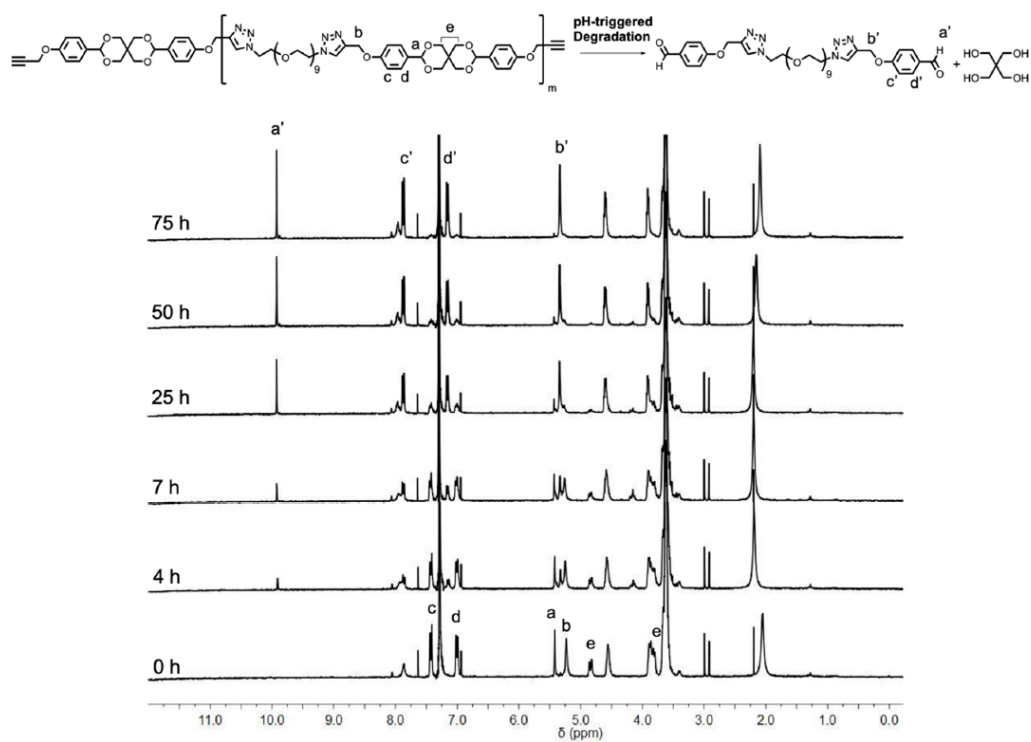


Figure A11. pH-triggered degradation of polymer **8** in 80 mM trifluoroacetic acid in CDCl_3 monitored by $^1\text{H-NMR}$ spectroscopy.

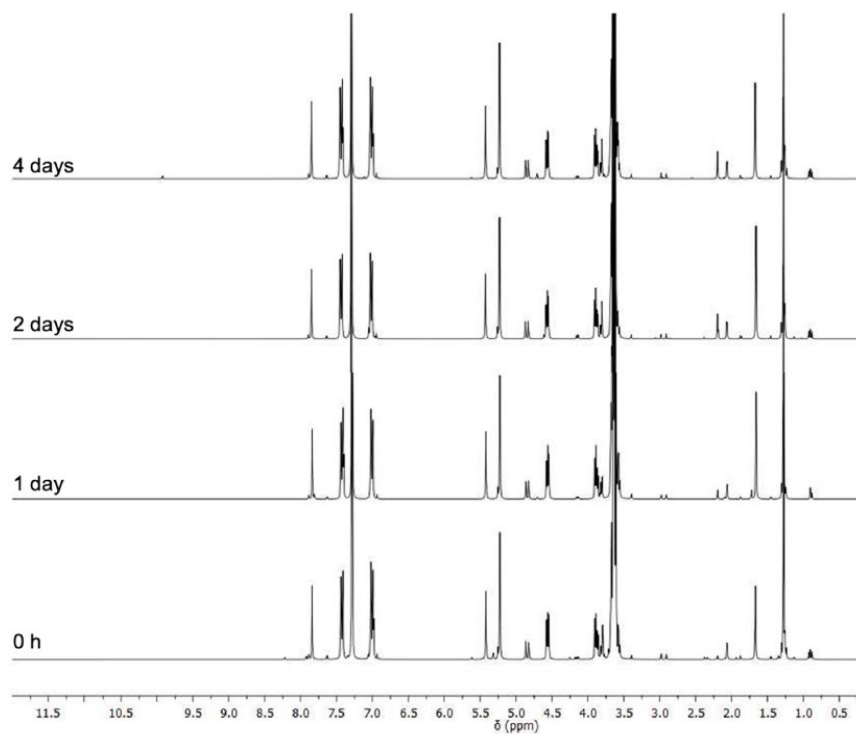


Figure A12. Stability of (7) in non-acidic CDCl_3 monitored by $^1\text{H-NMR}$ spectroscopy.

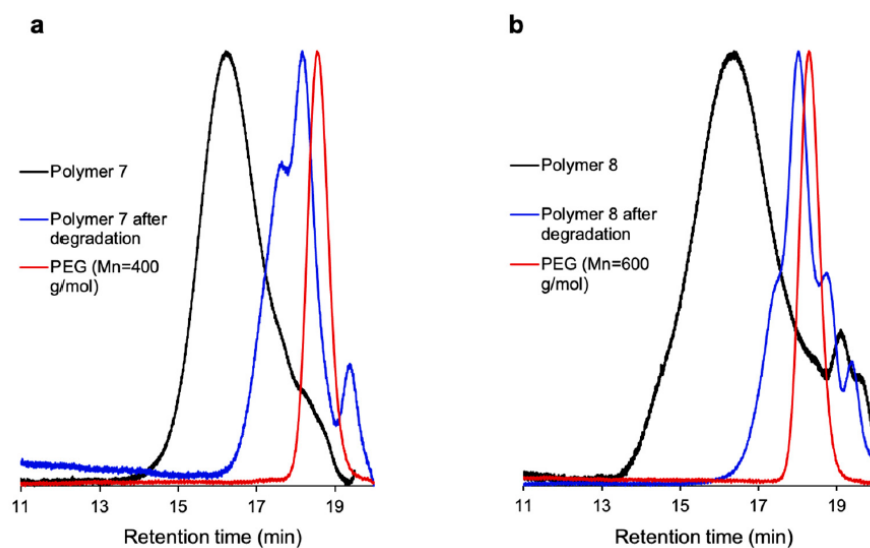


Figure A13. Refractive index (RI) traces in the SEC analysis of (a) polymer (7) before and after degradation as well as the PEG starting material ($M_n=$

400 g/mol) and **(b)** polymer **8** before and after degradation as well as the PEG starting material ($M_n = 600$ g/mol).

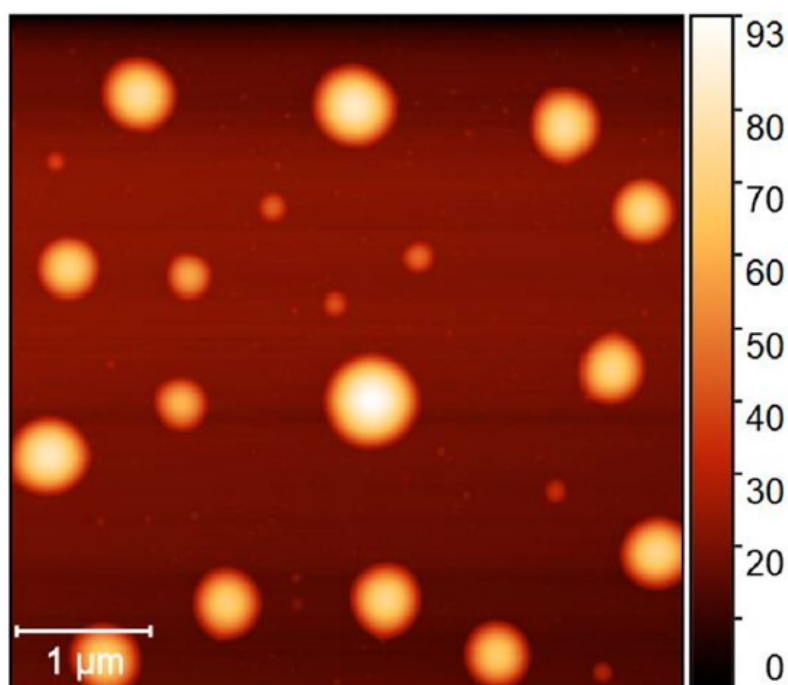


Figure A14. AFM image of Nile red-loaded particles (**P1**) formed by polymer **(8)**.

APPENDIX B

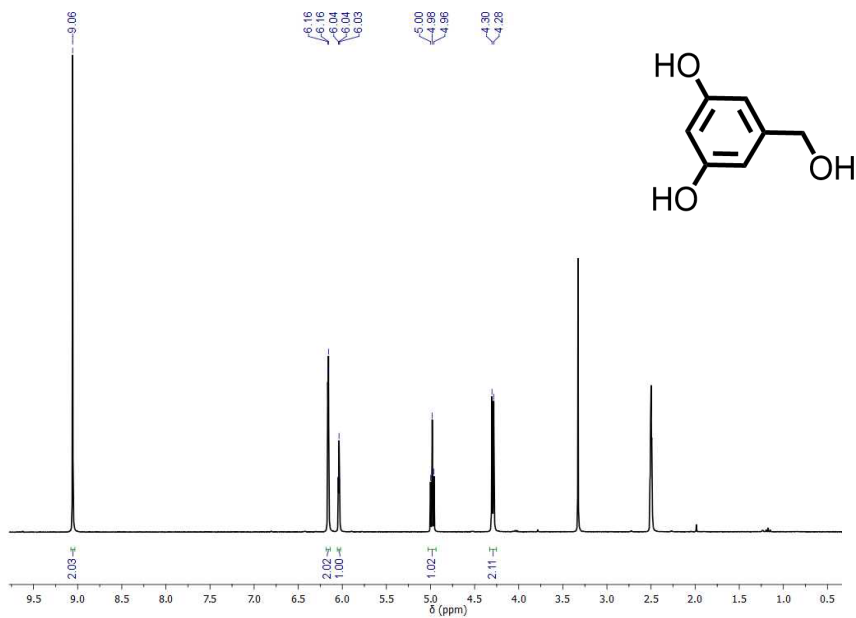


Figure B1. $^1\text{H-NMR}$ of **9** in DMSO-d_6 (300 MHz).

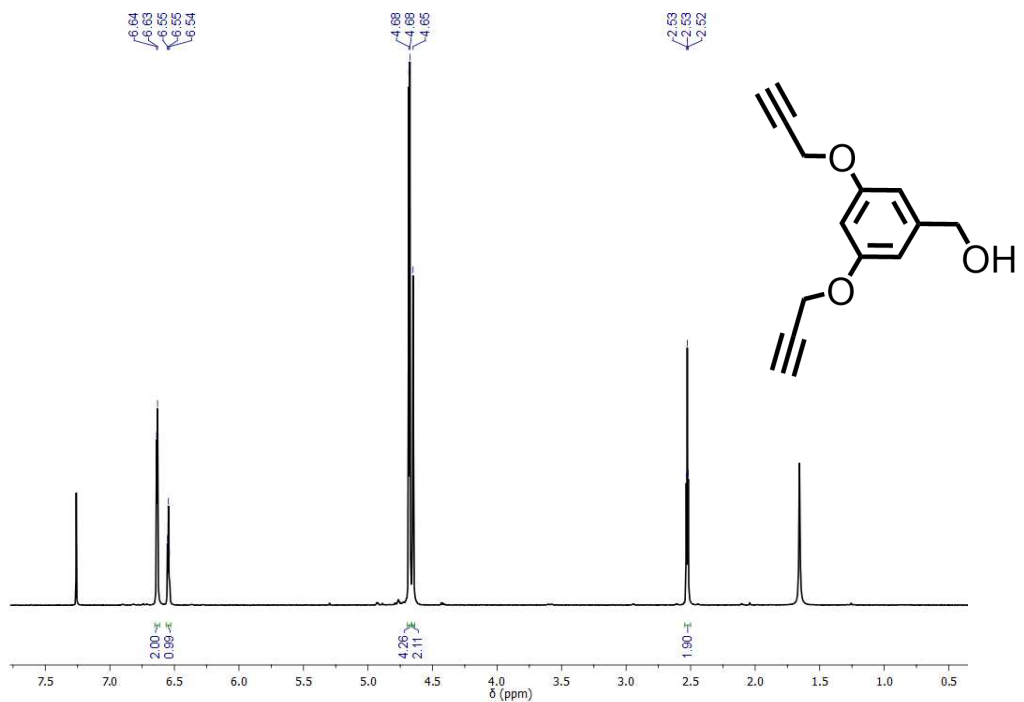
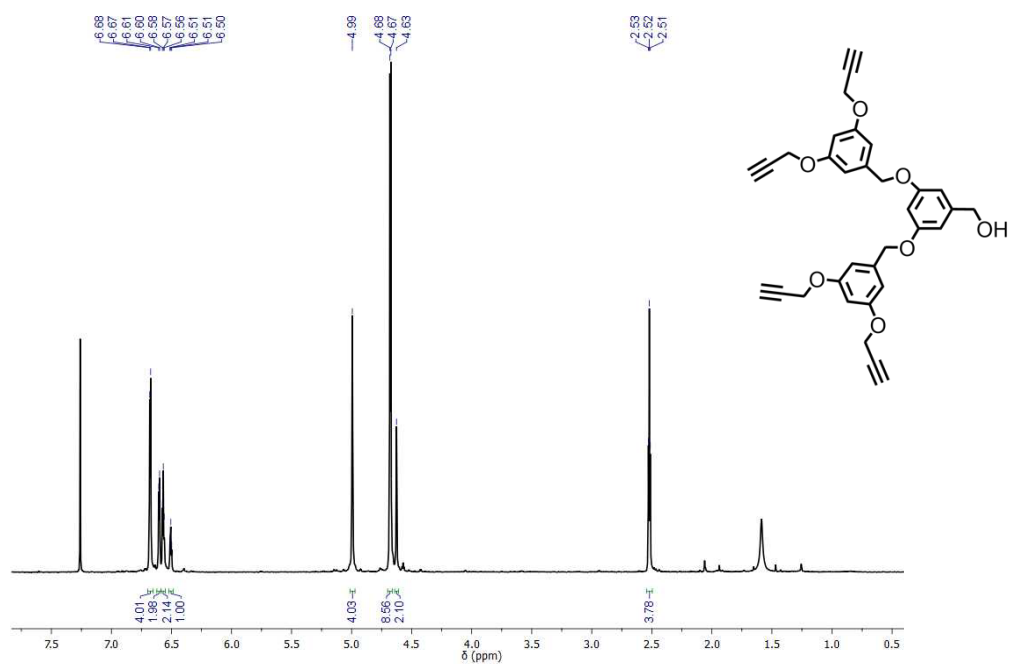
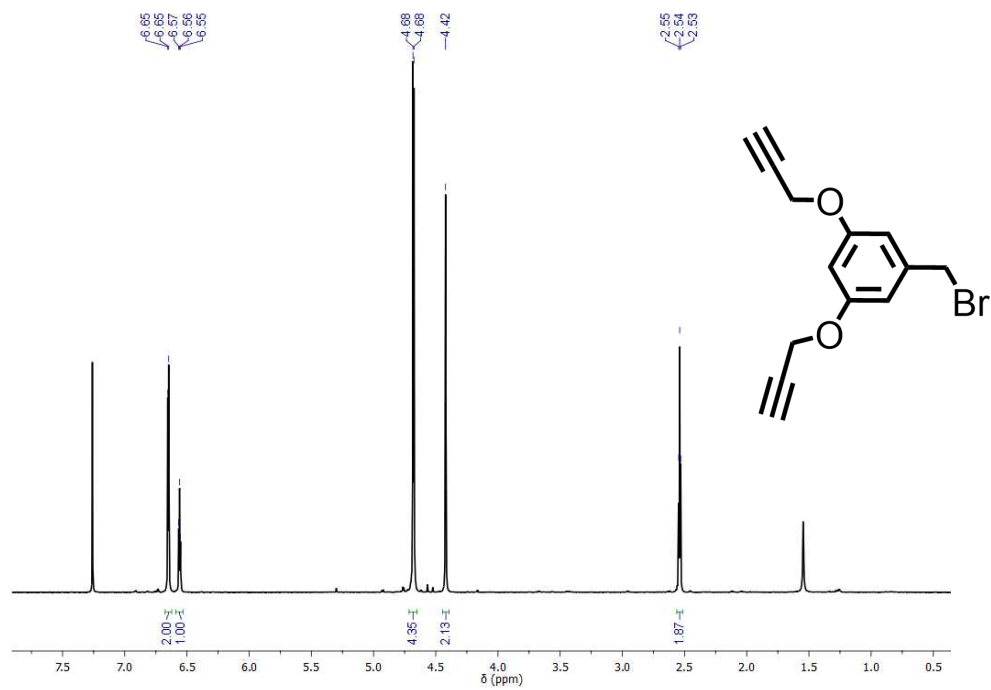


Figure B2. $^1\text{H-NMR}$ of **10** in CDCl_3 (300 MHz).



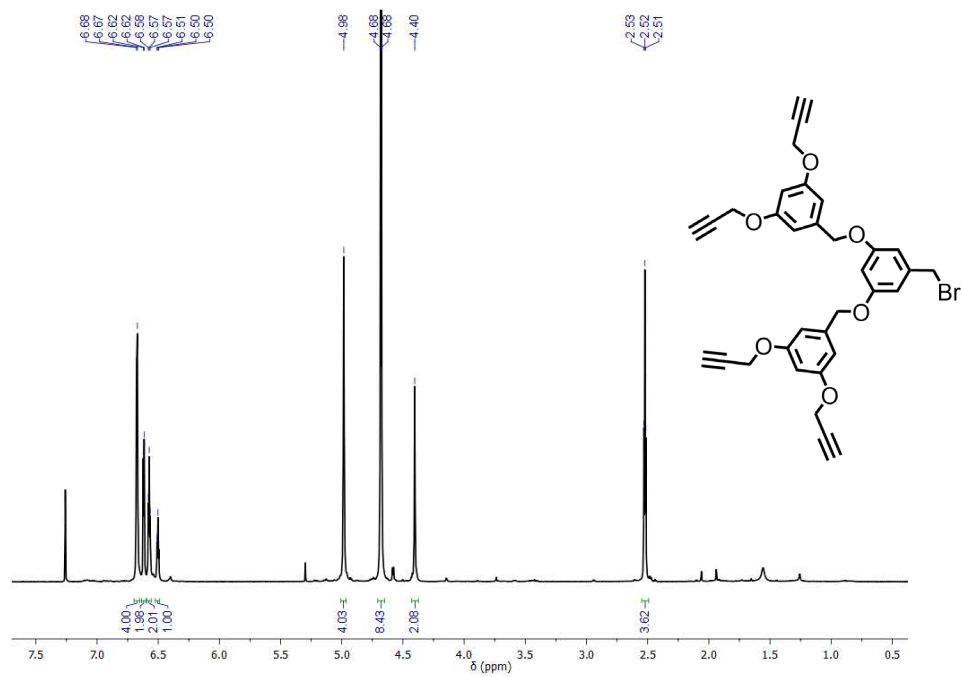


Figure B5. ¹H-NMR of **13** in CDCl₃(300 MHz).

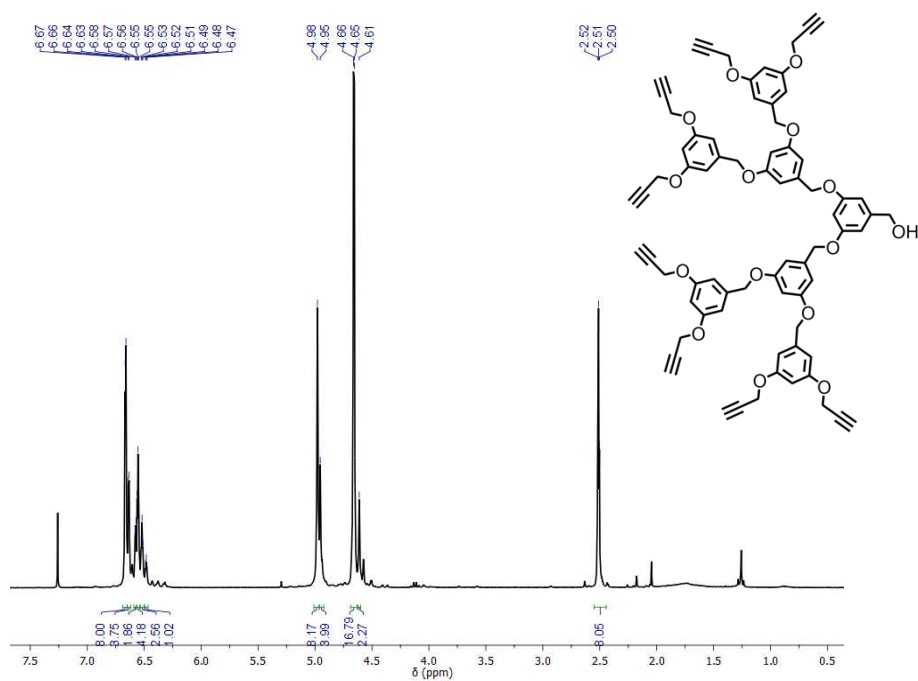


Figure B6. ¹H-NMR of **14** in CDCl₃(300 MHz).

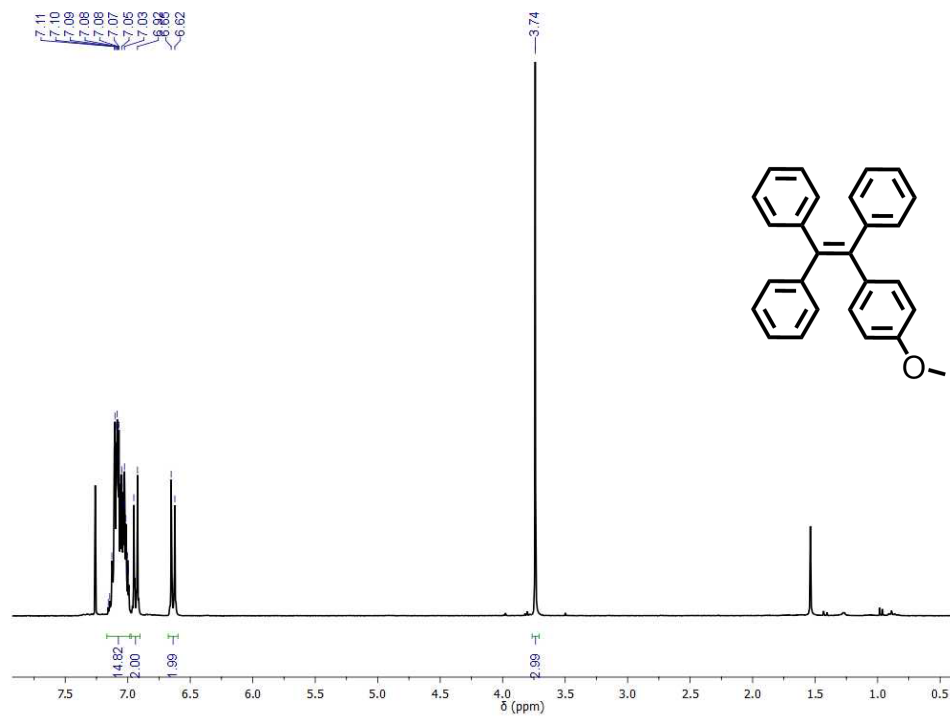


Figure B7. ¹H-NMR of **15** in CDCl₃(300 MHz).

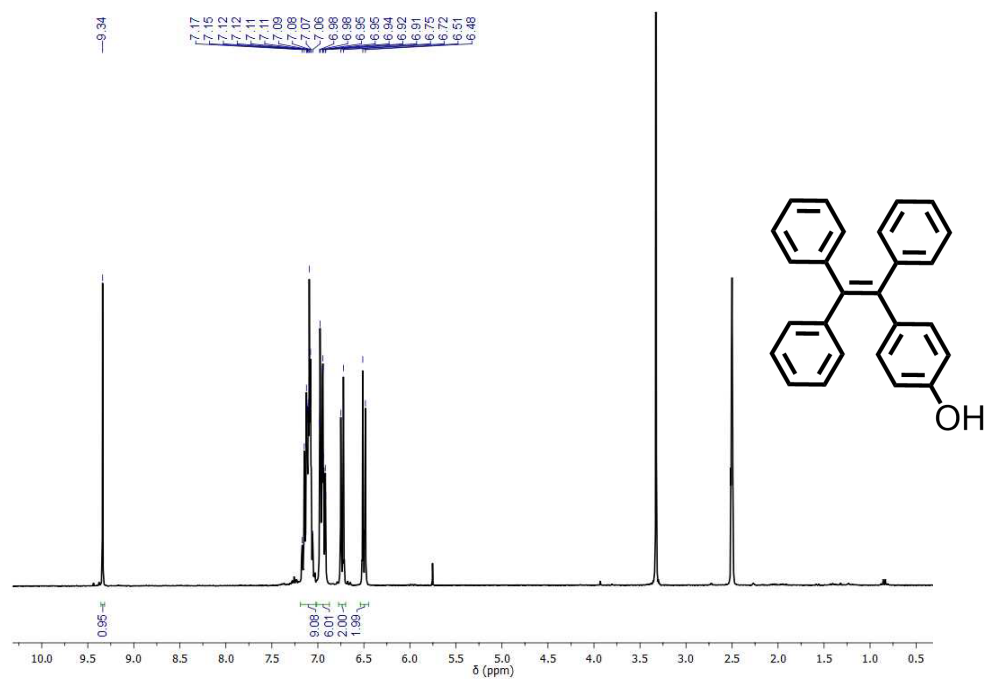


Figure B8. ¹H-NMR of **16** in DMSO-d₆(300 MHz).

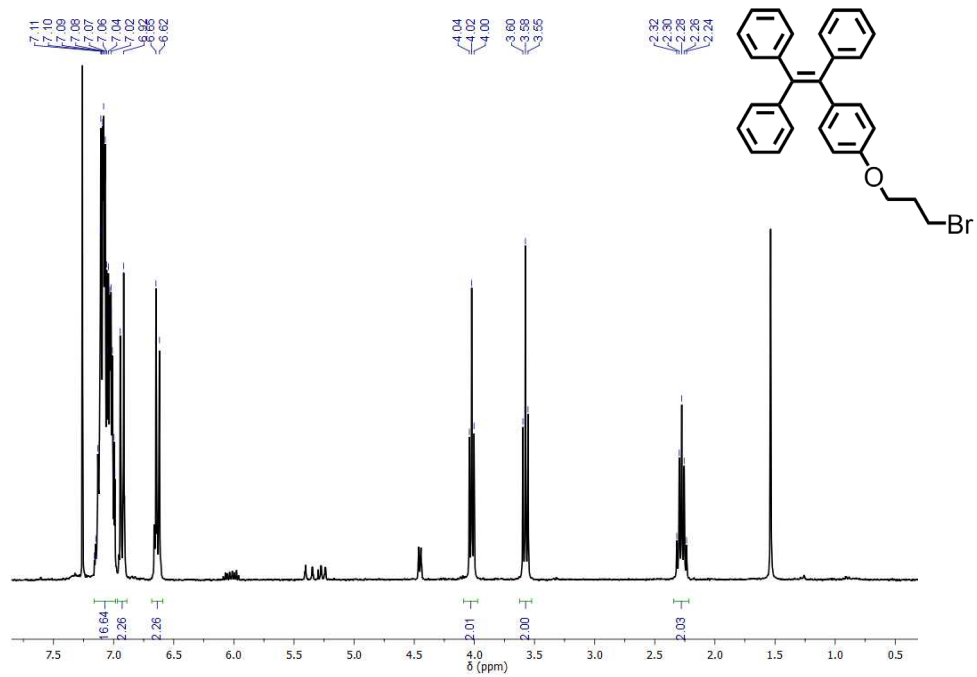


Figure B9. $^1\text{H-NMR}$ of **17** in CDCl_3 (300 MHz).

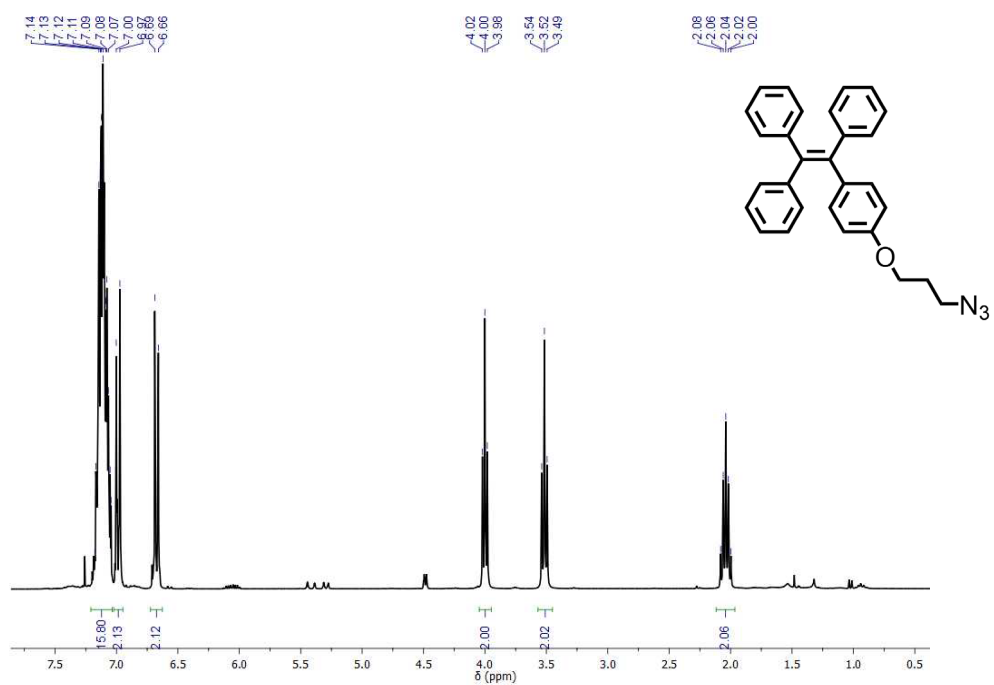


Figure B10. $^1\text{H-NMR}$ of **18** in CDCl_3 (300 MHz).

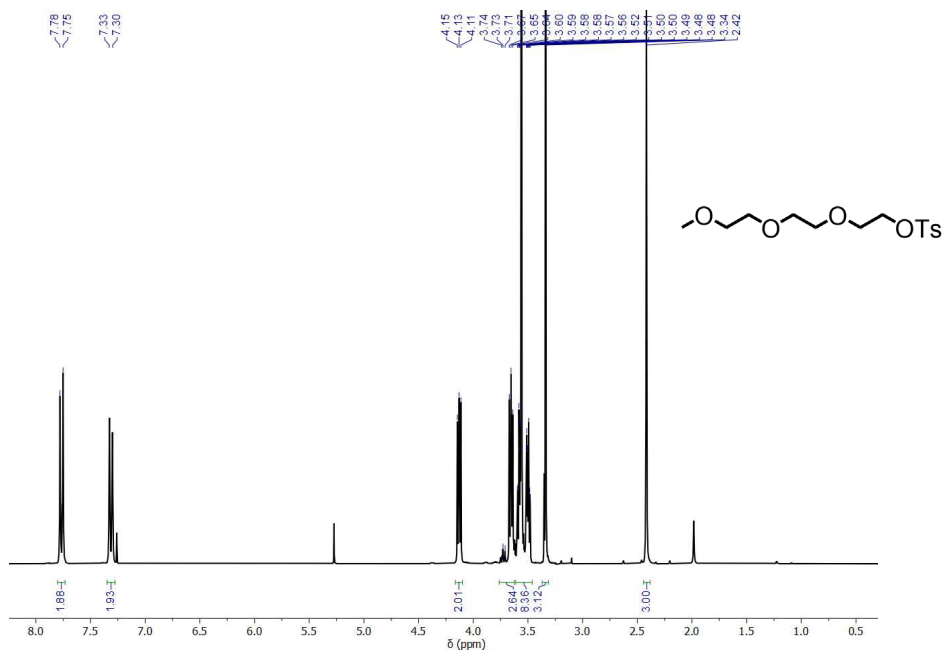


Figure B11. ¹H-NMR of **19** in CDCl₃(300 MHz).

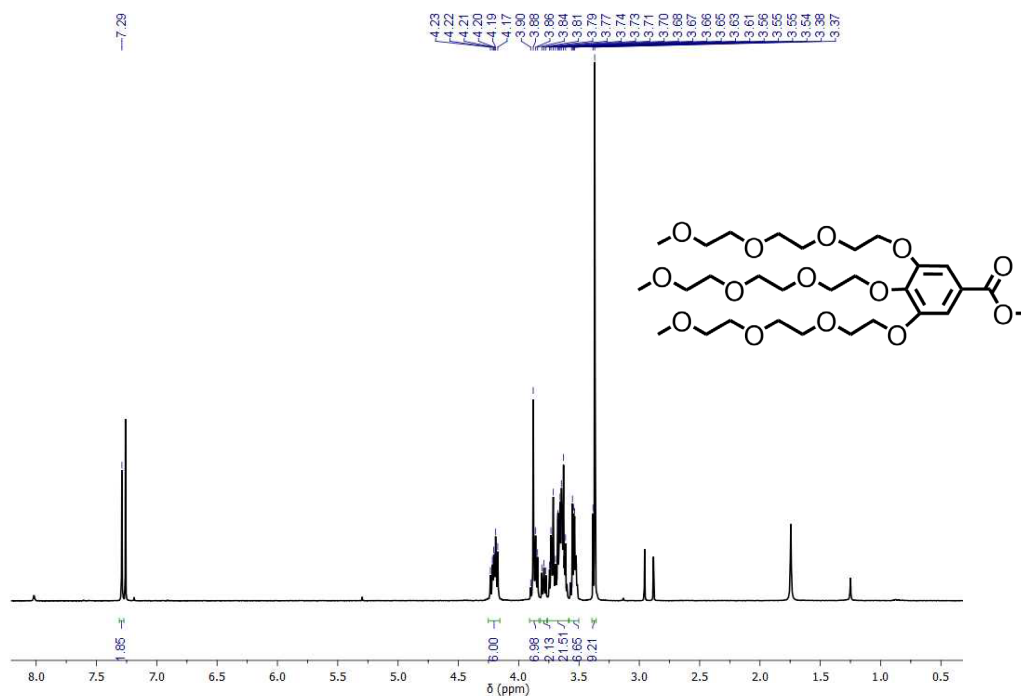


Figure B12. ¹H-NMR of **20** in CDCl₃(300 MHz).

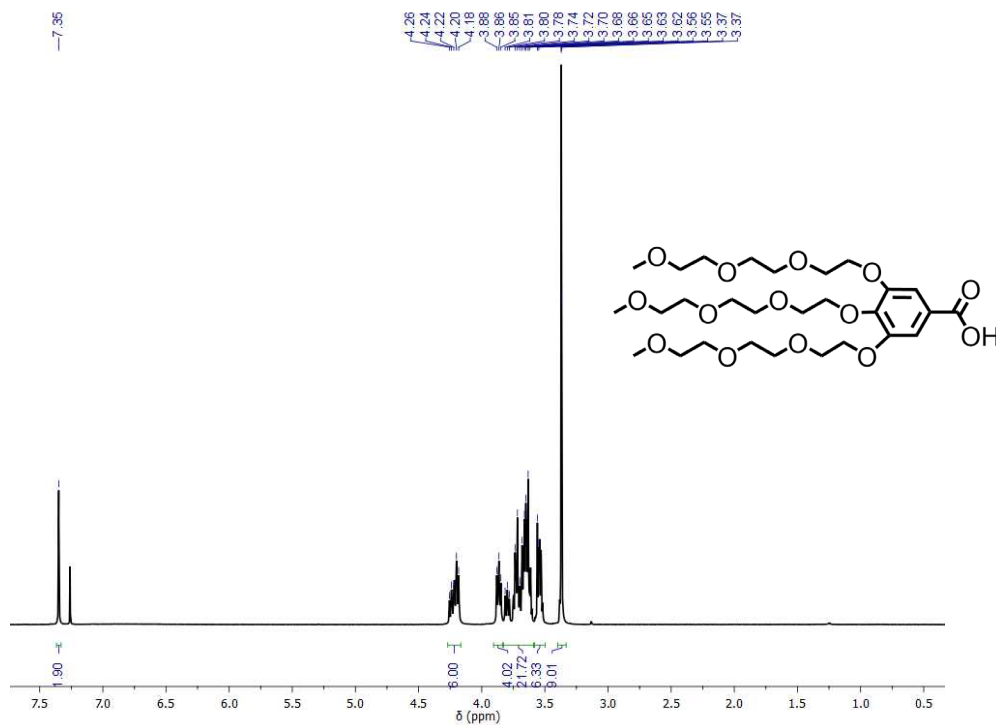


Figure B13. $^1\text{H-NMR}$ of **21** in CDCl_3 (300 MHz).

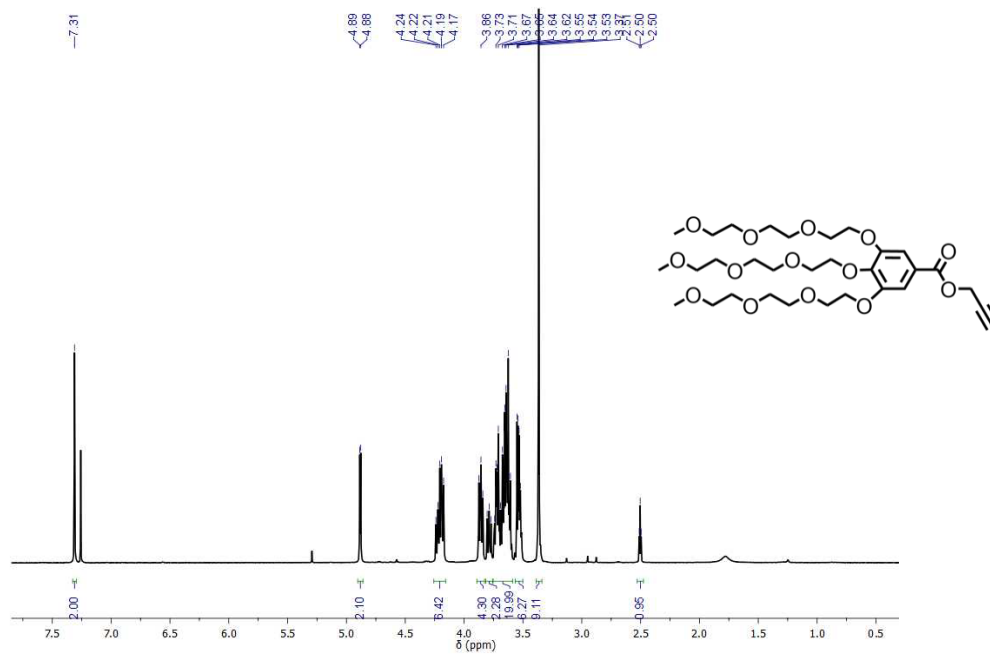


Figure B14. $^1\text{H-NMR}$ of **22** in CDCl_3 (300 MHz).

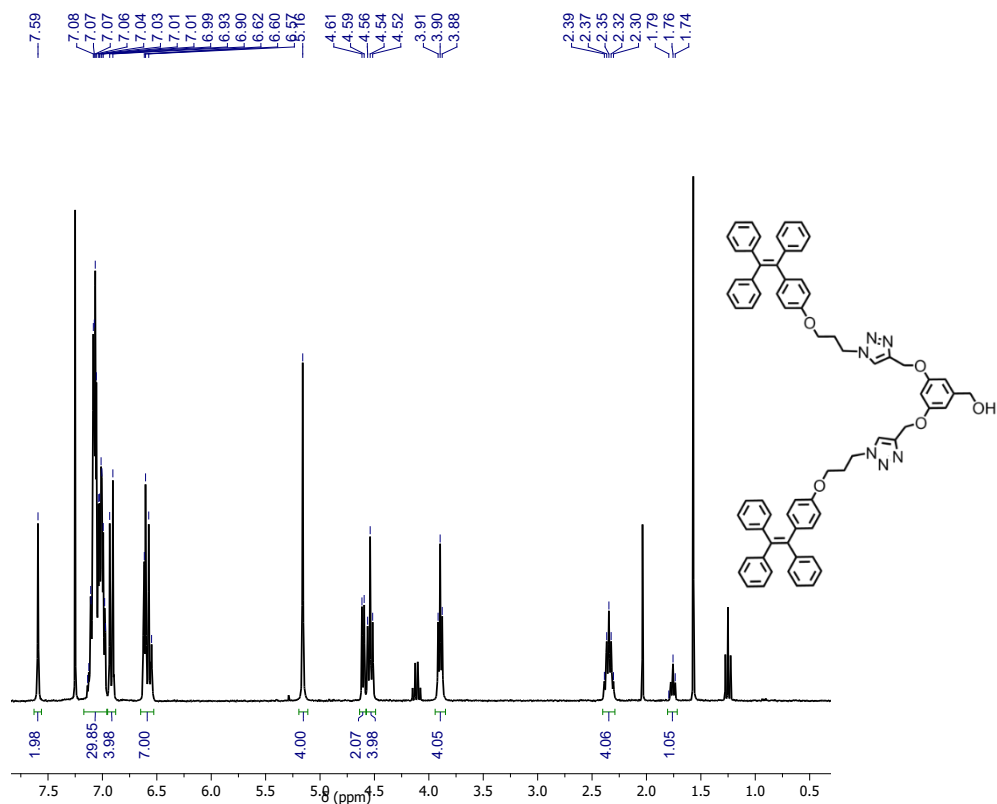


Figure B15. $^1\text{H-NMR}$ of **23** in CDCl_3 (300 MHz).

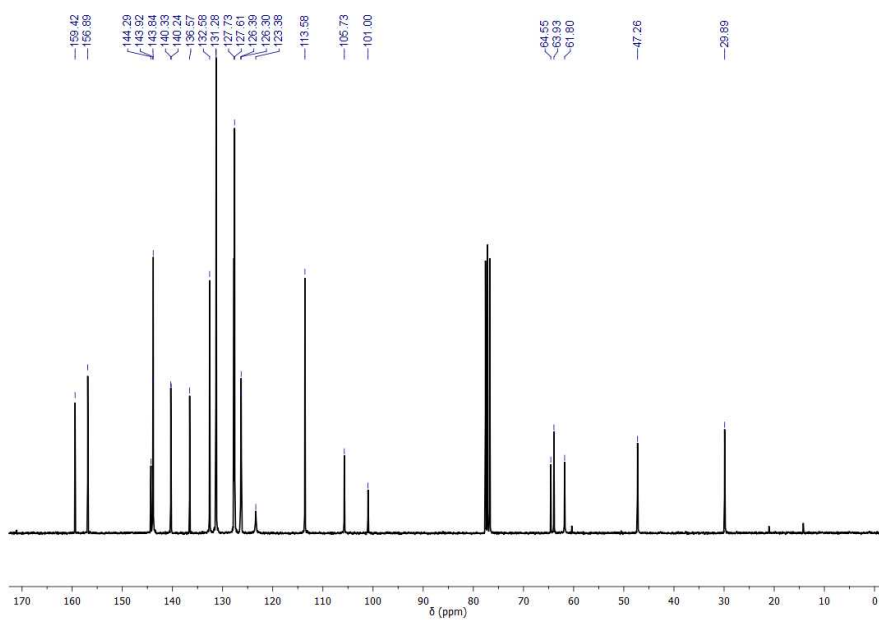


Figure B16. $^{13}\text{C-NMR}$ of **23** in CDCl_3 (75 MHz).

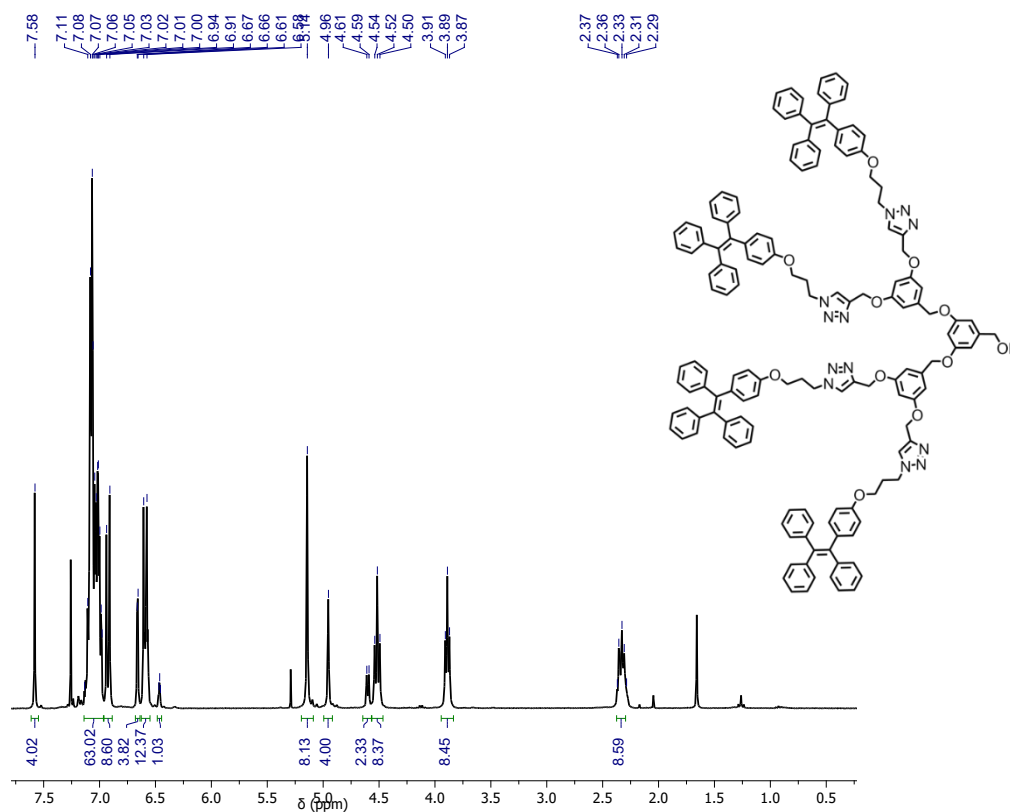


Figure B17. $^1\text{H-NMR}$ of **24** in CDCl_3 (300 MHz).

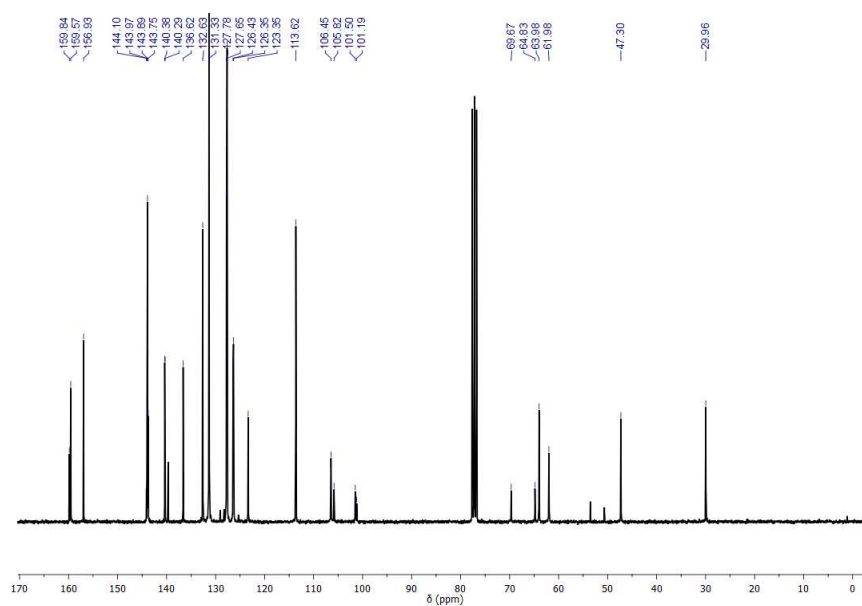


Figure B18. $^{13}\text{C-NMR}$ of **24** in CDCl_3 (75 MHz).

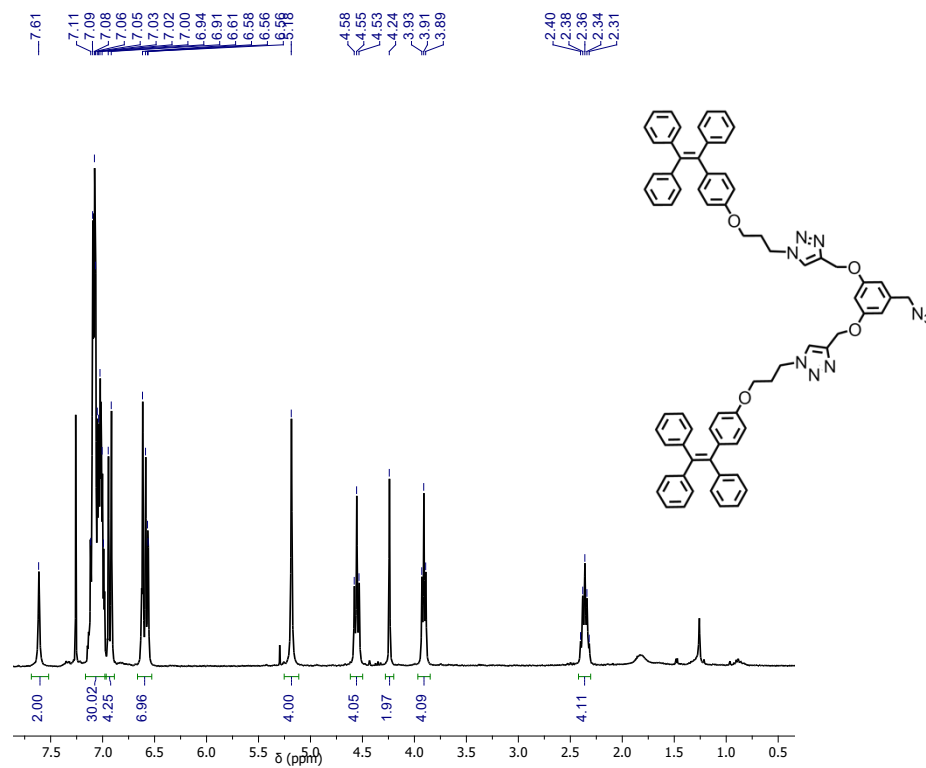


Figure B21. $^1\text{H-NMR}$ of **26** in CDCl_3 (300 MHz).

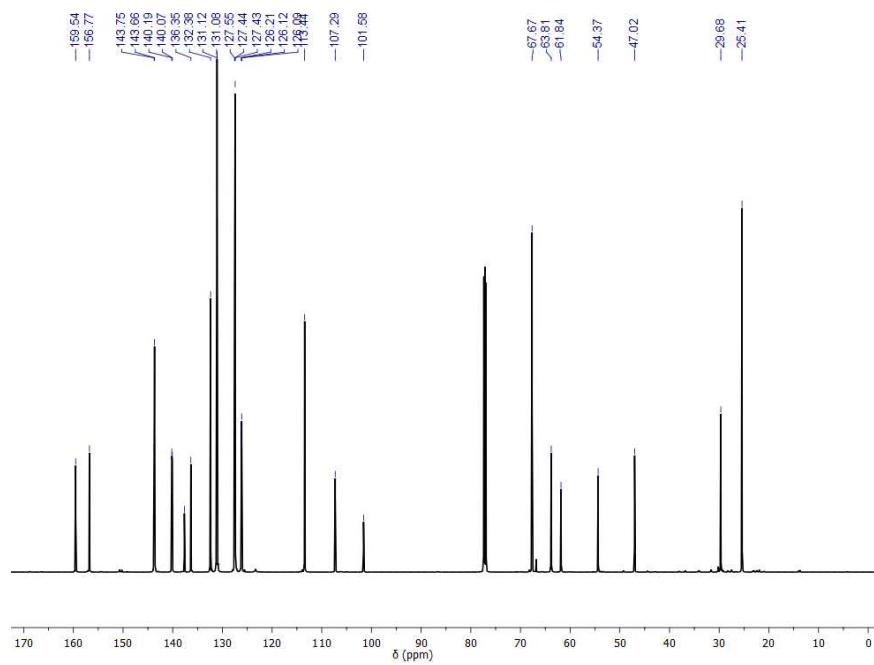


Figure B22. $^{13}\text{C-NMR}$ of **26** in CDCl_3 (150 MHz)

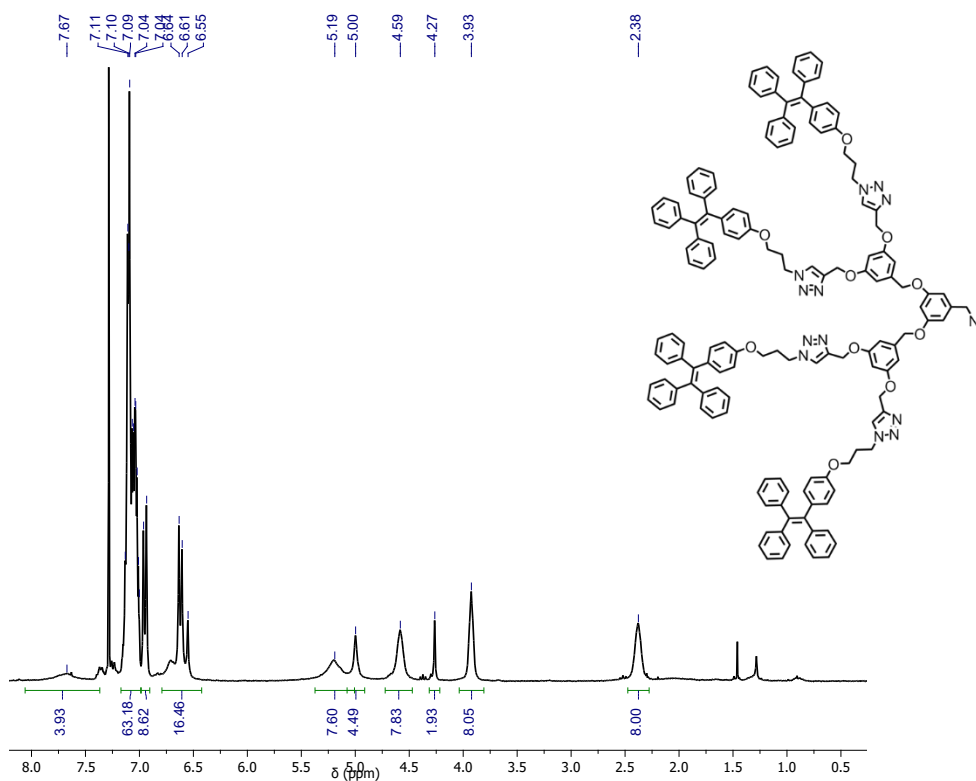


Figure B23. $^1\text{H-NMR}$ of **27** in CDCl_3 (300 MHz).

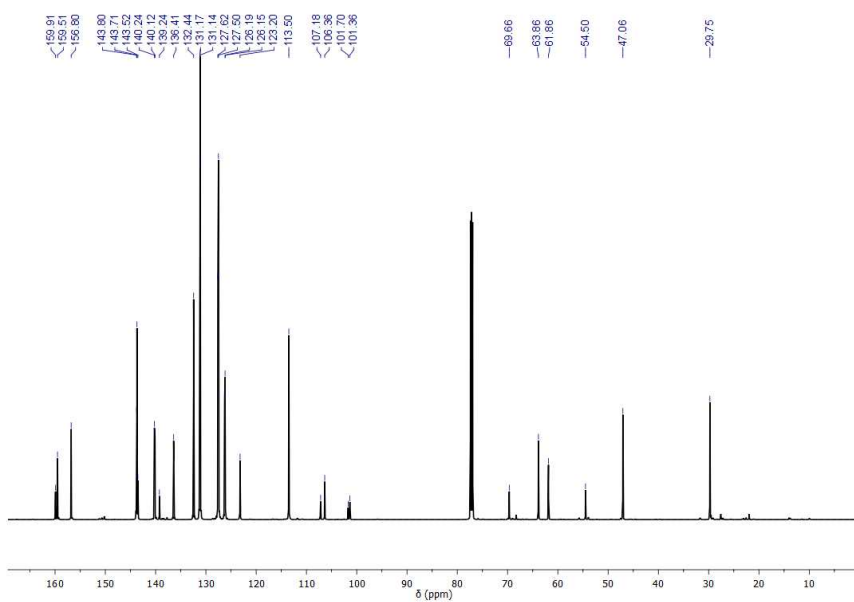


Figure B24. $^{13}\text{C-NMR}$ of **27** in CDCl_3 (150 MHz)

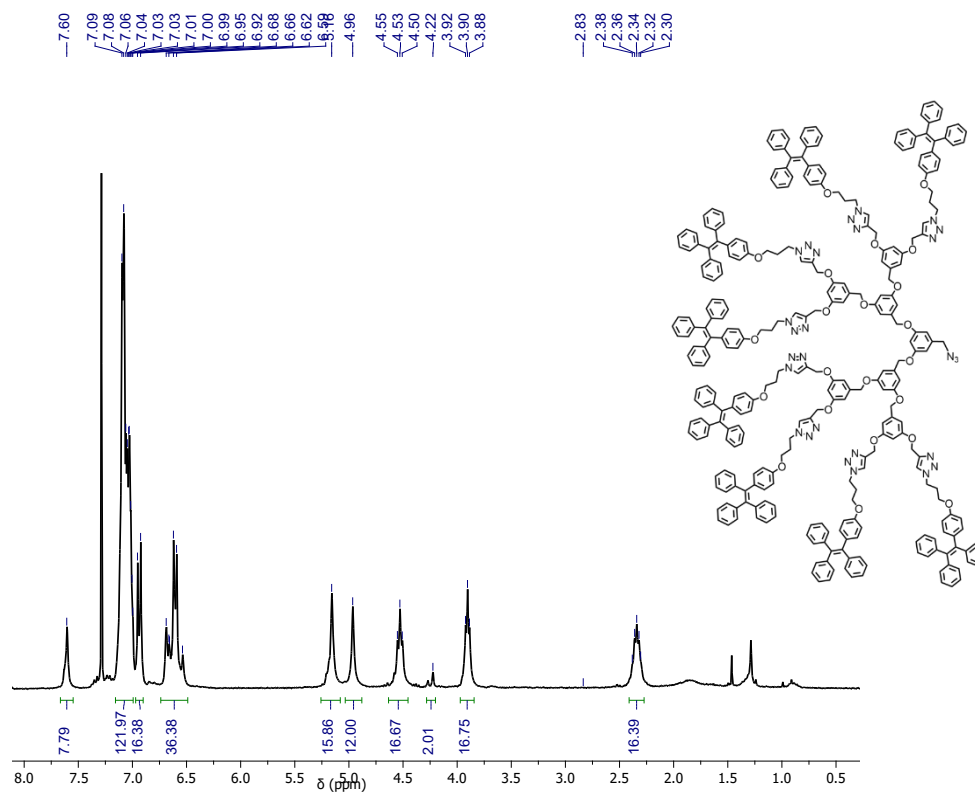


Figure B25. $^1\text{H-NMR}$ of **28** in CDCl_3 (300 MHz).

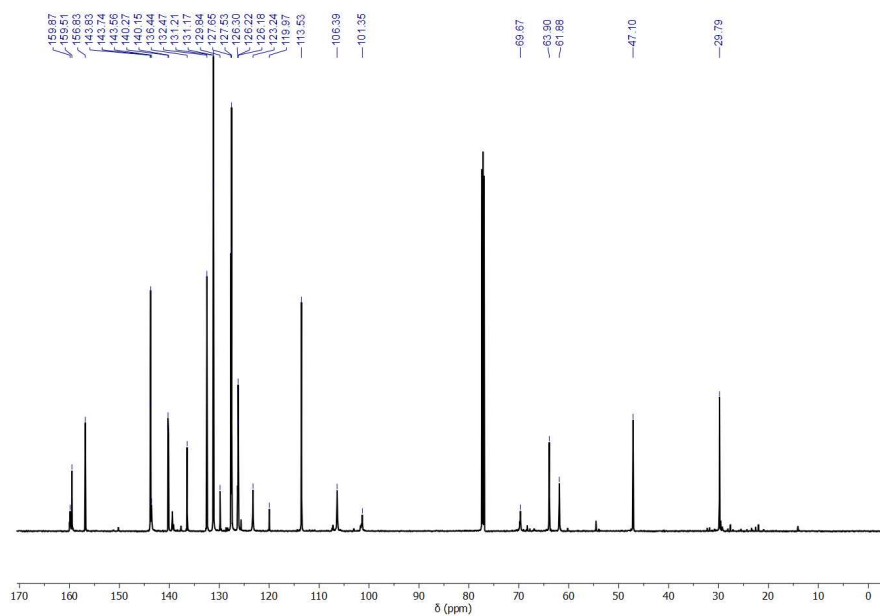


Figure B26. $^{13}\text{C-NMR}$ of **28** in CDCl_3 (150 MHz).

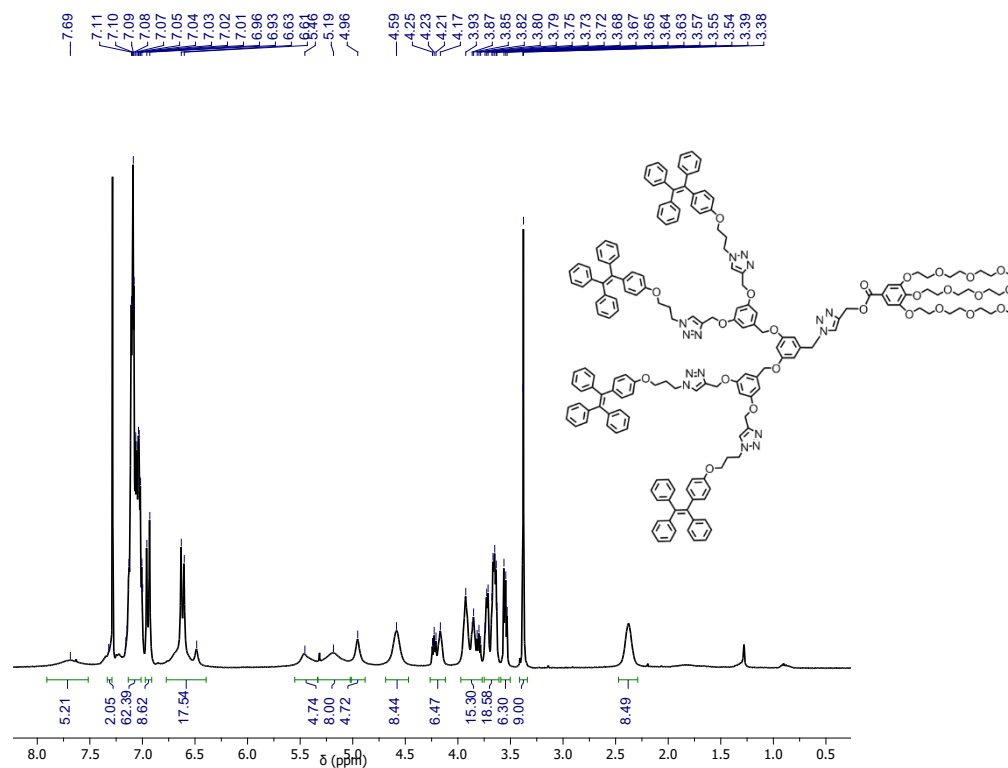


Figure B29. $^1\text{H-NMR}$ of **30** in CDCl_3 (300 MHz).

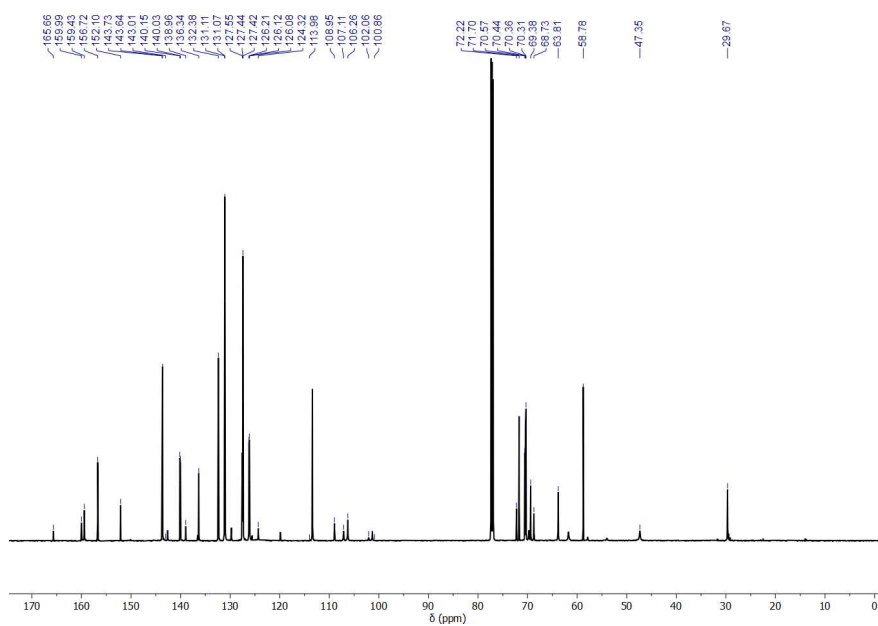


Figure B30. $^{13}\text{C-NMR}$ of **30** in CDCl_3 (150 MHz).

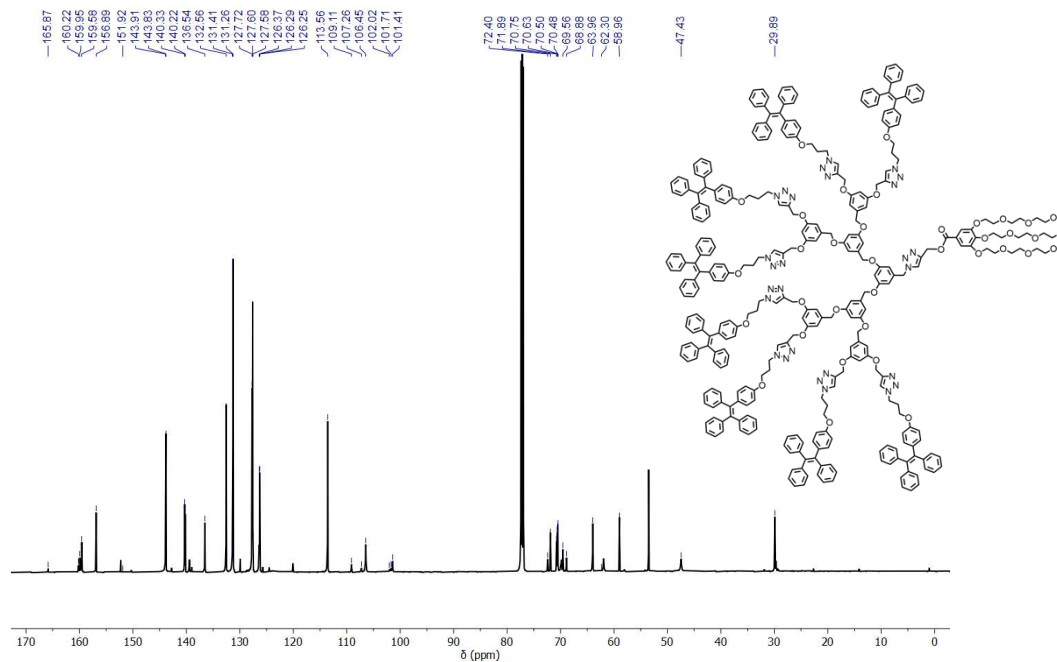


Figure B31. ^{13}C -NMR of **31** in CDCl_3 (150 MHz).

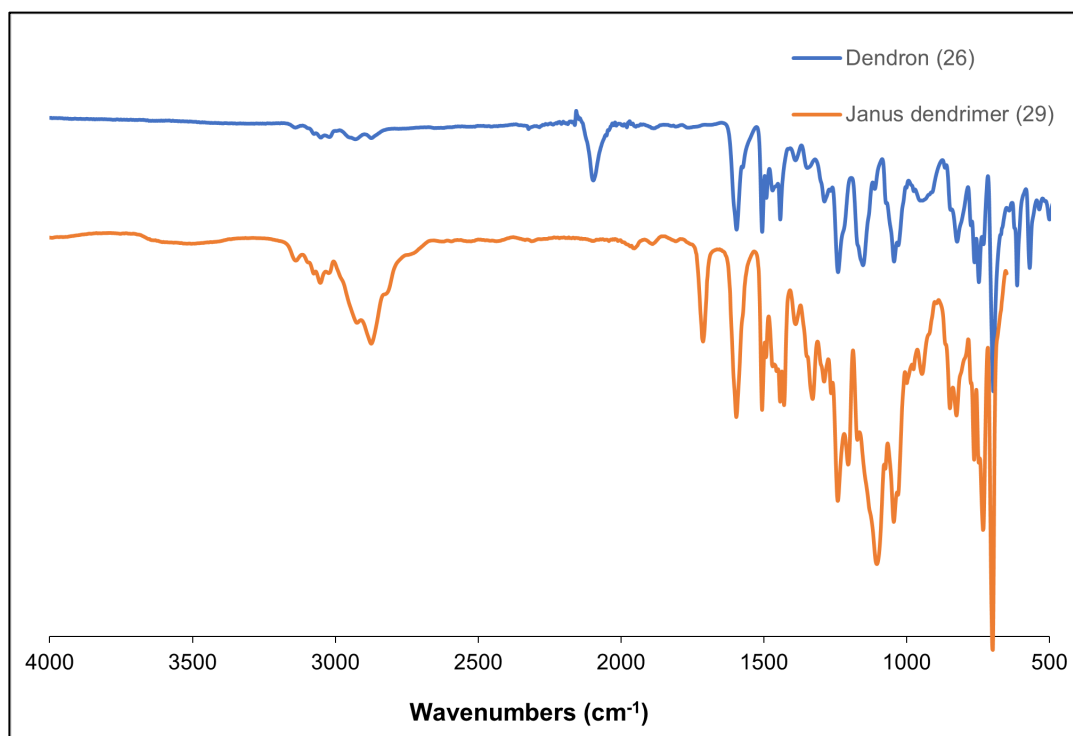


Figure B32. IR spectrum of dendron (**26**) and Janus dendrimer (**29**).

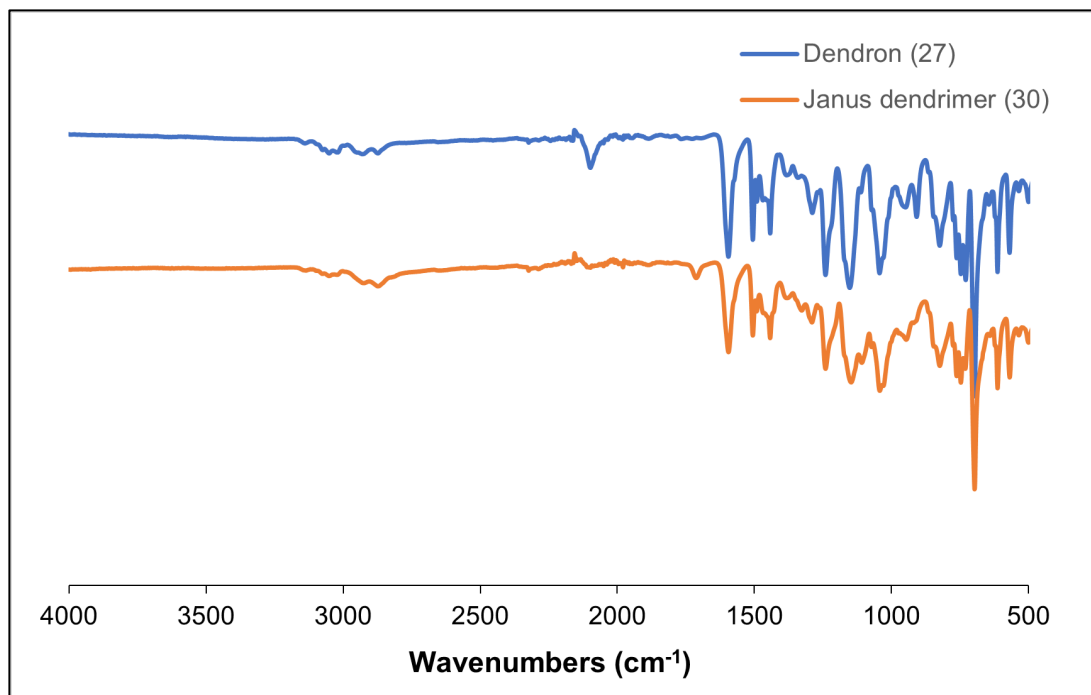


Figure B33. IR spectrum of dendron (27) and Janus dendrimer (30).

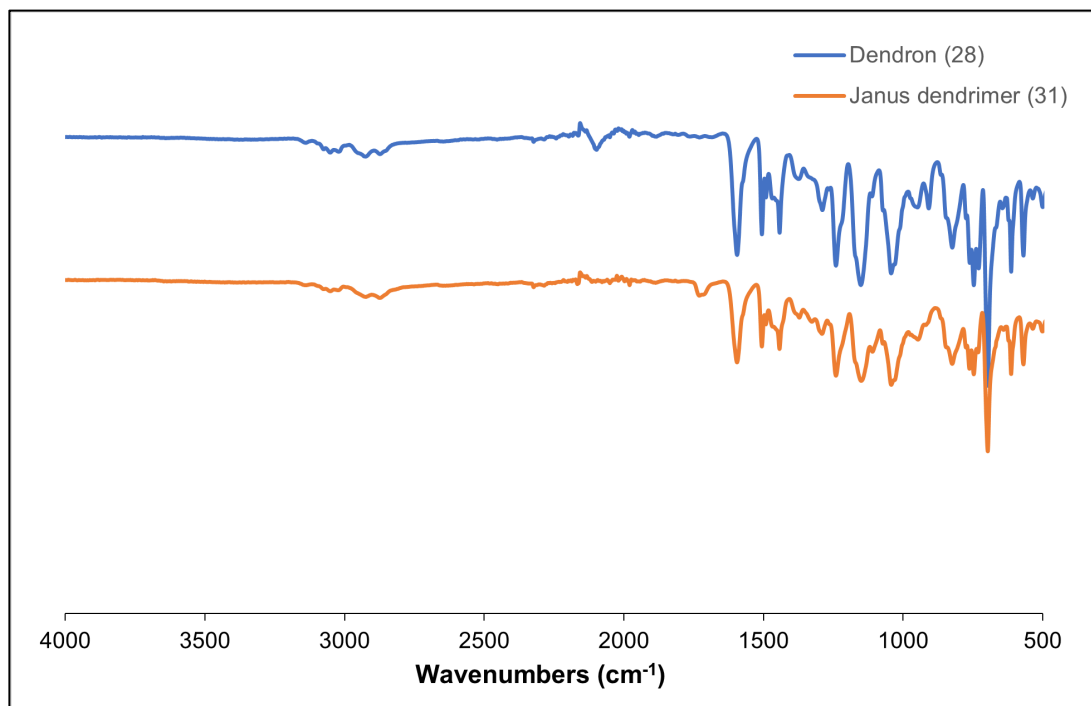


Figure B34. IR spectrum of dendron (28) and Janus dendrimer (31).

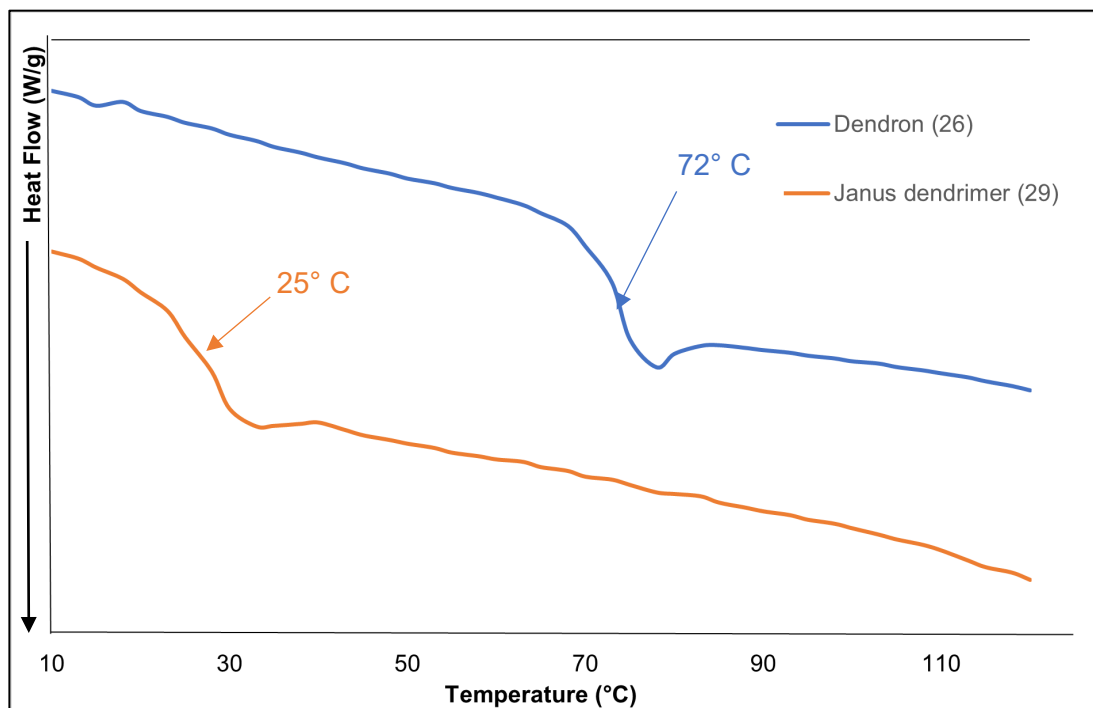


Figure B35. DSC comparison of dendron (26) and Janus dendrimer (29).

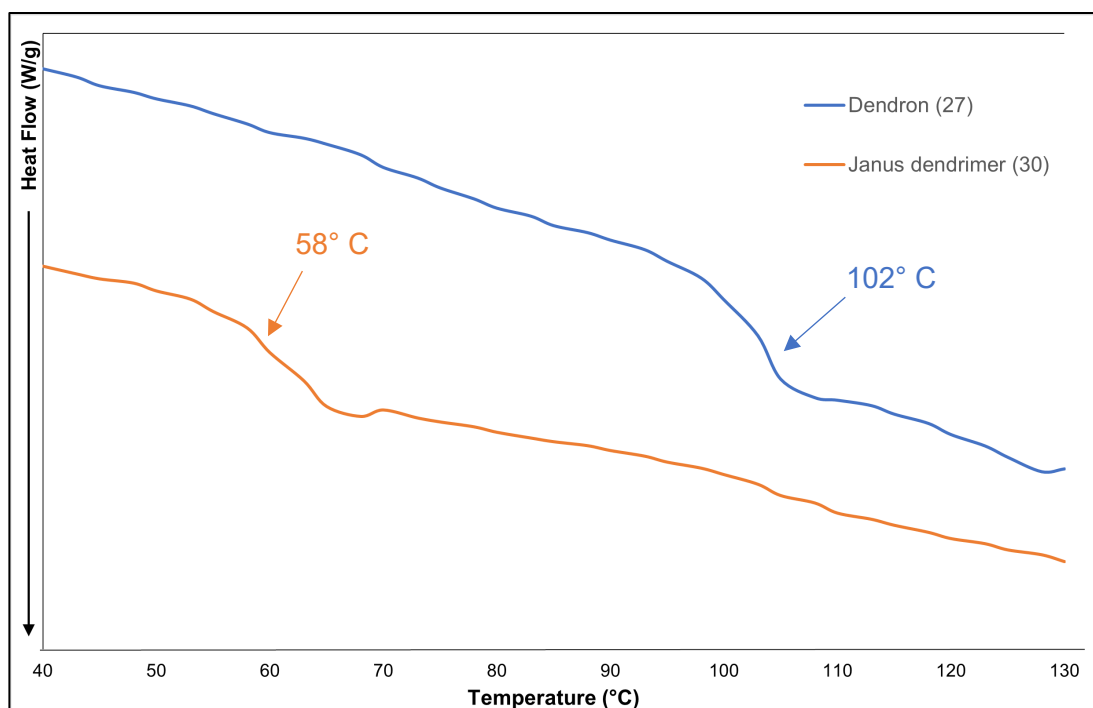


Figure B36. DSC comparison of dendron (27) and Janus dendrimer (30).

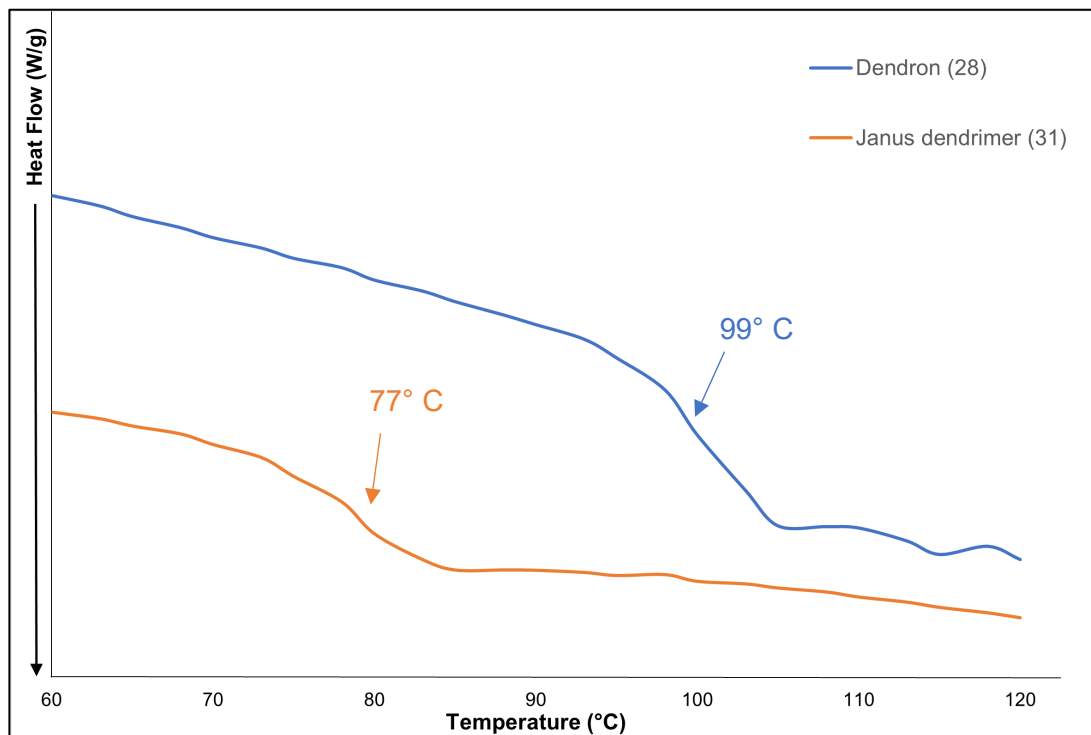


Figure B37. DSC comparison of dendron (28) and Janus dendrimer (31).

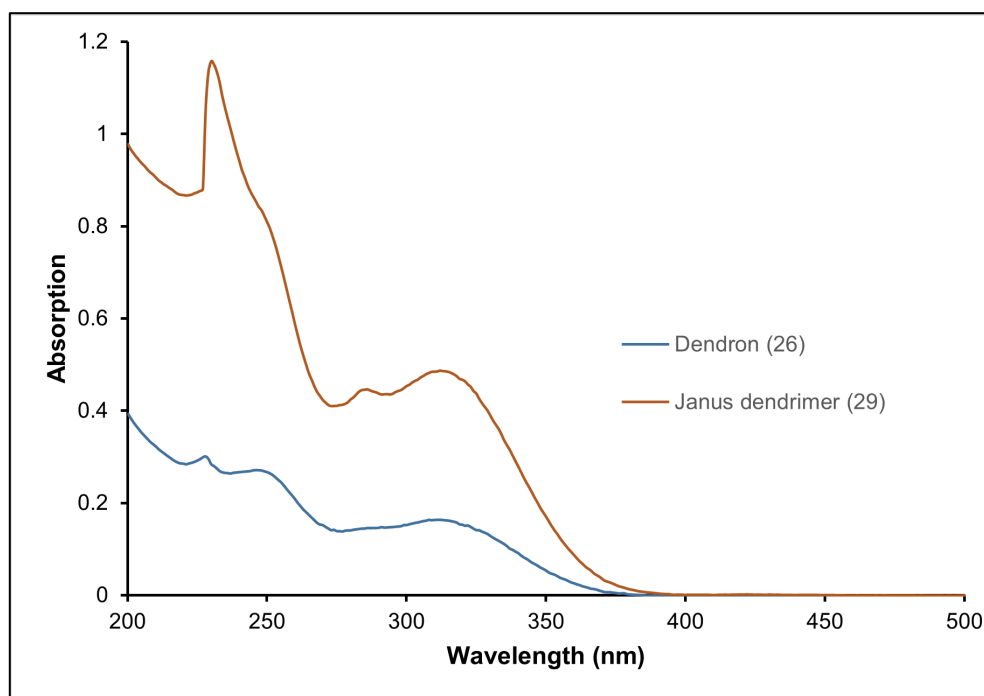


Figure B38. Absorption spectra of dendron (26) and Janus dendrimer (29).

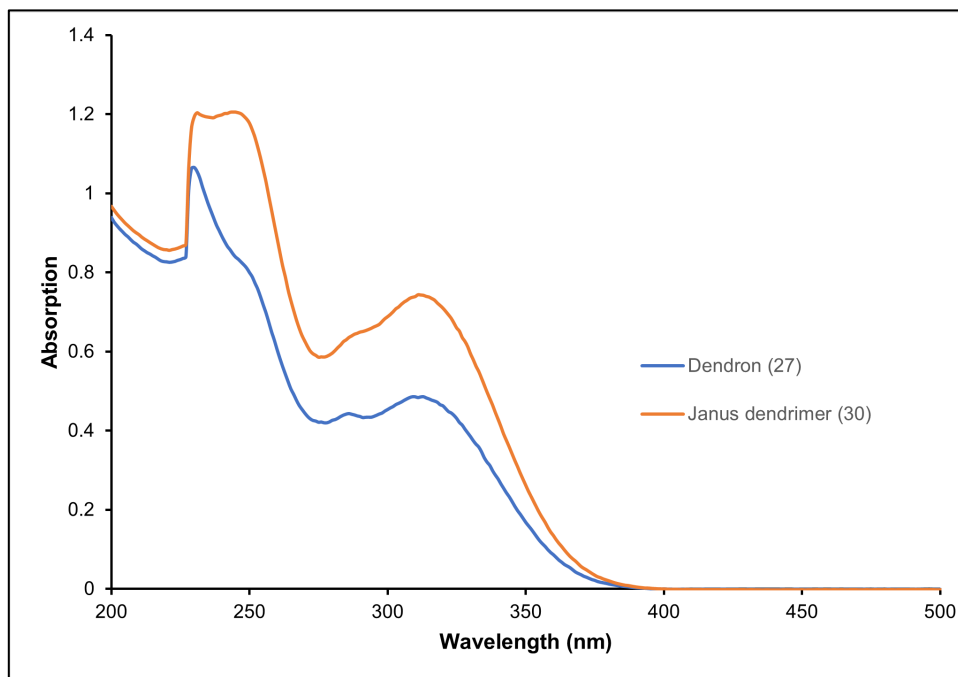


Figure B39. Absorption spectra of dendron (27) and Janus dendrimer (30).

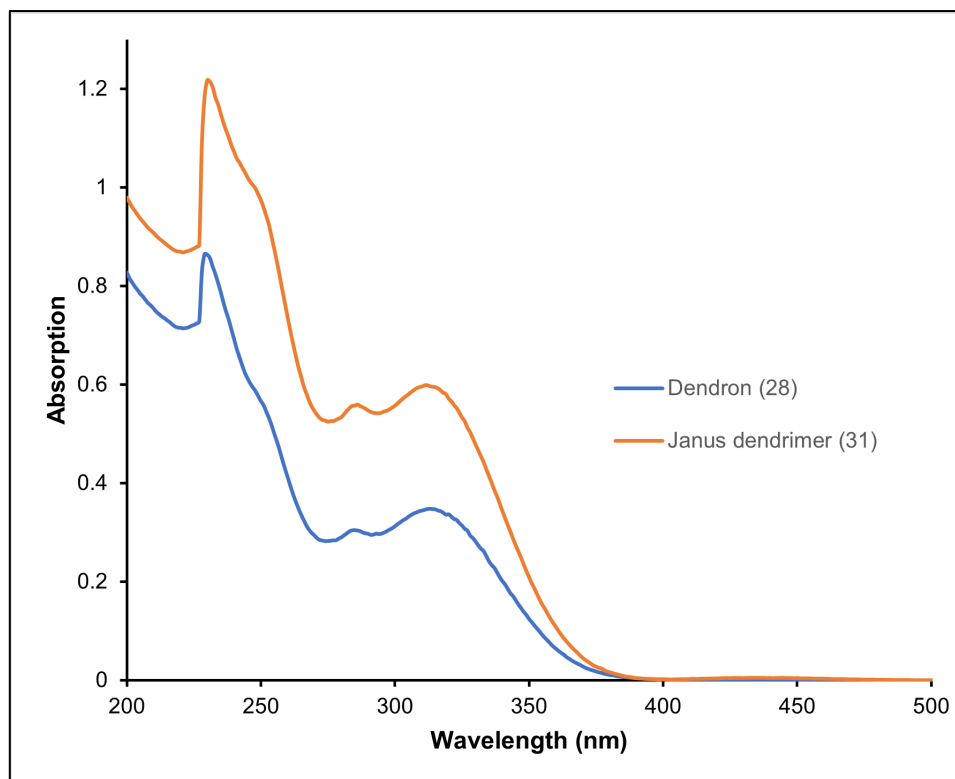


Figure B40. Absorption spectra of dendron (28) and Janus dendrimer (31).

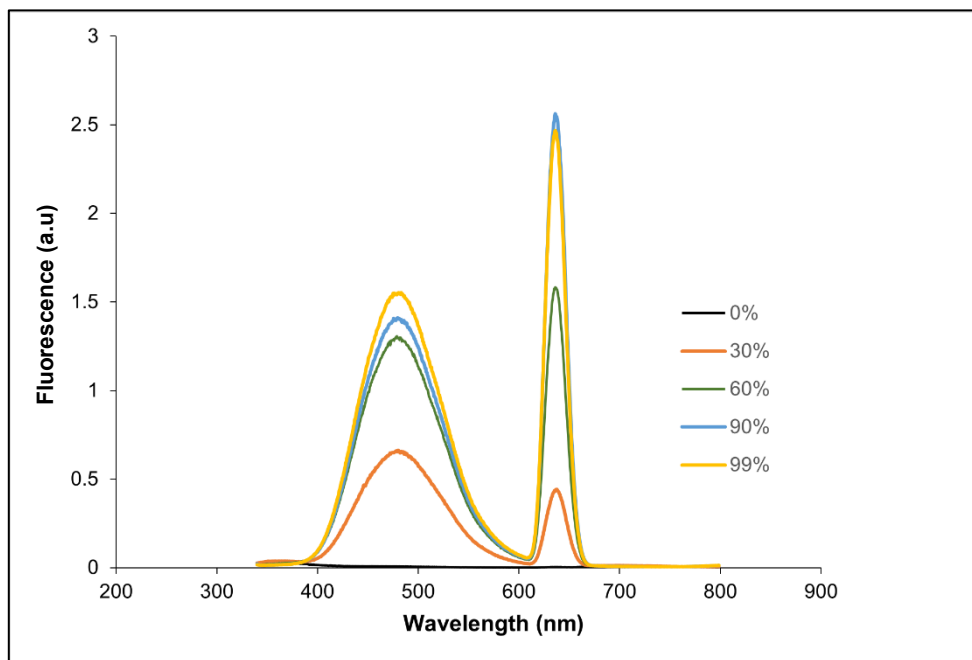


Figure B41. Fluorescence spectra of Janus dendrimer (**29**) at various water contents.

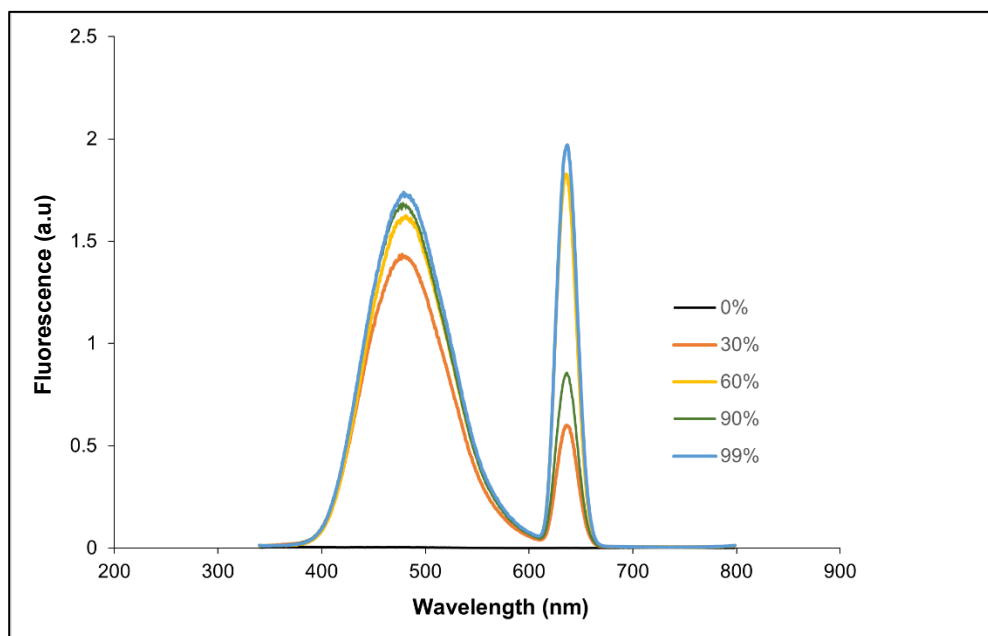


Figure B42. Fluorescence spectra of Janus dendrimer (**30**) at various water contents.

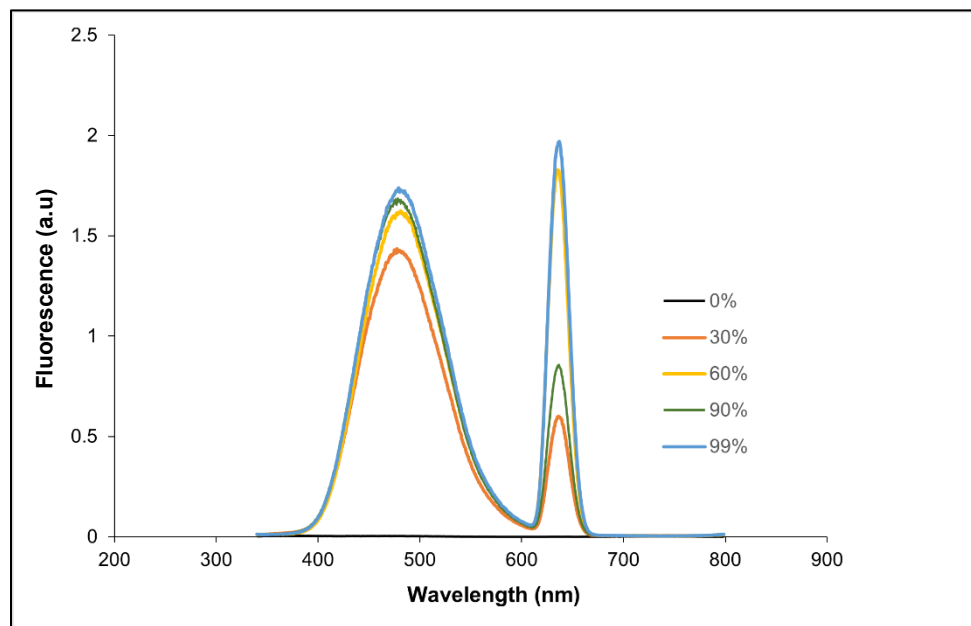


Figure B43. Fluorescence spectra of Janus dendrimer (**31**) at various water contents.

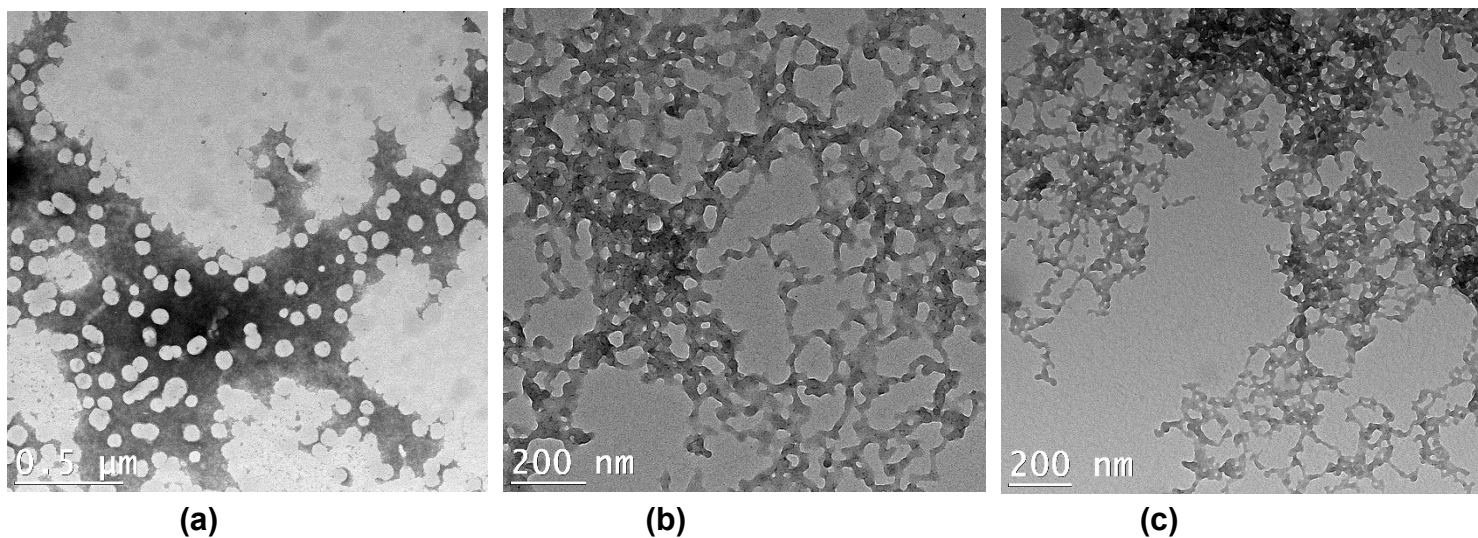


Figure B44. Additional TEM images under kinetic control: (a) Janus dendrimer (**29**), (b) Janus dendrimer (**30**) and (c) Janus dendrimer (**31**).

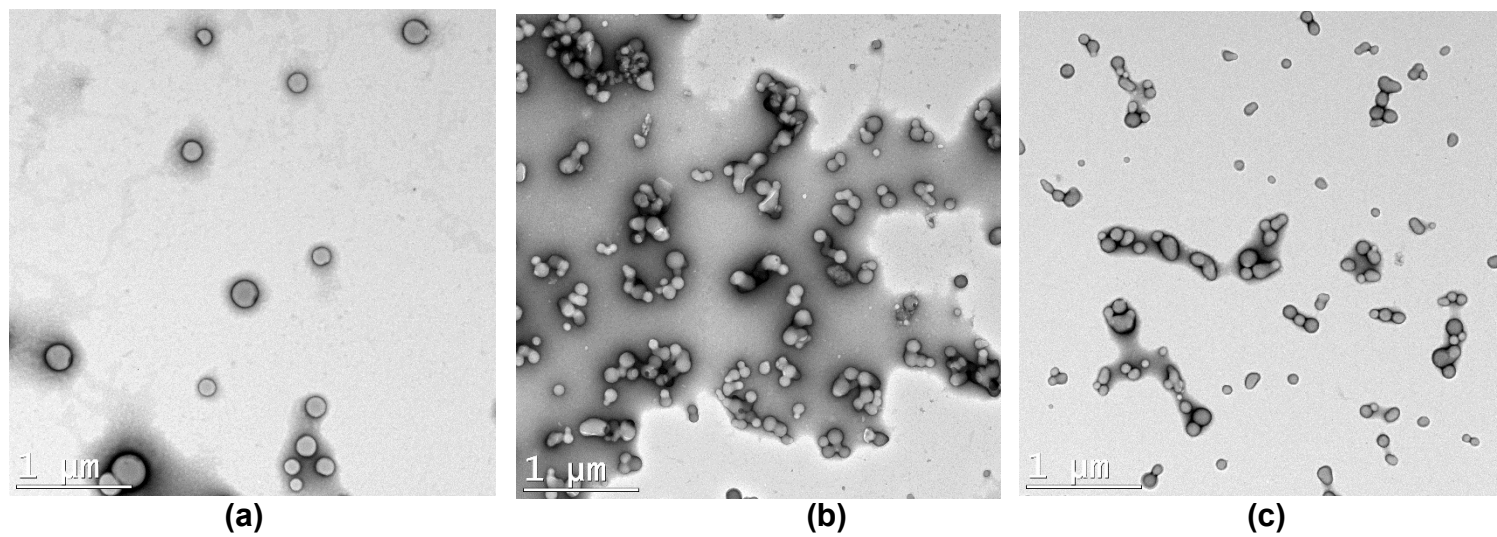


Figure B45. Supplemental TEM images under thermodynamic control: (a) Janus dendrimer (29), (b) Janus dendrimer (30) and (c) Janus dendrimer (31).

REFERENCES

1. Abedi-Gaballu, F., et al., *PAMAM dendrimers as efficient drug and gene delivery nanosystems for cancer therapy*. Applied materials today, 2018. **12**: p. 177-190.
2. Agrahari, V., V. Agrahari, and A.K. Mitra, *Nanocarrier fabrication and macromolecule drug delivery: challenges and opportunities*. Therapeutic delivery, 2016. **7**(4): p. 257-278.
3. Alder, R.W. and B. Reddy, *Attempted equilibration of an insoluble spiran polymer with monomers and oligomers through reversible chemical reactions: transketalization route to spiropolymers from 1, 4-cyclohexanedione and pentaerythritol*. Polymer, 1994. **35**(26): p. 5765-5772.
4. Ambekar, R.S., M. Choudhary, and B. Kandasubramanian, *Recent advances in dendrimer-based nanoplatform for cancer treatment: A review*. European Polymer Journal, 2020. **126**: p. 109546.
5. Andrade-Gagnon, B., et al., *Degradable Spirocyclic Polyacetal-Based Core-Amphiphilic Assemblies for Encapsulation and Release of Hydrophobic Cargo*. Nanomaterials, 2021. **11**(1): p. 161.
6. Antoni, P., et al., *Pushing the limits for Thiol– Ene and CuAAC reactions: Synthesis of a 6th generation dendrimer in a single day*. Macromolecules, 2010. **43**(16): p. 6625-6631.
7. Banerjee, M., et al., *Practical Synthesis of Unsymmetrical Tetraarylethylenes and Their Application for the Preparation of [Triphenylethylene– Spacer– Triphenylethylene] Triads*. The Journal of organic chemistry, 2007. **72**(21): p. 8054-8061.
8. Beginn, U., *Gradient copolymers*. Colloid and polymer science, 2008. **286**(13): p. 1465-1474.
9. Billiet, L., D. Fournier, and F. Du Prez, *Step-growth polymerization and 'click' chemistry: The oldest polymers rejuvenated*. Polymer, 2009. **50**(16): p. 3877-3886.
10. Binauld, S. and M.H. Stenzel, *Acid-degradable polymers for drug delivery: a decade of innovation*. Chemical communications, 2013. **49**(21): p. 2082-2102.

11. Binder, W.H. and R. Sachsenhofer, *'Click' chemistry in polymer and materials science*. Macromolecular Rapid Communications, 2007. **28**(1): p. 15-54.
12. Binder, W.H. and R. Sachsenhofer, *'Click' chemistry in polymer and material science: an update*. Macromolecular Rapid Communications, 2008. **29**(12-13): p. 952-981.
13. Blanz, A., S.P. Armes, and A.J. Ryan, *Self-assembled block copolymer aggregates: from micelles to vesicles and their biological applications*. Macromolecular rapid communications, 2009. **30**(4-5): p. 267-277.
14. Bose, T., et al., *Overview of nano-drugs characteristics for clinical application: the journey from the entry to the exit point*. Journal of nanoparticle research, 2014. **16**(8): p. 1-25.
15. Boyer, C., et al., *Copper-mediated living radical polymerization (atom transfer radical polymerization and copper (0) mediated polymerization): from fundamentals to bioapplications*. Chemical reviews, 2016. **116**(4): p. 1803-1949.
16. Caminade, A.-M. and C.-O. Turrin, *Dendrimers for drug delivery*. Journal of Materials Chemistry B, 2014. **2**(26): p. 4055-4066.
17. Caminade, A.-M., et al., *"Janus" dendrimers: syntheses and properties*. New Journal of Chemistry, 2012. **36**(2): p. 217-226.
18. Carlmark, A., et al., *New methodologies in the construction of dendritic materials*. Chemical Society Reviews, 2009. **38**(2): p. 352-362.
19. Carraher Jr, C.E., *Introduction to polymer chemistry*. 2012: CRC press.
20. Chatgililoglu, C., C. Ferreri, and K. Matyjaszewski, *Radicals and dormant species in biology and polymer chemistry*. ChemPlusChem, 2016. **81**(1): p. 11-29.
21. Chatterjee, S. and S. Ramakrishnan, *Hyperbranched polyacetals with tunable degradation rates*. Macromolecules, 2011. **44**(12): p. 4658-4664.
22. Crossley, S.W., et al., *Mn-, Fe-, and Co-catalyzed radical hydrofunctionalizations of olefins*. Chemical reviews, 2016. **116**(15): p. 8912-9000.
23. Deirram, N., et al., *pH-responsive polymer nanoparticles for drug delivery*. Macromolecular rapid communications, 2019. **40**(10): p. 1800917.
24. Deng, X.-X., F.-S. Du, and Z.-C. Li, *Combination of orthogonal ABB and ABC multicomponent reactions toward efficient divergent synthesis of dendrimers with structural diversity*. ACS Macro Letters, 2014. **3**(7): p. 667-670.

25. Donnelly, P.S., et al., 'Click' cycloaddition catalysts: copper (i) and copper (ii) tris (triazolymethyl) amine complexes. *Chemical communications*, 2008(21): p. 2459-2461.
26. Douka, A., et al., *A review on enzymatic polymerization to produce polycondensation polymers: The case of aliphatic polyesters, polyamides and polyesteramides*. *Progress in Polymer Science*, 2018. **79**: p. 1-25.
27. Elias, H.-G., *Macromolecules· 1: Volume 1: Structure and Properties*. 2012: Springer Science & Business Media.
28. Elizondo-García, M.E., et al., *Self-Assembly Behavior of Amphiphilic Janus Dendrimers in Water: A Combined Experimental and Coarse-Grained Molecular Dynamics Simulation Approach*. *Molecules*, 2018. **23**(4): p. 969.
29. Elsabahy, M. and K.L. Wooley, *Design of polymeric nanoparticles for biomedical delivery applications*. *Chemical Society Reviews*, 2012. **41**(7): p. 2545-2561.
30. Elsabahy, M., et al., *Polymeric nanostructures for imaging and therapy*. *Chemical reviews*, 2015. **115**(19): p. 10967-11011.
31. Fakirov, S., *Condensation polymers: Their chemical peculiarities offer great opportunities*. *Progress in Polymer Science*, 2019. **89**: p. 1-18.
32. Fernandez-Fernandez, A., R. Manchanda, and A.J. McGoron, *Theranostic applications of nanomaterials in cancer: drug delivery, image-guided therapy, and multifunctional platforms*. *Applied biochemistry and biotechnology*, 2011. **165**(7): p. 1628-1651.
33. Fréchet, J.M., *Functional polymers and dendrimers: reactivity, molecular architecture, and interfacial energy*. *Science*, 1994. **263**(5154): p. 1710-1715.
34. Fréchet, J.M., *Dendrimers and supramolecular chemistry*. *Proceedings of the National Academy of Sciences*, 2002. **99**(8): p. 4782-4787.
35. Gandini, A., *The furan/maleimide Diels–Alder reaction: A versatile click–unclick tool in macromolecular synthesis*. *Progress in Polymer Science*, 2013. **38**(1): p. 1-29.
36. Gao, M. and B.Z. Tang, *Aggregation-induced emission probes for cancer theranostics*. *Drug Discovery Today*, 2017. **22**(9): p. 1288-1294.
37. Garcia-Martinez, J.C., E. Diez-Barra, and J. Rodriguez-Lopez, *Conjugated dendrimers with oly (phenylenevinylene) and poly (phenyleneethynylene) scaffolds*. *Current Organic Synthesis*, 2008. **5**(3): p. 267-290.
38. Gerweck, L.E. and K. Seetharaman, *Cellular pH gradient in tumor versus normal tissue: potential exploitation for the treatment of cancer*. *Cancer research*, 1996. **56**(6): p. 1194-1198.

39. Goddard, E.D. and J.V. Gruber, *Principles of polymer science and technology in cosmetics and personal care*. 1999: CRC Press.
40. Gondi, S.R., A.P. Vogt, and B.S. Sumerlin, *Versatile pathway to functional telechelics via RAFT polymerization and click chemistry*. *Macromolecules*, 2007. **40**(3): p. 474-481.
41. Grosu, I., et al., *Synthesis and Structure of New Macrocycles Including Spiro-1, 3-Dioxane Units*. *European Journal of Organic Chemistry*, 2003. **2003**(16): p. 3153-3161.
42. Grubbs, R.B., *Nitroxide-mediated radical polymerization: limitations and versatility*. *Polymer Reviews*, 2011. **51**(2): p. 104-137.
43. Grubbs, R.B. and R.H. Grubbs, *50th Anniversary Perspective: Living Polymerization □ Emphasizing the Molecule in Macromolecules*. *Macromolecules*, 2017. **50**(18): p. 6979-6997.
44. Gurnani, P. and S. Perrier, *Controlled radical polymerization in dispersed systems for biological applications*. *Progress in Polymer Science*, 2020. **102**: p. 101209.
45. Hajduk, D.A., et al., *The gyroid: a new equilibrium morphology in weakly segregated diblock copolymers*. *Macromolecules*, 1994. **27**(15): p. 4063-4075.
46. Hopfinger, A., *Conformational properties of macromolecules*. 2012: Elsevier.
47. Hu, F.-F., et al., *Enthalpy-driven self-assembly of amphiphilic Janus dendrimers into onion-like vesicles: a Janus particle model*. *Nanoscale*, 2019. **11**(37): p. 17350-17356.
48. Hu, J., et al., *Precise modular synthesis and a structure–property study of acid-cleavable star-block copolymers for pH-triggered drug delivery*. *Polymer Chemistry*, 2015. **6**(9): p. 1553-1566.
49. Hu, L., et al., *Stimuli-responsive polymers for sensing and actuation*. *Materials Horizons*, 2019. **6**(9): p. 1774-1793.
50. Hu, Y., et al., *Newly developed techniques on polycondensation, ring-opening polymerization and polymer modification: Focus on poly (lactic acid)*. *Materials*, 2016. **9**(3): p. 133.
51. Huang, D., et al., *Facile synthesis and self-assembly behaviour of pH-responsive degradable polyacetal dendrimers*. *Polymer Chemistry*, 2016. **7**(40): p. 6154-6158.
52. Huang, G., et al., *Dendron-Containing Tetraphenylethylene Compounds: Dependence of Fluorescence and Photocyclization Reactivity on the Dendron Generation*. *Chemistry—A European Journal*, 2012. **18**(13): p. 3886-3892.

53. Huang, Y., et al., *A new design of cleavable acetal-containing amphiphilic block copolymers triggered by light*. Journal of Polymer Science Part A: Polymer Chemistry, 2018. **56**(16): p. 1815-1824.
54. Hufendiek, A., S. Lingier, and F.E. Du Prez, *Thermoplastic polyacetals: chemistry from the past for a sustainable future?* Polymer Chemistry, 2019. **10**(1): p. 9-33.
55. Hufendiek, A., et al., *Polycycloacetals via polytransacetalization of diglycerol bisacetone*. Polymer Chemistry, 2018. **9**(38): p. 4789-4797.
56. Jain, V., S. Jain, and S. Mahajan, *Nanomedicines based drug delivery systems for anti-cancer targeting and treatment*. Current drug delivery, 2015. **12**(2): p. 177-191.
57. Jana, D. and B.K. Ghorai, *Synthesis and photophysical properties of tetraphenylethylene-based conjugated dendrimers with triphenylamine core*. Tetrahedron letters, 2012. **53**(2): p. 196-199.
58. Jazani, A.M. and J.K. Oh, *Dual location, dual acidic pH/reduction-responsive degradable block copolymer: Synthesis and investigation of ketal linkage instability under ATRP conditions*. Macromolecules, 2017. **50**(23): p. 9427-9436.
59. Johnson, J.A., et al., *Construction of linear polymers, dendrimers, networks, and other polymeric architectures by copper-catalyzed azide-alkyne cycloaddition "click" chemistry*. Macromolecular rapid communications, 2008. **29**(12-13): p. 1052-1072.
60. Keddie, D.J., *A guide to the synthesis of block copolymers using reversible-addition fragmentation chain transfer (RAFT) polymerization*. Chemical Society Reviews, 2014. **43**(2): p. 496-505.
61. Kermagoret, A. and D. Gigmes, *Combined nitroxide mediated radical polymerization techniques for block copolymer synthesis*. Tetrahedron, 2016. **72**(48): p. 7672-7685.
62. Kesharwani, P., K. Jain, and N.K. Jain, *Dendrimer as nanocarrier for drug delivery*. Progress in Polymer Science, 2014. **39**(2): p. 268-307.
63. Kolb, H.C., M. Finn, and K.B. Sharpless, *Click chemistry: diverse chemical function from a few good reactions*. Angewandte Chemie International Edition, 2001. **40**(11): p. 2004-2021.
64. Krishnan, N., et al., *Self-assembly of tetraphenylethylene-based dendron into blue fluorescent nanoparticles with aggregation induced enhanced emission*. Journal of Chemical Sciences, 2018. **130**(10): p. 1-8.

65. Krishnan, N., et al., *Self-assembly of DNA–tetraphenylethylene amphiphiles into DNA-grafted nanosheets as a support for the immobilization of gold nanoparticles: a recyclable catalyst with enhanced activity*. *Nanoscale*, 2018. **10**(36): p. 17174-17181.
66. Krishnan, N., et al., *Galactose-Grafted 2D Nanosheets from the Self-Assembly of Amphiphilic Janus Dendrimers for the Capture and Agglutination of Escherichia coli*. *Chemistry—A European Journal*, 2020. **26**(5): p. 1037-1041.
67. Kwon, J., et al., *Inflammation-responsive antioxidant nanoparticles based on a polymeric prodrug of vanillin*. *Biomacromolecules*, 2013. **14**(5): p. 1618-1626.
68. Lallana, E., et al., *Click chemistry with polymers, dendrimers, and hydrogels for drug delivery*. *Pharmaceutical research*, 2012. **29**(4): p. 902-921.
69. Law, A.C., et al., *Synthesis and material properties of elastomeric high molecular weight polycycloacetals derived from diglycerol and meso-erythritol*. *Journal of Applied Polymer Science*, 2020. **137**(23): p. 48780.
70. Lee, C.C., et al., *Designing dendrimers for biological applications*. *Nature biotechnology*, 2005. **23**(12): p. 1517-1526.
71. Leiro, V., et al., *The present and the future of degradable dendrimers and derivatives in theranostics*. *Bioconjugate chemistry*, 2015. **26**(7): p. 1182-1197.
72. Liang, L. and D. Astruc, *The copper (I)-catalyzed alkyne-azide cycloaddition (CuAAC) “click” reaction and its applications. An overview*. *Coordination Chemistry Reviews*, 2011. **255**(23-24): p. 2933-2945.
73. Lingier, S., et al., *Rigid polyurethanes, polyesters, and polycarbonates from renewable ketal monomers*. *Macromolecules*, 2017. **50**(14): p. 5346-5352.
74. Lingier, S., et al., *Renewable thermoplastic polyurethanes containing rigid spiroacetal moieties*. *European Polymer Journal*, 2015. **70**: p. 232-239.
75. Liu, B. and S. Thayumanavan, *Substituent effects on the pH sensitivity of acetals and ketals and their correlation with encapsulation stability in polymeric nanogels*. *Journal of the American Chemical Society*, 2017. **139**(6): p. 2306-2317.
76. Liu, X., Y. Yang, and M.W. Urban, *Stimuli-responsive polymeric nanoparticles*. *Macromolecular rapid communications*, 2017. **38**(13): p. 1700030.
77. Lombardo, D., et al., *Amphiphiles self-assembly: basic concepts and future perspectives of supramolecular approaches*. *Advances in Condensed Matter Physics*, 2015. **2015**.

78. Lowe, A.B., *Thiol-ene “click” reactions and recent applications in polymer and materials synthesis*. Polymer Chemistry, 2010. **1**(1): p. 17-36.
79. Lu, H., et al., *Silver nanocrystals by hyperbranched polyurethane-assisted photochemical reduction of Ag⁺*. Materials Chemistry and Physics, 2003. **81**(1): p. 104-107.
80. Lyu, Z., et al., *Poly (amidoamine) dendrimers: Covalent and supramolecular synthesis*. Materials Today Chemistry, 2019. **13**: p. 34-48.
81. Magenau, A.J., et al., *Investigation of electrochemically mediated atom transfer radical polymerization*. Macromolecules, 2013. **46**(11): p. 4346-4353.
82. Mai, Y. and A. Eisenberg, *Self-assembly of block copolymers*. Chemical Society Reviews, 2012. **41**(18): p. 5969-5985.
83. Makhseed, S. and N.B. McKeown, *Novel spiro-polymers with enhanced solubility*. Chemical Communications, 1999(3): p. 255-256.
84. Malkoch, M. and S. García-Gallego, *Introduction to dendrimers and other dendritic polymers*. 2020.
85. Malkoch, M., et al., *Structurally diverse dendritic libraries: A highly efficient functionalization approach using click chemistry*. Macromolecules, 2005. **38**(9): p. 3663-3678.
86. Maślińska-Solich, J. and S. Kukowka, *Synthesis of poly (spiroacetal-ether) s*. Polymer international, 2003. **52**(10): p. 1633-1640.
87. Matsukizono, H. and T. Endo, *Reworkable polyhydroxyurethane films with reversible acetal networks obtained from multifunctional six-membered cyclic carbonates*. Journal of the American Chemical Society, 2018. **140**(3): p. 884-887.
88. Matsukizono, H., K. Matsumoto, and T. Endo, *Multifunctional cyclic carbonates comprising hyperbranched polyacetals: Synthesis and applications to polymer electrolytes and networked polymer materials*. Journal of Polymer Science Part A: Polymer Chemistry, 2019. **57**(23): p. 2295-2303.
89. Mellman, I., R. Fuchs, and A. Helenius, *Acidification of the endocytic and exocytic pathways*. Annual review of biochemistry, 1986. **55**(1): p. 663-700.
90. Mialon, L., et al., *Polyalkylenehydroxybenzoates (PAHBs): Biorenewable aromatic/aliphatic polyesters from lignin*. Macromolecular rapid communications, 2011. **32**(17): p. 1386-1392.
91. Miller, S.A., *Sustainable polymers: opportunities for the next decade*. 2013, ACS Publications.

92. Morachis, J.M., E.A. Mahmoud, and A. Almutairi, *Physical and chemical strategies for therapeutic delivery by using polymeric nanoparticles*. Pharmacological reviews, 2012. **64**(3): p. 505-519.
93. Nazemi, A. and E.R. Gillies, *Dendrimersomes with photodegradable membranes for triggered release of hydrophilic and hydrophobic cargo*. Chemical Communications, 2014. **50**(76): p. 11122-11125.
94. Pan, J., et al., *Design and synthesis of novel amphiphilic Janus dendrimers for bone-targeted drug delivery*. Tetrahedron, 2012. **68**(14): p. 2943-2949.
95. Pan, X., et al., *Externally controlled atom transfer radical polymerization*. Chemical Society Reviews, 2018. **47**(14): p. 5457-5490.
96. Peer, D., et al., *Nanocarriers as an emerging platform for cancer therapy*. Nano-Enabled Medical Applications, 2020: p. 61-91.
97. Pemba, A.G., et al., *Cyclic and spirocyclic polyacetal ethers from lignin-based aromatics*. Polymer Chemistry, 2014. **5**(9): p. 3214-3221.
98. Peng, H.-Q., et al., *Visualizing the initial step of self-assembly and the phase transition by stereogenic amphiphiles with aggregation-induced emission*. ACS nano, 2018. **13**(1): p. 839-846.
99. Percec, V., et al., *Self-assembly of Janus dendrimers into uniform dendrimersomes and other complex architectures*. Science, 2010. **328**(5981): p. 1009-1014.
100. Perrier, S., *50th Anniversary Perspective: RAFT Polymerization □ A User Guide*. Macromolecules, 2017. **50**(19): p. 7433-7447.
101. Peterca, M., et al., *Predicting the size and properties of dendrimersomes from the lamellar structure of their amphiphilic Janus dendrimers*. Journal of the American Chemical Society, 2011. **133**(50): p. 20507-20520.
102. Ramkumar, J., S. Banerjee, and A. Tyagi, *Nafion perfluorosulphonate membrane: Unique properties and various applications*. Funct. Materials: Preparation, Processes and Applications, Elsevier Ltd., London, 2012: p. 549-577.
103. Rivas, C.J.M., et al., *Nanoprecipitation process: From encapsulation to drug delivery*. International journal of pharmaceutics, 2017. **532**(1): p. 66-81.
104. Rodrigues, P.R. and R.P. Vieira, *Advances in atom-transfer radical polymerization for drug delivery applications*. European Polymer Journal, 2019. **115**: p. 45-58.
105. Rodríguez-Acosta, G.L., et al., *Nanomaterial Applications of Amphiphilic Dendrimeric Micelles*. Current Medicinal Chemistry, 2021.

106. Rostagno, M., et al., *Sustainable polyacetals from erythritol and bioaromatics*. Journal of Applied Polymer Science, 2016. **133**(45).
107. Samanta, S., et al., *Polyacetals: water-soluble, pH-degradable polymers with extraordinary temperature response*. Macromolecules, 2016. **49**(5): p. 1858-1864.
108. Sánchez-Ruiz, A., et al., *Aggregation-Induced Emission Properties in Fully π -Conjugated Polymers, Dendrimers, and Oligomers*. Polymers, 2021. **13**(2): p. 213.
109. Schacher, F.H., P.A. Rupar, and I. Manners, *Functional block copolymers: nanostructured materials with emerging applications*. Angewandte Chemie International Edition, 2012. **51**(32): p. 7898-7921.
110. Schacht, E., et al., *Polyacetal and poly (ortho ester)–poly (ethylene glycol) graft copolymer thermogels: Preparation, hydrolysis and FITC-BSA release studies*. Journal of controlled release, 2006. **116**(2): p. 219-225.
111. Schmaljohann, D., *Thermo- and pH-responsive polymers in drug delivery*. Advanced drug delivery reviews, 2006. **58**(15): p. 1655-1670.
112. Shaker, S., A.R. Gardouh, and M.M. Ghorab, *Factors affecting liposomes particle size prepared by ethanol injection method*. Research in pharmaceutical sciences, 2017. **12**(5): p. 346.
113. Sherman, S.E., Q. Xiao, and V. Percec, *Mimicking complex biological membranes and their programmable glycan ligands with dendrimersomes and glycodendrimersomes*. Chemical reviews, 2017. **117**(9): p. 6538-6631.
114. Sikwal, D.R., R.S. Kalhapure, and T. Govender, *An emerging class of amphiphilic dendrimers for pharmaceutical and biomedical applications: Janus amphiphilic dendrimers*. European Journal of Pharmaceutical Sciences, 2017. **97**: p. 113-134.
115. Singh, R., et al., *Exploration of energy modulations in novel RhB-TPE-based bichromophoric materials via interactions of Cu²⁺ ion under various semiaqueous and micellar conditions*. ACS applied materials & interfaces, 2016. **8**(10): p. 6751-6762.
116. Sorroza-Martínez, K., et al., *Efficient modification of PAMAM G1 dendrimer surface with β -cyclodextrin units by CuAAC: impact on the water solubility and cytotoxicity*. RSC Advances, 2020. **10**(43): p. 25557-25566.
117. Sowinska, M. and Z. Urbanczyk-Lipkowska, *Advances in the chemistry of dendrimers*. New Journal of Chemistry, 2014. **38**(6): p. 2168-2203.
118. Staff, R.H., K. Landfester, and D. Crespy, *Recent advances in the emulsion solvent evaporation technique for the preparation of nanoparticles and*

- nanocapsules*. Hierarchical Macromolecular Structures: 60 Years after the Staudinger Nobel Prize II, 2013: p. 329-344.
119. Sutthasupa, S., M. Shiotsuki, and F. Sanda, *Recent advances in ring-opening metathesis polymerization, and application to synthesis of functional materials*. Polymer journal, 2010. **42**(12): p. 905-915.
 120. Taabache, S. and A. Bertin, *Vesicles from amphiphilic dumbbells and janus dendrimers: Bioinspired self-assembled structures for biomedical applications*. Polymers, 2017. **9**(7): p. 280.
 121. Tang, R., W. Ji, and C. Wang, *Amphiphilic Block Copolymers Bearing Ortho Ester Side-Chains: pH-Dependent Hydrolysis and Self-Assembly in Water*. Macromolecular bioscience, 2010. **10**(2): p. 192-201.
 122. Taratula, O., et al., *A multifunctional theranostic platform based on phthalocyanine-loaded dendrimer for image-guided drug delivery and photodynamic therapy*. Molecular pharmaceutics, 2013. **10**(10): p. 3946-3958.
 123. Teodorescu, M. and K. Matyjaszewski*, *Controlled polymerization of (meth)acrylamides by atom transfer radical polymerization*. Macromolecular rapid communications, 2000. **21**(4): p. 190-194.
 124. Tezuka, Y. and H. Oike, *Topological polymer chemistry: systematic classification of nonlinear polymer topologies*. Journal of the American Chemical Society, 2001. **123**(47): p. 11570-11576.
 125. Tritschler, U., et al., *50th anniversary perspective: Functional nanoparticles from the solution self-assembly of block copolymers*. Macromolecules, 2017. **50**(9): p. 3439-3463.
 126. Ummadisetti, C., B.N.P. Rachapudi, and L.A.P.D. Bethala, *Glycerol-based SO₃H-Carbon Catalyst: A green recyclable catalyst for the chemoselective synthesis of pentaerythritol diacetals*. European Journal of Chemistry, 2014. **5**(3): p. 536-540.
 127. Vilar, G., J. Tulla-Puche, and F. Albericio, *Polymers and drug delivery systems*. Current drug delivery, 2012. **9**(4): p. 367-394.
 128. Viswanath, V. and K. Santhakumar, *Perspectives on dendritic architectures and their biological applications: From core to cell*. Journal of Photochemistry and Photobiology B: Biology, 2017. **173**: p. 61-83.
 129. Wang, F., et al., *A highly efficient photocatalytic system for hydrogen production by a robust hydrogenase mimic in an aqueous solution*. Angewandte Chemie International Edition, 2011. **50**(14): p. 3193-3197.

130. Wittenberg, J.B. and L. Isaacs, *Cucurbit [6] uril dimer induces supramolecular polymerisation of a cationic polyethylene glycol derivative*. *Supramolecular Chemistry*, 2014. **26**(3-4): p. 157-167.
131. Xiao, Q., et al., *Self-sorting and coassembly of fluorinated, hydrogenated, and hybrid Janus dendrimers into dendrimersomes*. *Journal of the American Chemical Society*, 2016. **138**(38): p. 12655-12663.
132. Xiong, H., et al., *Theranostic dendrimer-based lipid nanoparticles containing PEGylated BODIPY dyes for tumor imaging and systemic mRNA delivery in vivo*. *Journal of Controlled Release*, 2020. **325**: p. 198-205.
133. Xu, J.-F., et al., *Hydrogen bonding directed self-assembly of small-molecule amphiphiles in water*. *Organic letters*, 2014. **16**(15): p. 4016-4019.
134. Yokozawa, T. and Y. Ohta, *Transformation of step-growth polymerization into living chain-growth polymerization*. *Chemical reviews*, 2016. **116**(4): p. 1950-1968.
135. Young, R.J. and P.A. Lovell, *Introduction to polymers*. 2011: CRC press.
136. Zaremski, M.Y., D. Kalugin, and V. Golubev, *Gradient copolymers: Synthesis, structure, and properties*. *Polymer Science Series A*, 2009. **51**(1): p. 103-122.
137. Zeng, F. and S.C. Zimmerman, *Dendrimers in supramolecular chemistry: from molecular recognition to self-assembly*. *Chemical reviews*, 1997. **97**(5): p. 1681-1712.
138. Zhang, Q., et al., *Acid-Labile Thermoresponsive Copolymers That Combine Fast pH-Triggered Hydrolysis and High Stability under Neutral Conditions*. *Angewandte Chemie International Edition*, 2015. **54**(37): p. 10879-10883.
139. Zhang, S., et al., *Self-assembly of amphiphilic Janus dendrimers into uniform onion-like dendrimersomes with predictable size and number of bilayers*. *Proceedings of the National Academy of Sciences*, 2014. **111**(25): p. 9058-9063.
140. Zhang, S., et al., *"Single-single" amphiphilic janus dendrimers self-assemble into uniform dendrimersomes with predictable size*. *ACS nano*, 2014. **8**(2): p. 1554-1565.
141. Zhang, Y., et al., *Small molecule-initiated light-activated semiconducting polymer dots: an integrated nanoplatfom for targeted photodynamic therapy and imaging of cancer cells*. *Analytical chemistry*, 2014. **86**(6): p. 3092-3099.
142. Zhu, L., et al., *On the Mechanism of Copper (I)-Catalyzed Azide-Alkyne Cycloaddition*. *The Chemical Record*, 2016. **16**(3): p. 1501-1517.

